AN ABSTRACT OF THE THESIS OF

THEODORE ANTHONY SHUGAR for the DOCTOR OF PHILOSOPHY
(Name) (Degree)

in CIVIL ENGINEERING presented on Feb. 26, 1971
(Major) (Date)

Title: STRUCTURAL ANALYSIS OF SYMMETRICAL PENSTOCK BIFURCATIONS BY THE FINITE ELEMENT METHOD

Redacted for privacy

Abstract approved: _____
Harold I. Laursen

A need has existed for an in-depth structural analysis of penstock bifurcations because they form an integral part of hydroelectric power plants. Their geometrical complexity has prevented classical structural analysis from providing an accurate and overall picture of the stresses in the structure.

Digital computers and the development of finite element methods have provided an alternative to past methods of analysis. A finite element solution is developed and described which treats the structure as a continuous entity. The basic finite element is a flat plate element which superimposes bending action and membrane action. It is classified as a mixed formulation and is derived from Reissner's principle. Convergence of the solution, with decreasing element size, is discussed.

Verification of the basic formulation is established by comparing

results for several simple structures for which classical solutions are available. Verification of the finite element model for penstock bifurcations is established by comparison with experimental data obtained from a prototype bifurcation.

Application of the finite element solution is made to a penstock bifurcation which is currently being designed for the Lost Creek project on the Rogue River in southern Oregon. Results of this analysis are presented and discussed.

The computer program was developed so that it can be applied to most symmetrical penstock bifurcations. Included in the Appendices are a user's manual, program description, and program listing.

Structural Analysis of Symmetrical Penstock Bifurcations by the Finite Element Method

by

Theodore Anthony Shugar

A THESIS

submitted to

Oregon State University

in partial fulfillment of
the requirements for the
degree of

Doctor of Philosophy

June 1971

APPROVED:

Redacted for privacy

Professor of Civil Engineering

in charge of major

Redacted for privacy

Head of Department of Civil Engineering

Redacted for privacy

Dean of Graduate School

Date thesis is submitted February 26, 1971

Typed by Clover Redfern for Theodore Anthony Shugar

ACKNOWLEDGMENTS

This dissertation was sponsored by the Corps of Engineers Graduate Fellowship Program. As such, its reproduction has been authorized in whole, or in part, for any purpose of the United States Government. The author wishes to express his appreciation for the hospitality and cooperation extended him at the Portland District Office of the Corps of Engineers during the development and preparation of the dissertation.

A sincere appreciation is expressed to Harold I. Laursen, Professor of Civil Engineering, who served as faculty advisor. His counsel, encouragement, and example were invaluable during this research effort and will always be remembered.

The author would like to thank Randal W. Dickinson of the Portland District, Corps of Engineers, whose friendly cooperation helped to expedite the computer program development.

It has been a privilege to have known the many professors at Oregon State University with whom the author has come to know. A special thanks goes to the professors composing the author's graduate committee; John Peterson, Charles E. Smith, Solon A. Stone and William M. Stone.

Finally, the author would like to express his gratitude to his wife Joan for her continuous support in so many tangible and intangible ways.

TABLE OF CONTENTS

LIST OF TABLES

LIST OF FIGURES

STRUCTURAL ANALYSIS OF SYMMETRICAL PENSTOCK BIFURCATIONS BY THE FINITE ELEMENT METHOD

I. INTRODUCTION

For many years penstock bifurcations have been designed by various governmental agencies and private companies engaged in hydroelectric power generation. Their function, generally, is to divert the kinetic energy of water from one penstock into two generators. As a result of these efforts, methods of analysis have been developed and are continually being improved (22). These analyses have been adequate in the sense that they have provided a design basis for many successful penstock bifurcations. Only a relatively few structural failures have been noted and some were due to inferior materials and fabrication methods.

Until recent years, however, analyses have provided stresses only in certain parts of the structure and have not provided an overall picture. Furthermore, the results have been based on extensive assumptions that have been cause for concern among engineers. The digital computer, combined with the advent of certain matrix methods, has provided an alternative approach. This approach could conceivably result in a substantial improvement by yielding an overall stress analysis without the need for extensive simplifying assumptions.

Consequently, the U.S. Army Corps of Engineers, Portland

District, initiated an investigation of the true structural behavior of penstock bifurcations. The immediate objective was to apply the results to the Lost Creek Reservoir project on the Rogue River. The overall objective was to provide a capability for analyzing stress in other symmetrical penstock bifurcations of the same general configuration.

1.1 Statement and Scope of the Problem

Early work of mathematicians and engineers has provided the classical methods and useful solutions to simplified, typical situations which the practicing engineer still uses today, but which sometimes do not permit an extension to real engineering situations. Owing to its complex geometry, the symmetrical penstock bifurcation, as shown in Figure 1.1, is a difficult structure to analyze even under such simple loading conditions as uniform internal pressure.

The need for the reinforcing girders is best understood with the aid of Figure 1.2. The effect of the crotch girder is to provide reaction R_v due to the discontinuity in hoop stresses all along the intersection a-b. The ring girders have a similar effect along intersection a-c except their behavior is complicated by a lack of symmetry. Therefore, it must be assumed that they provide vertical reactions, horizontal reactions, and bending moment reactions along a-c.

Heretofore, it has been necessary to make simplifying

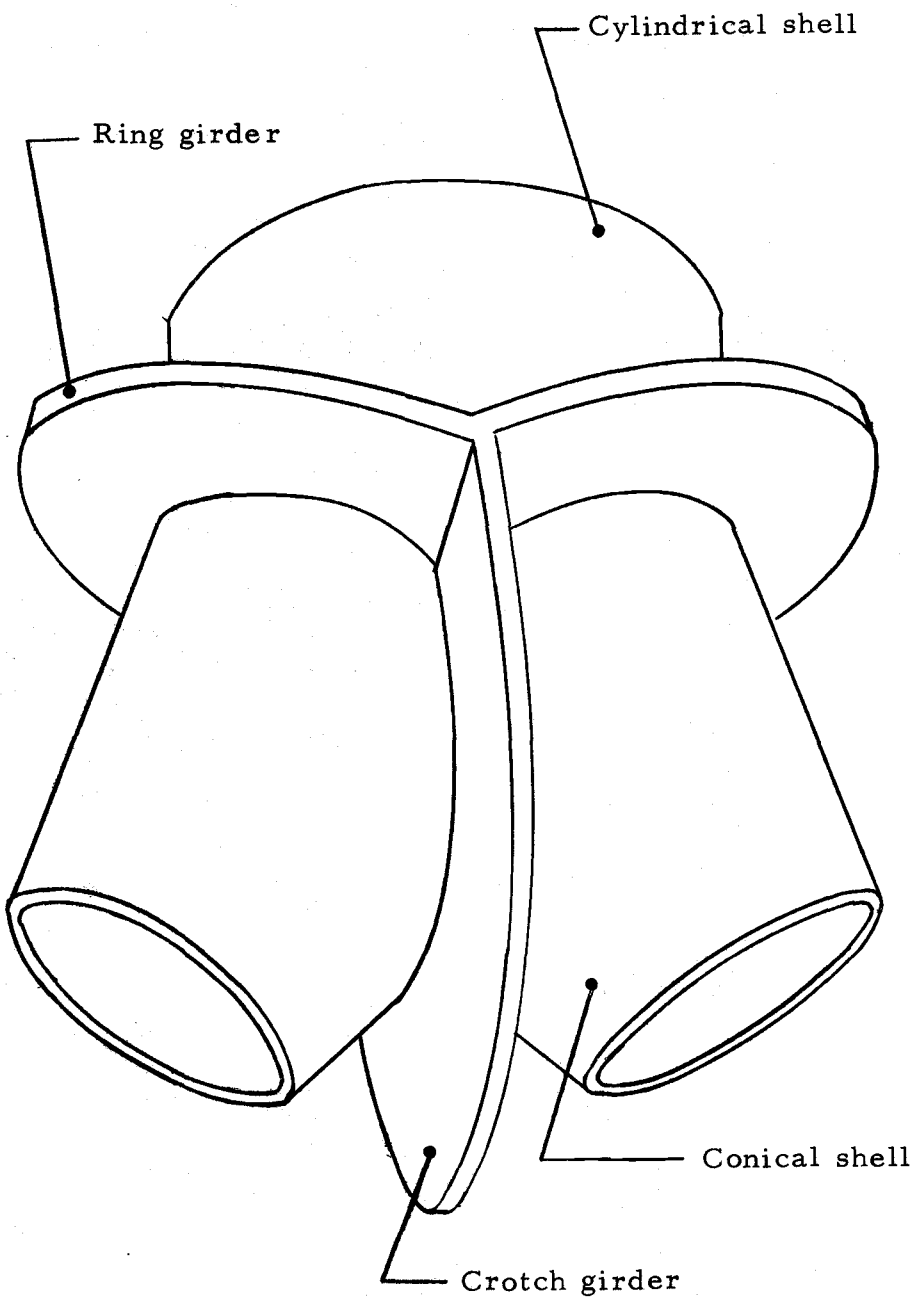

Figure 1.1. Typical penstock bifurcation.

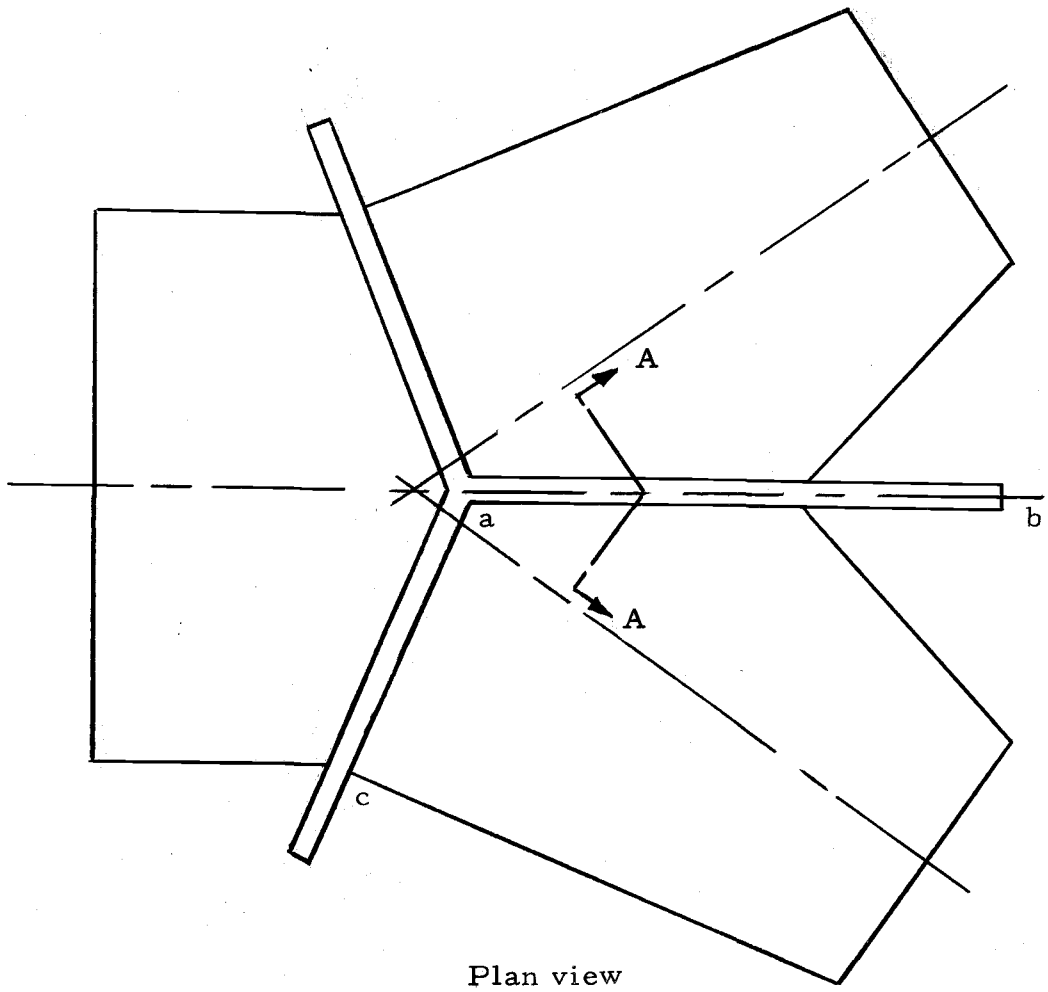

Figure 1.2. Illustration of crotch girder function.

assumptions in order to accomplish a tractable analysis via the aforementioned classical methods. Specifically, these assumptions are as follows:

(1) The effect of the shells on the girders is a linearly varying plane stress load.

(2) The bending rigidity of the shells is neglected.

(3) The girders behave as beams as opposed to plates.

It may be that under certain low pressure and small diameter applications these assumptions are reasonable but the engineer can seldom say when this is so. The shell-girder interaction is basic to the behavior of the structure and as the above assumptions compromise this interaction, the end product, a rational design basis, would likewise be compromised.

The primary objective of this presentation is to obtain stresses, strains, and displacements throughout the structure while subjected to uniform internal pressure. The interaction problem will be circumvented by viewing the entire structure as a continuous entity as opposed to disregarding the shell except as a load transferring mechanism and analyzing the girders as if they were a three-dimensional space frame composed of curved beams.

Two load conditions will be studied; hydrostatic test condition and operating condition. In the former, bulkheads are applied to the bifurcation inlet and outlet apertures and in the latter no bulkheads are

assumed. The internal design pressure is a statically equivalent pressure that takes into account the static head, the effect of water hammer and a factor of safety.

The effect of concrete encasement will not be considered because present design conditions assume all the load to be taken by the bifurcation disregarding its interaction with encasement.

1.2 Method of Solution

Certainly it is possible with more ingenious analytical approaches to overcome the necessity for the aforementioned assumptions. The procedure of this presentation, however, will be to use the approximate numerical approach of the finite element method (28). By dividing the entire structure into a large number of elements, each element can legitimately be treated with the simplified theories of plane stress and/or plate bending, provided the boundary conditions around each element and around the structure are satisfied. Thus the approach is not to abandon simplified methods, but to be more efficient in applying them. This is the central idea behind any numerical approximation, and as long as the desired result is insight rather than numbers, the idea is valid.

The structure is thought of as being composed of four substructures for purposes of explanation. The crotch girder, the ring girder, the cylindrical shell, and the conical shell. Two planes of

symmetry are evident from geometry and the symmetry of uniform internal pressure as shown in Figure 1.3. Because of these conditions the crotch girder is subjected to plane stress loads only. The ring girder is more complicated in that it must be assumed to contain plate bending moments as well as plane stress components. Both the cylindrical and conical shells must be assumed to contain bending stresses along with membrane stresses for a completely general solution.

In order to model such varied stress conditions, it would appear that several different finite element types are required. This, however, immediately leads to difficulties unless the elements have the same number and types of degrees of freedom per node. Further, it is particularly important to insure interelement displacement compatibility and this may not be provided by some otherwise possible combinations. If inconsistent displacement functions are involved, then the displacements will be continuous at the nodes but not along the element edges. Despite these difficulties, some results have been achieved with elements of mixed degrees of freedom (5).

An alternative approach, and the one used here, is to select a finite element that will model, in its most sophisticated state, the shell stress condition (bending and plane stress) and degenerate to model the more simple plane stress condition found in the crotch girder. This is a difficult proposition with a plate bending element

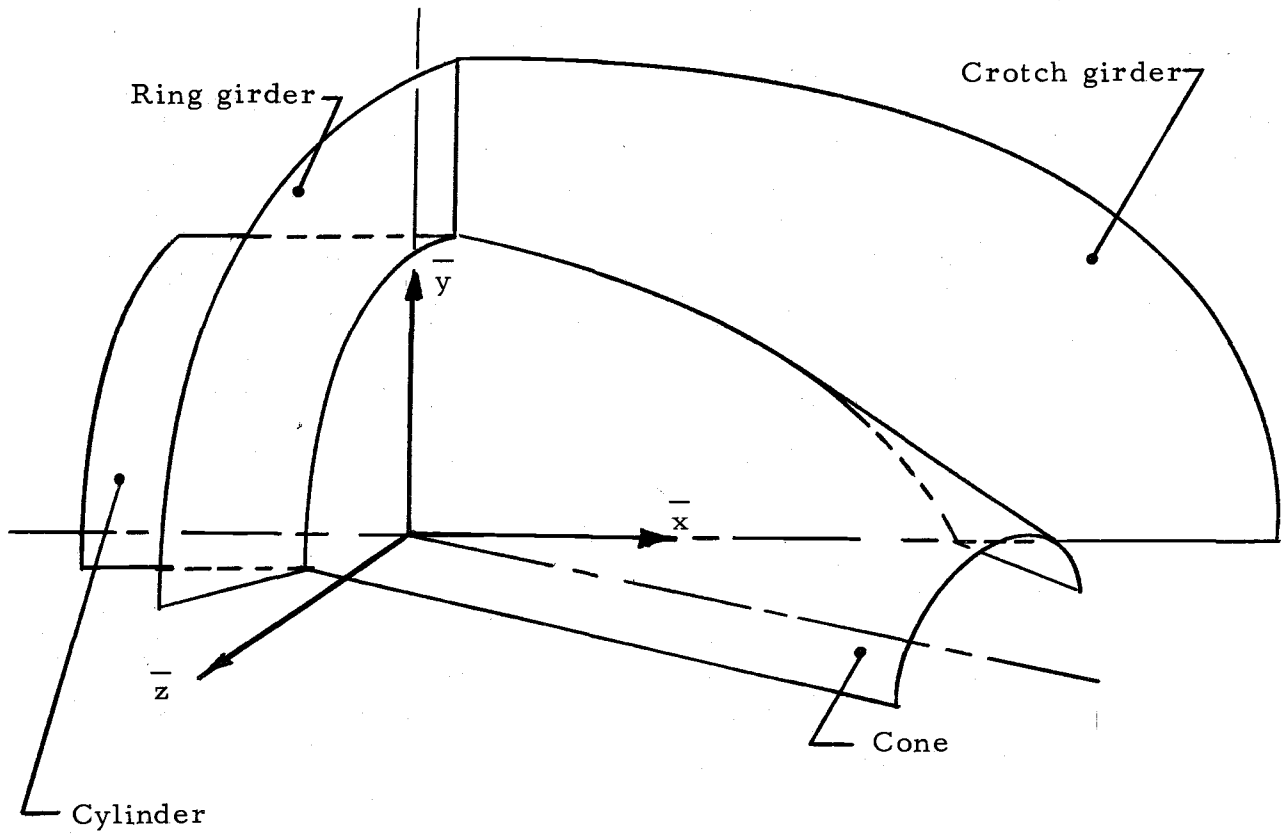

Note: $\bar{x}$-$\bar{y}$ plane and $\bar{x}$-$\bar{z}$ plane are planes of symmetry

Figure 1.3. Global coordinate system.

based on the pure displacement formulation such as found in (1, 2, 3) because this element invariably contains rotation as a degree of freedom. Since a plane stress element does not contain a rotational degree of freedom, it may be difficult to combine it with a plate bending element based on the displacement method. Therefore, while there are many adequate shell finite elements based on the pure displacement formulation, they are not easily adapted when there is need to combine them with plane stress elements as in this analysis.

Recently, the development of the finite element method has produced the mixed methods (10, 11, 19). Unlike the displacement formulations which yield elements containing only displacements and their derivatives as unknowns, the mixed methods result in elements which contain displacements, stresses and/or stress resultants as unknowns. The mixed methods are all derivable from Reissner's variational principle (21) or a modification of it. In fact, all finite element methods, whether they be displacement, mixed or equilibrium methods are derivable from a variational statement. This point of view is very well presented in (17).

The displacement method traces back to the minimum potential energy theorem, the mixed method to Reissner's principle, and the equilibrium method to the minimum complementary energy theorem. It should be added that Reissner's variational principle can be derived by applying appropriate conditions of constraint to either the potential

energy or complementary energy theorems (26). Thus, the variational theorems of minimum potential energy and minimum complementary energy are fundamental in the finite element method.

The basic formulation used in this presentation is due to L. R. Herrmann (12) and is a mixed method. The primary reason for this choice is that it has the ability to model the stresses occurring in intersecting shells and easily combines with plane stress elements without violating displacement compatibility. No rotational degrees of freedom exist in the formulation.

The structure is analyzed in the following manner:

(1) The crotch girder is represented as a series of plane stress elements and the ring girder, cylindrical shell and conical shell are represented as a series of flat-plate elements.

(2) The bending and membrane characteristics of a plate element is expressed by combining a plate-bending element with a plane stress element.

(3) The compatible response of adjacent elements is assured.

II. VARIATIONAL PRINCIPLE

The purpose of this chapter is to present a generalized variational principle and the sequence of specialization that leads to the particular variational principle used. In this manner the validity of the principle is presented and at the same time sufficient information is given to establish convergence of the method.

2.1 Discussion of Basic Theorems

The theorem of minimum potential energy states the stationary condition of the potential energy functional Π_P which is defined (23) as

$$\Pi_P = \iiint_V W(\epsilon_{ij})dV - \iiint_V F_i^a u_i dV - \iint_{S_T} T_k^a u_k dS. \tag{2.1}$$

The indices $i, j,$ and k take on values 1, 2, and 3. The strain energy density function $W(\epsilon_{ij})$ is assumed to be positive definite. The prescribed body forces F_i^a and the prescribed surface forces T_k^a on the portion of surface S_T where they act are assumed to be conservative forces. The strains ϵ_{ij} are related to the displacement components u_i in the volume, V, according to the expansion

$$\epsilon_{ij} = \frac{1}{2}(u_{i,j}+u_{j,i}) \quad \text{in} \quad V. \tag{2.2}$$

Finally, the displacement components u_k on the boundary are to satisfy the prescribed boundary displacement components u_k^a on the surface, S_u,

$$u_k = u_k^a \quad \text{on} \quad S_u. \tag{2.3}$$

The variation of the functional Π_P set equal to zero, leads to the Euler equations,

$$\sigma_{ij,j} + F_i^a = 0 \quad \text{(equilibrium)} \tag{2.4}$$

and

$$\sigma_{ij}\nu_j = T_i^a \qquad \text{(natural boundary conditions)} \tag{2.5}$$

where σ_{ij} are the stresses and ν_j [1/] are direction cosines of the outward surface normal. Equations (2.2) and (2.3) can be removed as subsidiary conditions and placed in the framework of the variational statement. This is done by introducing as Lagrange multipliers σ_{ij} and T_k and rewriting Equation (2.1) as

---

[1/] The term ν is also used to designate Poisson's ratio and should not be confused with it.

$$\Pi_G = \iiint_V W(\epsilon_{ij})dV - \iiint_V F_i^a u_i dV - \iiint_V [\epsilon_{ij} - \frac{1}{2}(u_{i,j}+u_{j,i})]\sigma_{ij}dV$$

$$- \iint_{S_T} T_k^a u_k dS - \iint_{S_u} (u_k - u_k^a)T_k dS. \qquad (2.6)$$

The generalized variational principle (26) states the stationary condition of Π_G. The independent quantities subject to variation now include the Lagrange multipliers. Setting the variation of Π_G equal to zero will now include Equations (2.2) and (2.3) along with Equations (2.4) and (2.5) as Euler equations. The fact that the Euler equations are the governing equations of an elastic body verifies the generalized principle and the principle of minimum potential energy. Alternatively, the proof can be found by deriving the principles from the principle of virtual work as in (23).

2.2 Hellinger-Reissner Principle

Using the appropriate stress-strain relationship, the strain energy $W(\epsilon_{ij})$ can be written in terms of stresses. The complementary energy is defined as

$$B(\sigma_{ij}) = \epsilon_{ij}\sigma_{ij} - W(\sigma_{ij}). \qquad (2.7)$$

Using Equation (2.2) the functional Π_G may be rewritten as

$$\Pi_R = \iiint_V [-B(\sigma_{ij}) + \sigma_{ij}\epsilon_{ij} - F_i^a u_i]dV$$

$$- \iint_{S_T} T_k^a u_k dS - \iint_{S_u} (u_k - u_k^a) T_k dS. \qquad (2.8)$$

The Hellinger-Reissner principle states the stationary property of the functional in Equation (2.8). While the principle of minimum potential energy has greater significance in the finite element analysis of plane stress or plane strain problems, this principle has its merit in the finite element analysis of plates and shells (17).

The classical plate bending formulation makes the assumption that lines perpendicular to the middle surface remain straight and perpendicular to the deformed middle surface. Figure 2.1 shows the coordinate system for a plate. This premise, referred to as the Kirckhoff hypothesis, leads to the following relationship between the transverse displacement w and the in-plane displacements u_i:

$$u_i = \begin{cases} -zw_{,i} & i = 1, 2 \\ w & i = 3 \end{cases} \qquad (2.9)$$

Substituting this equation into Equation (2.2) the strains are written as

$$\epsilon_{ij} = \begin{cases} -zw_{,ij} & i, j = 1, 2 \\ 0 & i \text{ or } j = 3 \end{cases} \qquad (2.10)$$

Note that the transverse shear strains are zero under the Kirckhoff hypothesis. The stress resultants which participate in the complementary energy function, now written in terms of the resultants as $B(M_{ij})$, are defined as

$$M_{ij} = \begin{cases} -\int_{-h/2}^{h/2} \sigma_{ij} z dz & i,j = 1,2 \\ 0 & i \text{ or } j = 3 \end{cases} \tag{2.11}$$

The minus sign is a matter of choice and in this manner it leads to a positive relationship between curvature $w_{,ij}$ and moment M_{ij}. The prescribed stress resultants on the boundary are defined as

$$M_n^a = -\int_{-h/2}^{h/2} T_1^a z dz \tag{2.12}$$

$$M_{nt}^a = -\int_{-h/2}^{h/2} T_2^a z dz \tag{2.13}$$

$$Q_n^a = -\int_{-h/2}^{h/2} T_3^a dz \tag{2.14}$$

Substituting Equations (2.9) through (2.14) into Equation (2.8) and integrating on dz, the Π_R functional may be written for plates as

$$\Pi_R = \iint_A [-B(M_{ij})+M_{ij}w_{,ij}-pw]dA - \int_{C_T} (M_n^a w_{,n}+M_{nt}^a w_{,t}-Q_n^a w)d\ell$$

$$- \int_{C_u} [M_n(w_{,n}-w_{,n}^a)+M_{nt}(w_{,t}-w_{,t}^a) - Q_n(w-w^a)]d\ell, \qquad (2.15)$$

$$i,j = 1,2$$

The sign convention for the displacements and stress resultants are shown in Figure 2.2.

2.3 Discussion of Convergence

The variational formulations offer more elegant and concise procedures for deriving finite element analysis techniques than do less rigorous formulations. One of the advantages is that they permit statements to be made regarding convergence to exact solutions with vanishing element size as in references (14) and (15). Convergence of the finite element method depends on two requirements; 1) the elements are connected in such a way that no discontinuities of deformation occur, and 2) the elements are in equilibrium subject to the external loads and the forces they exert on each other. Generally, one of these requirements is stated explicitly and the other follows implicitly according to the mechanics of the particular method being used. For example, in the direct-stiffness method, continuity of deformation is explicitly required by choosing appropriate deformation

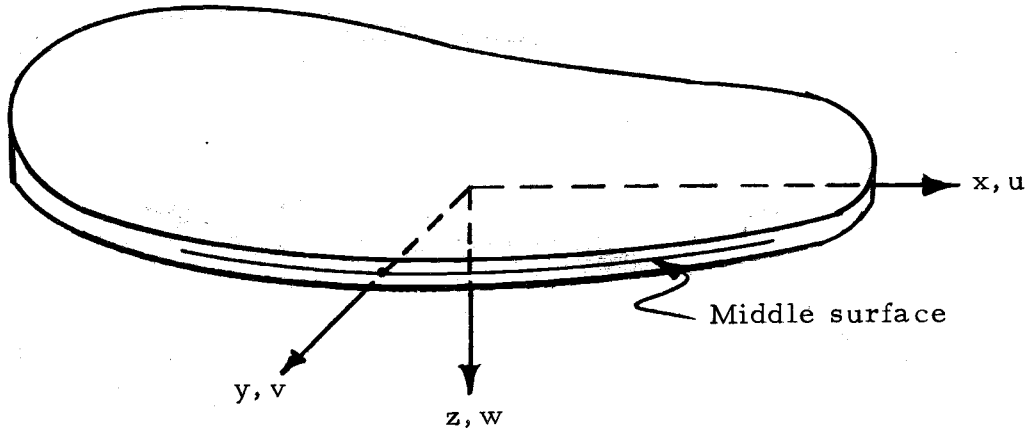

Figure 2.1. Coordinate system.

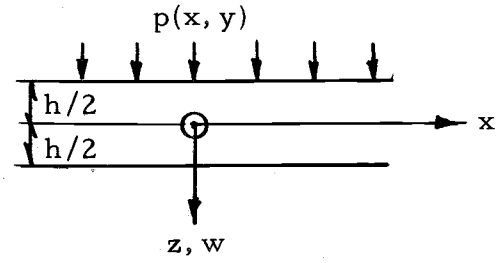

Load and deflection notation

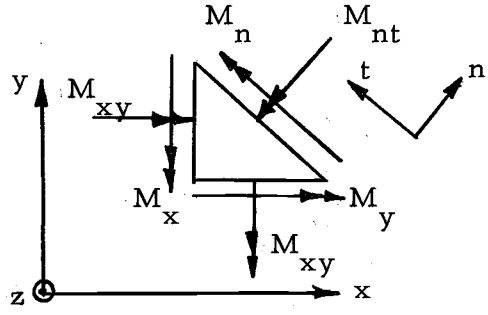

Moment notation

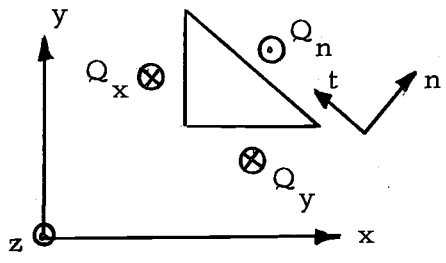

Shear notation

Figure 2.2. Sign convention for plate.

functions for each element while the equilibrium requirement is implicit in the finite element solution process.

The finite element process begins by dividing the plate into a finite number of elements as shown in Figure 2.3a. It is then assumed that if Π_R^e represents the contribution of a typical element to Π_R that

$$\Pi_R = \sum \Pi_R^e$$

This is generally true if no infinite values of the first integral in Equation (2.15) occur on the element interfaces. Thus, in the variational approach to finite element analysis, the compatibility condition is defined by the requirement that the variational functional be definable on the element interface (17). As a result, for different variational functionals, different compatibility conditions will occur.

Infinite values or delta functions will occur when a discontinuous function is differentiated. Therefore, since only the second term of the first integral in Equation (2.15) involves differentiation, it alone will be considered. For convenience, this term is rewritten, choosing the local n-t coordinate system at an interelement boundary, as

$$\iint_A (M_n w_{,nn} + 2M_{nt} w_{,nt} + M_t w_{,tt}) dA$$

The question now is under what conditions for the above integral will

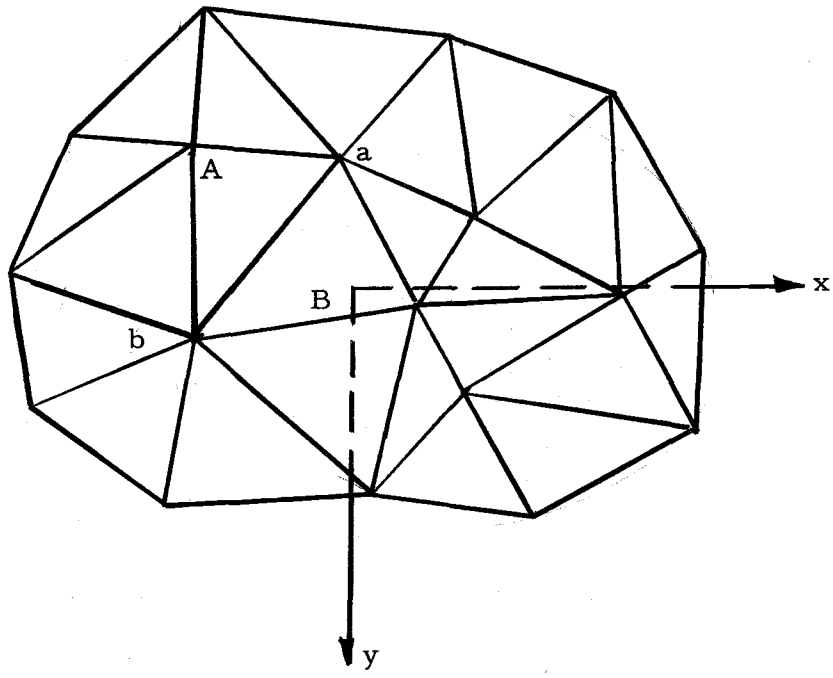

Figure 2.3a. Discretized plate.

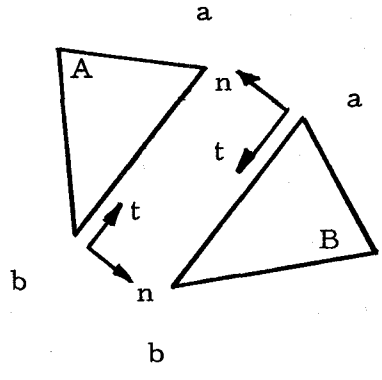

Figure 2.3b. Adjacent elements.

the functional Π_R be definable. There is more than one solution and each leads to an entirely different finite element formulation (17). Since a smooth function for w within any individual element is a natural occurrence in the finite element method, only a differentiation in the normal direction, n, may yield a delta function. But the functional Π_R will still be definable if the normal moment M_n is continuous. Therefore, one set of conditions that will satisfy the continuity requirement is to choose interpolating functions for w and M_n that are continuous across interelement boundaries. Thus, these variables become the primary variables in the formulation and their continuity satisfies explicitly the requirements of continuity of displacement and equilibrium of normal moment.

The equilibrium requirements of the other stress resultants contained in Π_R are satisfied implicitly and, of course, approximately in the finite element solution process. Because of the allowance of discontinuity in normal slope $w_{,n}$ we may add a subsidiary constraint equation to the formulation of the form

$$w_{,n}\Big|_A = -w_{,n}\Big|_B \tag{2.16}$$

These slopes are evaluated at a common interface a-b between two elements A and B as shown in Figure 2.3b. The minus sign is a consequence of the opposite orientations of the local normal directions

for two such elements. This constraint equation can be incorporated in the framework of the functional Π_R through the use of a Lagrange multiplier λ. Equation (2.16) can be rewritten as

$$\int_a^b \lambda w,_n dt\Big|_A + \int_a^b \lambda w,_n dt\Big|_B = 0 \tag{2.17}$$

The Lagrange multipliers are to be treated as additional variables. When all the interelement boundaries have been considered, the integral Π_R over the entire plate area is equal to the sum of the integrals Π_R^e over each elemental area. That is, Equation (2.15) becomes

$$\begin{aligned}\Pi_R = \sum_m \iint_{A_m} [-B(M_{ij})+M_{ij}w,_{ij}-pw]dA + \int_{C_m} M_n w,_n d\ell \\ - \int_{C_{T_m}} (M_n^a w,_n + M_{nt}^a w,_t - Q_n^a w)d\ell \\ - \int_{C_{u_m}} [M_n(w,_n - w,_n^a)+M_{nt}(w,_t - w,_t^a)-Q_n(w-w^a)]\ d\ell .\end{aligned} \tag{2.18}$$

By taking the variation of Π_R with respect to w and λ it can be shown that the Lagrange multiplier λ is equal to M_n. Thus M_n has replaced λ in the second integral of Equation (2.18).

This line integral is to be evaluated around each element m. Now that the constraint Equation (2.16) is incorporated, normal slope compatibility will be satisfied implicitly, analogous to the element equilibrium requirement for the direct-stiffness method. This analogy and other similarities has lead R.E. Jones in reference (15) to term the variational approach as a generalized direct-stiffness method. Indeed, the final system of simultaneous algebraic equations are assembled and solved using the same algorithms that are used for the direct-stiffness method.

2.4 L.R. Herrmann's Formulation for Plates

The modified Reissner functional Π_R in Equation (2.18) is similar to a version of the energy functional proposed by L.R. Herrmann (11). To obtain this version, Equation (2.18) is integrated by parts using Green's Theorem,[2/]

$$\iint_{A_m} (Q_{,n} - P_{,t})dA = \int_{C_m} Pdn + Qdt.$$

The second term of the first integral in Equation (2.18) expanded in the local n-t coordinate system becomes

---

[2/] The functions Q and P are used here temporarily and are not to be confused with shear Q_n or subsequent terms.

$$\iint_{A_m} M_{ij} w_{,ij} dA = \iint_{A_m} (M_n w_{,nn} + 2M_{nt} w_{,nt} + M_t w_{,tt}) dA.$$

If in Green's Theorem the functions Q and P, defined as

$$Q = M_n w_{,n} + M_{nt} w_{,t}$$

$$P = -(M_t w_{,t} + M_{nt} w_{,n})$$

are substituted and the indicated differentiations are carried out, a substitute expression can be found for this second term. This substitute expression is

$$\iint_{A_m} M_{ij} w_{,ij} dA = -\iint_{A_m} M_{ij,j} w_{,i} dA + \int_{C_m} -(M_t w_{,t} + M_{nt} w_{,n}) dn + (M_n w_{,n} + M_{nt} w_{,t}) dt. \tag{2.19}$$

But since dn is everywhere perpendicular to the boundary C_m, the first portion of the line integral vanishes. Further, by specifying the displacement function w to be linear within each element and the moments M_{ij} as constants within each element, the terms $w_{,ij}$, $M_{ij,j}$ and Q_n will vanish. Therefore, rewriting Equation (2.19) under these conditions, the following relationship is obtained:

$$\int_{C_m} M_n w_{,n} dt = -\int_{C_m} M_{nt} w_{,t} dt \tag{2.20}$$

This relationship may now be used in Equation (2.18) to form the following functional where dt has replaced $d\ell$.

$$\Pi_R = \sum_m \left\{ \iint_{A_m} [-B(M_{ij}) - pw] dA - \int_{C_m} M_{nt} w_{,t} dt \right.$$

$$+ \int_{C_{T_m}} [(M_n^a - M_n) w_{,n} + (M_{nt}^a - M_{nt}) w_{,t} - Q_n^a w] dt$$

$$\left. - \int_{C_{u_m}} (M_n w_{,n}^a + M_{nt} w_{,t}^a) dt \right\} . \tag{2.21}$$

In going from Equation (2.18) to Equation (2.21), the transverse displacement boundary requirement is removed from the variational statement, but it will, of course, be an added requirement in the formulation. L.R. Herrmann makes use of Equation (2.21) with the added stipulation that the prescribed normal moment boundary requirement be satisfied; that is, this requirement is removed from the variational statement as was the transverse displacement boundary condition. Subsequently, in the formation of the linear algebraic equations that result from $\delta\Pi = 0$, these boundary conditions will be

included by merely specifying the prescribed value in place of a corresponding algebraic equation and corresponding unknown. This is possible because the unknowns are the transverse displacements at each corner of an element and the normal moment at each side of an element.

The boundary condition that is not explicitly satisfied is the twisting moment at each element side. Since there does not exist an unknown variable for twisting moment, a prescribed value can not be input into the solution process.

If the above considerations are accepted, then the functional which is attributed to L. R. Herrmann (11) becomes

$$\Pi_H = \sum_m \left\{ \iint_{A_m} [-B(M_{ij})-pw]dA - \int_{C_m} M_{nt} w_{,t} dt \right.$$

$$\left. - \int_{C_{T_m}} Q_n^a w dt - \int_{C_{u_m}} M_n w_{,n}^a dt \right\} . \qquad (2.22)$$

An alternate method is to choose a linear moment field. While this approach would be expected to furnish better results particularly as far as moments are concerned, it would require the solution of a substantially larger system of equations (18).

III. FINITE ELEMENT FORMULATION

As stated at the end of Chapter I, the basic finite element used in this study is a flat element combining plate bending components with plane stress components. This combination is an uncoupled superposition of both of these components and therefore disregards the natural coupling occurring due to curvature of the structure surface. Thus, the crotch girder and ring girder are approximated more accurately than the cone and cylinder portions of the penstock bifurcation.

To formulate such an element, the functional Π_P in Equation (2.1) and Π_H in Equation (2.23) are added to form a combined functional Π_S. Thus,

$$\Pi_S = \Pi_P + \Pi_H \tag{3.1}$$

where the variational statement, $\delta\Pi_S = 0$, will be used to select the approximate solution from a family of trial solutions. This method is connected closely with the Ritz technique (4). However, the basic idea of the Ritz technique is altered in the finite element method since the process is facilitated by representing the structure as a series of elements and applying the Ritz technique individually to each element instead of to the entire structure.

The variational statement may be written

$$\delta\Pi_S^e = \delta\Pi_P^e + \delta\Pi_H^e \tag{3.2}$$

where the superscript indicates the contribution to each functional from a single element. The variation $\delta\Pi_P^e$ set equal to zero forms the plane stress matrix equations for the element and the variation $\delta\Pi_H^e$ set equal to zero forms the plate bending matrix equations for the element.

3.1 Plane Stress Matrix Equations

Equation (2.1) may be written in matrix form for an individual flat element as

$$\Pi_P^e = \iiint_{V^e} \frac{1}{2} \begin{bmatrix} \epsilon_x & \epsilon_y & \gamma_{xy} \end{bmatrix} \begin{Bmatrix} \sigma_x \\ \sigma_y \\ \sigma_{xy} \end{Bmatrix} dV - \iiint_{V^e} \begin{bmatrix} F_x^a & F_y^a \end{bmatrix} \begin{Bmatrix} u \\ v \end{Bmatrix} dV$$

$$- \iint_{S^e} \begin{bmatrix} T_x^a & T_y^a \end{bmatrix} \begin{Bmatrix} u \\ v \end{Bmatrix} dS. \tag{3.3}$$

The term γ introduced here is the shear strain which is equal to twice the tensor quantity ϵ_{ij}. Admissible forms for the inplane element displacements u and v are now chosen so that displacement continuity is maintained across element boundaries. Therefore, assume as trial functions

$$u = a_1 + a_2 x + a_3 y$$

and (3.4)

$$v = a_4 + a_5 x + a_6 y$$

Let u_i and v_i refer to the x and y displacements, respectively, of any corner node i of the element as shown in Figure 3.1. Using the displacement boundary conditions for u at each corner, the following matrix expression is obtained:

$$\begin{Bmatrix} u_1 \\ u_2 \\ u_3 \end{Bmatrix} = \begin{bmatrix} 1 & x_1 & y_1 \\ 1 & x_2 & y_2 \\ 1 & x_3 & y_3 \end{bmatrix} \begin{Bmatrix} a_1 \\ a_2 \\ a_3 \end{Bmatrix} . \quad (3.5)$$

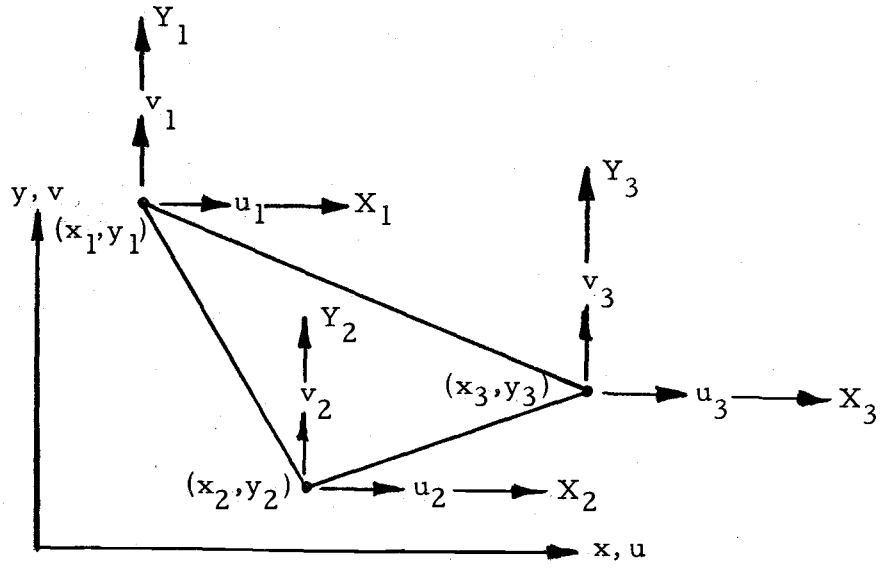

Figure 3.1. Plane stress element.

The constants α_i are obtained by inversion as

$$\begin{Bmatrix} \alpha_1 \\ \alpha_2 \\ \alpha_3 \end{Bmatrix} = \frac{1}{2A} \begin{bmatrix} x_2y_3 - x_3y_2 & x_3y_1 - x_1y_3 & x_1y_2 - x_2y_1 \\ y_2 - y_3 & y_3 - y_1 & y_1 - y_2 \\ x_3 - x_2 & x_1 - x_3 & x_2 - x_1 \end{bmatrix} \begin{Bmatrix} u_1 \\ u_2 \\ u_3 \end{Bmatrix} \tag{3.6}$$

where A is the area of the triangular element. Since the constants α_i are seen to depend on the coordinates and displacements at each corner, the displacements in Equation (3.4) will be continuous across any interelement boundary. Rewriting Equation (3.6) as

$$\begin{Bmatrix} \alpha_1 \\ \alpha_2 \\ \alpha_3 \end{Bmatrix} = \frac{1}{2A} \begin{bmatrix} a_1 & a_2 & a_3 \\ b_1 & b_2 & b_3 \\ c_1 & c_2 & c_3 \end{bmatrix} \begin{Bmatrix} u_1 \\ u_2 \\ u_3 \end{Bmatrix} \equiv [\overline{T}] \begin{Bmatrix} u_1 \\ u_2 \\ u_3 \end{Bmatrix} \tag{3.7}$$

and substituting into the first of Equations (3.4), the displacement u becomes

$$u = \frac{1}{2A} (N_1u_1 + N_2u_2 + N_3u_3) \tag{3.8}$$

where

$$N_1 = a_1 + b_1x + c_1y$$

$$N_2 = a_2 + b_2x + c_2y$$

$$N_3 = a_3 + b_3x + c_3y.$$

Similarly, the displacement v may be written

$$v = \frac{1}{2A} (N_1 v_1 + N_2 v_2 + N_3 v_3). \tag{3.9}$$

Using the strain-displacement relationship of Equation (2.2), the strains can be found from the displacements described in Equations (3.8) and (3.9) as

$$\begin{Bmatrix} \epsilon_x \\ \epsilon_y \\ \gamma_{xy} \end{Bmatrix} = \frac{1}{2A} \begin{bmatrix} b_1 & b_2 & b_3 & 0 & 0 & 0 \\ 0 & 0 & 0 & c_1 & c_2 & c_3 \\ c_1 & c_2 & c_3 & b_1 & b_2 & b_3 \end{bmatrix} \begin{Bmatrix} u_i \\ v_i \end{Bmatrix} \tag{3.10}$$

where the displacement vector on the right side stands for the vector of six inplane displacements for an element. Equation (3.10) can be written in a simplified form as

$$\begin{Bmatrix} \epsilon_x \\ \epsilon_y \\ \gamma_{xy} \end{Bmatrix} = [\overline{A}] \begin{Bmatrix} u_i \\ v_i \end{Bmatrix} \tag{3.11}$$

The stress-strain relationship for an isotropic material with Young's modulus E and Poisson's ratio ν is

$$\begin{Bmatrix} \sigma_x \\ \sigma_y \\ \sigma_{xy} \end{Bmatrix} = \frac{E}{1-\nu^2} \begin{bmatrix} 1 & \nu & 0 \\ \nu & 1 & 0 \\ 0 & 0 & \frac{1-\nu}{2} \end{bmatrix} \begin{Bmatrix} \epsilon_x \\ \epsilon_y \\ \gamma_{xy} \end{Bmatrix} \equiv [\overline{D}] \begin{Bmatrix} \epsilon_x \\ \epsilon_y \\ \gamma_{xy} \end{Bmatrix} \tag{3.12}$$

Substituting Equation (3.11) into Equation (3.12), the stresses become

$$\begin{Bmatrix} \sigma_x \\ \sigma_y \\ \sigma_{xy} \end{Bmatrix} = [\bar{D}][\bar{A}] \begin{Bmatrix} u_i \\ v_i \end{Bmatrix} . \tag{3.13}$$

If Equations (3.8), (3.9), (3.11) and (3.13) are substituted into Equation (3.3), the contribution to the total potential energy of one element becomes

$$\begin{aligned} \Pi_P^e = & \iiint_{V^e} \frac{1}{2} \begin{bmatrix} u_i & v_i \end{bmatrix} [\bar{A}]^T [\bar{D}][\bar{A}] \begin{Bmatrix} u_i \\ v_i \end{Bmatrix} dV \\ & - \iiint_{V^e} \frac{1}{2A} \begin{bmatrix} F_x^a & F_y^a \end{bmatrix} \begin{bmatrix} N_1 & N_2 & N_3 & 0 & 0 & 0 \\ 0 & 0 & 0 & N_1 & N_2 & N_3 \end{bmatrix} \begin{Bmatrix} u_i \\ v_i \end{Bmatrix} dV \\ & - \sum_{k=1}^{3} \iint_{S_{T_k}^e} \frac{1}{2A} \begin{bmatrix} T_{xk}^a & T_{yk}^a \end{bmatrix} \begin{bmatrix} N_1 & N_2 & N_3 & 0 & 0 & 0 \\ 0 & 0 & 0 & N_1 & N_2 & N_3 \end{bmatrix} \begin{Bmatrix} u_i \\ v_i \end{Bmatrix} dS . \end{aligned} \tag{3.14}$$

The sum on the last term arises because the prescribed surface forces could conceivably differ on each of the three element edges.

Next, the variational statement

$$\delta \Pi_P^e = 0$$

is applied with respect to each displacement to form the matrix equations. For each displacement, it yields a corresponding linear

algebraic equation and since there are six displacements, six simultaneous equations develop. In matrix form, these equations become

$$\left[\begin{array}{c|c} K_a & K_b \\ \hline K_b^T & K_c \end{array}\right]^e \left\{\begin{array}{c} u_i \\ \hline v_i \end{array}\right\} - \left\{\begin{array}{c} X_i \\ \hline Y_i \end{array}\right\} = \left\{\begin{array}{c} 0 \\ \hline 0 \end{array}\right\} \tag{3.15}$$

where

$$\left[\begin{array}{c|c} K_a & K_b \\ \hline K_b^T & K_c \end{array}\right]^e \equiv [K]^e = hA[\bar{A}]^T[\bar{D}][\bar{A}]$$

is the element stiffness matrix and

$$X_i = \frac{1}{3} hAF^a_{xi} + \frac{1}{2} h\ell T^a_{xi}$$

$$Y_i = \frac{1}{3} hAF^a_{yi} + \frac{1}{2} h\ell T^a_{yi}$$

are the load components shown in Figure 3.1. It has been assumed in taking the variations and in the subsequent integrations that the material properties, material thickness, body force components, and surface force components are constants for the element.

The body force components are included only for generality and will not be used in the analysis of the penstock bifurcation because the weight is assumed negligible in comparison with the applied load. The inclusion of the surface force components, however, is necessary for the hydrostatic test case where the tensioning effect of the

bulkheads is produced by applying inplane loads on the bulkhead boundaries. Otherwise, for the large majority of elements, the load components X_i and Y_i will be zero. It is interesting to note that the variational process yields the 1/3 and 1/2 factors for the load components that would be expected for equivalent static loading.

3.2 Plate Bending Matrix Equations

The trial functions used in conjunction with the Ritz process for plate bending elements are, as stated in Section 2.4, a transverse displacement function w that is linear in x and y and constants for the moments M_x, M_y, and M_{xy} within each element. The linear variations of w is expressed as a function of the node values w_i as in the treatment of the inplane displacements in Section 3.1. The element values of M_x, M_y, and M_{xy} are expressed in terms of the values of the normal moment M_{n_i} at the element sides (see Figure 3.2 for a typical plate element).

The family of trial functions described in this manner satisfies the admissibility requirements established in Section 2.3 and insures the existence of the functional Π_H in Equation (2.22).

Equation (2.22) may be written for an individual plate element as

$$\Pi_H^e = \iint_{A^e} \left\{ -pw - \frac{12}{Eh^3} \left[\frac{1}{2} M_x^2 + \frac{1}{2} M_y^2 + (1+\nu) M_{xy}^2 - \nu M_x M_y \right] \right\} dA$$

$$- \int_{C^e} M_{nt} w_{,t} dt - \int_{C_T^e} Q_n^a w dt - \int_{C_u^e} M_n w_{,n}^a dt \qquad (3.16)$$

Next, all the variables must be written in terms of the unknowns w_i and M_{n_i}.

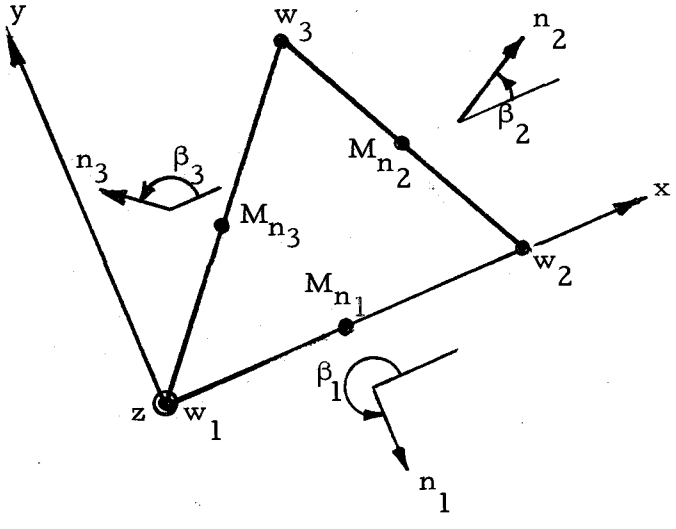

Figure 3.2. Plate bending element.

The transverse displacement may be written in matrix form as

$$w = \begin{bmatrix} 1 & x & y \end{bmatrix} \begin{Bmatrix} d_1 \\ d_2 \\ d_3 \end{Bmatrix} \quad . \tag{3.17}$$

The constants d_i are then expressed in terms of the corner point displacements w_i as

$$\begin{Bmatrix} d_1 \\ d_2 \\ d_3 \end{Bmatrix} = [\overline{T}] \begin{Bmatrix} w_1 \\ w_2 \\ w_3 \end{Bmatrix} \tag{3.18}$$

where $[\overline{T}]$ is defined in Equation (3.7). Substituting Equation (3.18) into Equation (3.17), the transverse displacement becomes

$$w = \begin{bmatrix} 1 & x & y \end{bmatrix} [\overline{T}] \begin{Bmatrix} w_1 \\ w_2 \\ w_3 \end{Bmatrix} \quad . \tag{3.19}$$

The Cartesian components of the moments within the element are expressed as

$$\begin{Bmatrix} M_x \\ M_y \\ M_{xy} \end{Bmatrix} = \begin{Bmatrix} g_1 \\ g_2 \\ g_3 \end{Bmatrix}$$

Since the constants g_i are to be expressed in terms of the normal moments at the element's three sides, the following relationship is

required;

$$\begin{Bmatrix} M_{n_1} \\ M_{n_2} \\ M_{n_3} \end{Bmatrix} = \begin{bmatrix} \cos^2\beta_1 & \sin^2\beta_1 & 2\sin\beta_1\cos\beta_1 \\ \cos^2\beta_2 & \sin^2\beta_2 & 2\sin\beta_2\cos\beta_2 \\ \cos^2\beta_3 & \sin^2\beta_3 & 2\sin\beta_3\cos\beta_3 \end{bmatrix} \begin{Bmatrix} M_x \\ M_y \\ M_{xy} \end{Bmatrix} \equiv [\beta] \begin{Bmatrix} M_x \\ M_y \\ M_{xy} \end{Bmatrix} \tag{3.20}$$

Inverting this expression, the constant moments become

$$\begin{Bmatrix} M_x \\ M_y \\ M_{xy} \end{Bmatrix} = [\overline{B}] \begin{Bmatrix} M_{n_1} \\ M_{n_2} \\ M_{n_3} \end{Bmatrix} \tag{3.21}$$

where

$$[\overline{B}] = [\beta]^{-1}$$

The tangential slope $w,_t$ and the twisting moment M_{nt} must also be expressed in terms of the unknowns. The tangential slope can be written in terms of the Cartesian components of slope as

$$\begin{Bmatrix} w,_{t_1} \\ w,_{t_2} \\ w,_{t_3} \end{Bmatrix} = \begin{bmatrix} -\sin\beta_1 & \cos\beta_1 \\ -\sin\beta_2 & \cos\beta_2 \\ -\sin\beta_3 & \cos\beta_3 \end{bmatrix} \begin{Bmatrix} w,_x \\ w,_y \end{Bmatrix} . \tag{3.22}$$

Using Equations (3.17) and (3.18), the slopes $w,_x$ and $w,_y$ can be written

$$\begin{Bmatrix} w,_x \\ w,_y \end{Bmatrix} = \begin{Bmatrix} d_2 \\ d_3 \end{Bmatrix} = \begin{bmatrix} \overline{T}_{21} & \overline{T}_{22} & \overline{T}_{23} \\ \overline{T}_{31} & \overline{T}_{32} & \overline{T}_{33} \end{bmatrix} \begin{Bmatrix} w_1 \\ w_2 \\ w_3 \end{Bmatrix} \tag{3.23}$$

Substituting Equation (3.23) into Equation (3.22), the tangential slopes are appropriately expressed in terms of unknown displacements as

$$\begin{Bmatrix} w,_{t_1} \\ w,_{t_2} \\ w,_{t_3} \end{Bmatrix} = [\overline{P}] \begin{Bmatrix} w_1 \\ w_2 \\ w_3 \end{Bmatrix} \tag{3.24}$$

where

$$\overline{P}_{ij} = - \overline{T}_{2j} \sin \beta_i + \overline{T}_{3j} \cos \beta_i .$$

For the twisting moments, the following relationships are needed:

$$\begin{Bmatrix} M_{nt_1} \\ M_{nt_2} \\ M_{nt_3} \end{Bmatrix} = \begin{bmatrix} -\sin \beta_1 \cos \beta_1 & \sin \beta_1 \cos \beta_1 & \cos 2\beta_1 \\ -\sin \beta_2 \cos \beta_2 & \sin \beta_2 \cos \beta_2 & \cos 2\beta_2 \\ -\sin \beta_3 \cos \beta_3 & \sin \beta_3 \cos \beta_3 & \cos 2\beta_3 \end{bmatrix} \begin{Bmatrix} M_x \\ M_y \\ M_{xy} \end{Bmatrix} = [\overline{\beta}] \begin{Bmatrix} M_x \\ M_y \\ M_{xy} \end{Bmatrix} \tag{3.25}$$

Substituting Equation (3.21) into Equation (3.25), the twisting moments are expressed in terms of the unknowns as

$$\begin{Bmatrix} M_{nt_1} \\ M_{nt_2} \\ M_{nt_3} \end{Bmatrix} = [\bar{\beta}][\bar{B}] \begin{Bmatrix} M_{n_1} \\ M_{n_2} \\ M_{n_3} \end{Bmatrix} \equiv [\bar{F}] \begin{Bmatrix} M_{n_1} \\ M_{n_2} \\ M_{n_3} \end{Bmatrix} . \tag{3.26}$$

Substituting Equations (3.19), (3.20), (3.24), and (3.25) into Equation (3.16), the contribution of one element to the energy functional Π_H becomes

$$\Pi_H^e = \iint_{A^e} \Bigg\langle -p \lfloor 1 \; x \; y \rfloor [\bar{T}] \begin{Bmatrix} w_1 \\ w_2 \\ w_3 \end{Bmatrix} - \frac{12}{Eh^3} \Bigg[\frac{1}{2} \Bigg(\lfloor \bar{B}_{11} \; \bar{B}_{12} \; \bar{B}_{13} \rfloor \begin{Bmatrix} M_{n_1} \\ M_{n_2} \\ M_{n_3} \end{Bmatrix} \Bigg)^2$$

$$+ \frac{1}{2} \Bigg(\lfloor \bar{B}_{21} \; \bar{B}_{22} \; \bar{B}_{23} \rfloor \begin{Bmatrix} M_{n_1} \\ M_{n_2} \\ M_{n_3} \end{Bmatrix} \Bigg)^2 + (1+\nu) \Bigg(\lfloor \bar{B}_{31} \; \bar{B}_{32} \; \bar{B}_{33} \rfloor \begin{Bmatrix} M_{n_1} \\ M_{n_2} \\ M_{n_3} \end{Bmatrix} \Bigg)^2$$

$$- \nu \lfloor \bar{B}_{11} \; \bar{B}_{12} \; \bar{B}_{13} \rfloor \begin{Bmatrix} M_{n_1} \\ M_{n_2} \\ M_{n_3} \end{Bmatrix} \lfloor \bar{B}_{21} \; \bar{B}_{22} \; \bar{B}_{23} \rfloor \begin{Bmatrix} M_{n_1} \\ M_{n_2} \\ M_{n_3} \end{Bmatrix} \Bigg] \Bigg\rangle \, dA$$

$$- \sum_{k=1}^{3} \int_{C_k^c} \lfloor \bar{F}_{k1} \; \bar{F}_{k2} \; \bar{F}_{k3} \rfloor \begin{Bmatrix} M_{n_1} \\ M_{n_2} \\ M_{n_3} \end{Bmatrix} \lfloor \bar{P}_{k1} \; \bar{P}_{k2} \; \bar{P}_{k3} \rfloor \begin{Bmatrix} w_1 \\ w_2 \\ w_3 \end{Bmatrix} dt. \tag{3.27}$$

For clarity the last two integrals of Equation (3.16) have been

omitted from Equation (3.27). They represent the prescribed boundary conditions for shear and normal slope, respectively, and are not needed in the formulation because no such boundary conditions are specified on the structure to be analyzed. However, they will again be included in the final algebraic equations below for the sake of generality.

The functional Π_H^e in Equation (3.27) is now completely expressed in terms of the six unknown nodal values w_i and M_{n_i}, analogous to Equation (3.14). The variational statement $\delta\Pi_H^e = 0$ can now be applied with respect to each unknown for the element and six simultaneous linear algebraic equations will result. The indicated integrations are in some cases detailed and are excluded. It again will be mentioned that the material properties, plate thickness, and applied load are assumed constant for each element but can be varied from element to element. The six equations in matrix form are

$$\begin{bmatrix} G & H \\ H^T & 0 \end{bmatrix} \begin{Bmatrix} M_{n_i} \\ w_i \end{Bmatrix} + \begin{Bmatrix} L_i \\ L_i' \end{Bmatrix} = \begin{Bmatrix} 0 \\ 0 \end{Bmatrix} \tag{3.28}$$

where

$$G_{ij} = \frac{12A}{Eh^3}\left[\bar{B}_{1i}\,\bar{B}_{1j} + \bar{B}_{2i}\,\bar{B}_{2j} + 2(1+\nu)\bar{B}_{3i}\,\bar{B}_{3j} - \nu(\bar{B}_{1i}\,\bar{B}_{2j} + \bar{B}_{2i}\,\bar{B}_{1j})\right]$$

$$H_{ij} = \sum_{k=1}^{3} \ell_k \bar{F}_{ki} \bar{P}_{kj} \qquad (\ell \text{ is triangle side length})$$

$$L_i = w^a_{n_i} \ell_i$$

$$L'_i = \frac{pA}{3} + \frac{Q^a_{n_i} \ell_i}{2}$$

$$i, j = 1, 2, 3$$

The terms $\frac{1}{2} Q^a_{n_i} \ell_i$ and L_i are the contributions of the natural boundary conditions represented by the last two line integrals in Equation (3.16). In the analysis of the penstock bifurcation, these terms will be set equal to zero for every element.

3.3 Shell Element Matrix Equations

Equations (3.15) and (3.28) may now be combined to form an element that can be used to model shell behavior as well as plate bending and plane stress behavior. The variational statement $\delta \Pi^e_S = 0$ yields the matrix equations for a shell element (see Figure 3.3) as,

$$\begin{bmatrix} K_a & K_b & 0 & 0 \\ K_b^T & K_c & 0 & 0 \\ 0 & 0 & 0 & H^T \\ 0 & 0 & H & G \end{bmatrix} \begin{Bmatrix} u_i \\ v_i \\ w_i \\ M_{n_i} \end{Bmatrix} - \begin{Bmatrix} X_i \\ Y_i \\ -L'_i \\ -L_i \end{Bmatrix} = \begin{Bmatrix} 0 \\ 0 \\ 0 \\ 0 \end{Bmatrix} . \qquad (3.29)$$

This set of twelve equations is the contribution of one triangular element to the total set of simultaneous equations for the structure.

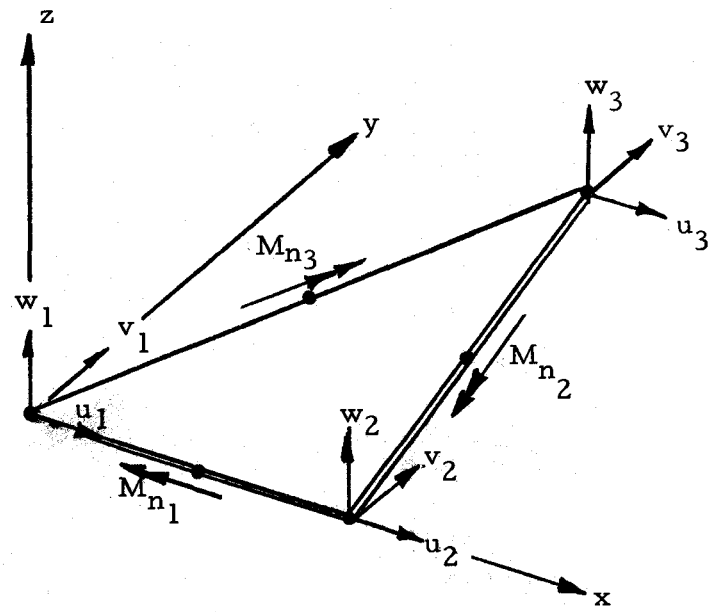

Figure 3.3. Shell element.

The K_{ij} coefficients can be termed stiffness coefficients, the G_{ij} coefficients can be termed flexibility coefficients and the H_{ij} coefficients can be termed coupling coefficients. Because of this mixture in the coefficient matrix, the method is often termed a mixed method.

For an element located on the crotch girder, a plane stress member, the coefficients G_{ij} and H_{ij} are set equal to zero so that plane stress conditions are modeled. The ring girder, cylindrical shell and conical shell will involve all coefficients. If the ring girder does not show significant out-of-plane bending after one analysis, then subsequent analyses can exclude the G_{ij} and H_{ij}

coefficients from ring girder elements as in the crotch girder elements and derive the benefits of a reduced number of equations without loss of accuracy. In this way the ring girder would be treated as a plane stress member.

The triangular element obtained in the foregoing fashion has 12 degrees of freedom. Four of these triangular elements can be combined to form a quadrilateral element with 16 degrees of freedom. First, however, the triangular element coefficient matrices must be referenced to a global coordinate system $\bar{x}$, $\bar{y}$, $\bar{z}$ as shown in Figure 3.4. Note that the local system, x, y, z is selected so that the element lies in the x-y plane and the x axis is collinear with the external side of the triangle. To facilitate the rotation of the coefficient matrix, it must be rearranged to correspond to the unknown vector which is regrouped so that u_i, v_i and w_i for a single node are together. Thus, Equation (3.29) can be rewritten as

$$[E]\{\phi\} = \{P\} \tag{3.30}$$

where $[E]$ is the rearranged element matrix in the local system corresponding to the unknown vector $\{\phi\}$ and load vector $\{P\}$ which are defined as

$$\{\phi\} \equiv \begin{Bmatrix} u_1 \\ v_1 \\ w_1 \\ M_{n_1} \\ \hline u_2 \\ v_2 \\ w_2 \\ M_{n_2} \\ \hline u_3 \\ v_3 \\ w_3 \\ M_{n_3} \end{Bmatrix} \quad \text{and} \quad \{P\} \equiv \begin{Bmatrix} X_1 \\ Y_1 \\ L_1 \\ L'_1 \\ \hline X_2 \\ Y_2 \\ L_2 \\ L'_2 \\ \hline X_3 \\ Y_3 \\ L_3 \\ L'_3 \end{Bmatrix} .$$

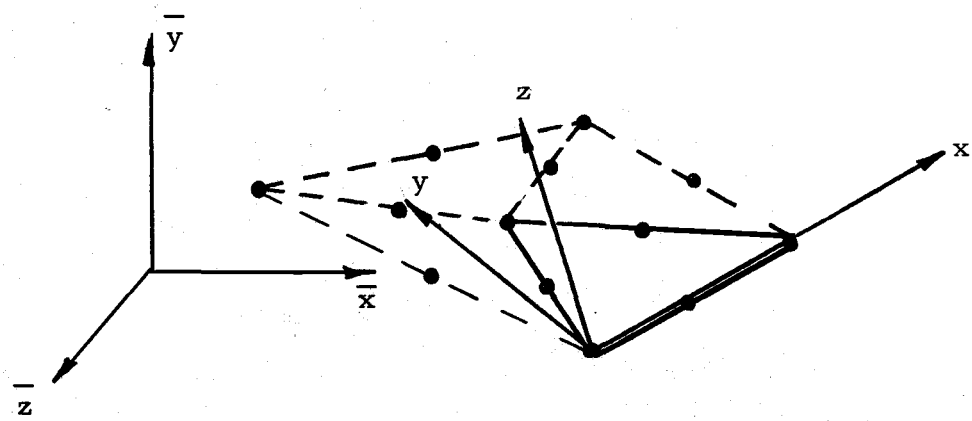

Figure 3.4. Local and global coordinate system.

Permutating the rows and columns of the element matrix is accomplished by premultiplying and postmultiplying the original 12 x 12 element matrix of Equation (3.29) by the appropriate 12 x 12 elementary matrices. An elementary matrix is simply an identity matrix whose rows or columns have been permutated in the same desired fashion (7).

The orthogonal rotation matrix $[R]$ relating the local unknowns to the system unknowns for an element is given by the equation

$$\begin{Bmatrix} u_j \\ v_j \\ w_j \end{Bmatrix} = [R] \begin{Bmatrix} \bar{u}_j \\ \bar{v}_j \\ \bar{w}_j \end{Bmatrix}$$

where the bar quantities represent the system unknowns. The nine coefficients R_{ij} are the direction cosines for the two coordinate systems and are given in Appendix A. The triangular element rotation matrix $[\bar{R}]$ is written as

$$[\bar{R}] = \begin{bmatrix} [R] & & & & \\ & 1 & & & \\ & & [R] & & \\ & & & 1 & \\ & & & & [R] \\ & & & & & 1 \end{bmatrix}$$

so that

$$\{\phi\} = [\bar{R}]\{\bar{\phi}\} \tag{3.31}$$

and

$$\{P\} = [\bar{R}]\{\bar{P}\} . \tag{3.32}$$

Substituting Equations (3.31) and (3.32) into Equation (3.30), the following expression is obtained:

$$[E][\bar{R}]\{\bar{\phi}\} = [\bar{R}]\{\bar{P}\} . \tag{3.33}$$

Premultiplying Equation (3.33) by $[\bar{R}]^{-1}$, the transformed system for a triangular shell element becomes

$$[\bar{E}]\{\bar{\phi}\} = [\bar{P}] \tag{3.34}$$

where, since the inverse of an orthogonal matrix $[\bar{R}]$ equals its transpose,

$$[\bar{E}] = [\bar{R}]^T[E][\bar{R}]$$

Equation (3.34) thus represents the contribution of one triangular shell element, as referenced in the global system, to the total system of equations.

3.4 Quadrilateral Shell Element

In order to reduce the required input without a corresponding loss of accuracy, it is advisable to combine four triangular shell elements into one quadrilateral element as shown in Figure 3.5. The coordinates of the center node are computed as the average of the four

corner point coordinates.

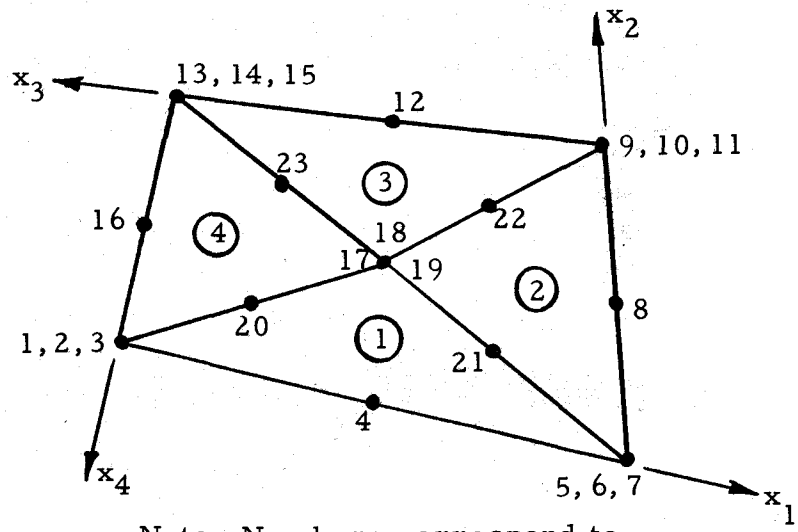

Note: Numbers correspond to unknowns at each node

Figure 3.5. Quadrilateral element.

A 16-degree-of-freedom quadrilateral element matrix is formed by first appropriately combining the four 12-degree-of-freedom triangular element matrices into a 23-degree-of-freedom element matrix (one degree of freedom for each unknown). Then through a process commonly known as static condensation (27) the internal seven unknowns are eliminated, resulting in a 16-degree-of-freedom quadrilateral element matrix.

The algorithm used to combine the four triangular element matrices was proposed in reference (24) and explained further in reference (16). Code numbers for each triangular element consisting of 12 entries, one for each element unknown are developed as shown in Table 1. These code numbers are the same for every quadrilateral

element in the system and are therefore generated only once in the computer program. After four triangular element matrices are generated for an individual quadrilateral element, they are used in conjunction with the FORTRAN statements in Table 2 to generate the 23 x 23 element matrix previously mentioned. If the load matrices $\{\bar{P}\}$ for each of the triangular elements are similarly superimposed, the 23 equations may be written

$$[E']\{\phi'\} = \{P'\} \tag{3.35}$$

where

$$\{\phi'\} \equiv \begin{Bmatrix} \phi'_1 \\ \vdots \\ \phi'_{16} \\ \hline \phi'_{17} \\ \vdots \\ \phi'_{23} \end{Bmatrix} \begin{matrix} \left.\begin{matrix} \\ \\ \\ \\ \end{matrix}\right\} \text{external unknowns} \quad \{\phi'_a\} \\ \left.\begin{matrix} \\ \\ \\ \\ \end{matrix}\right\} \text{internal unknowns} \quad \{\phi'_b\} \end{matrix}$$

and

$$\{P'\} \equiv \begin{Bmatrix} P'_1 \\ \vdots \\ P'_{16} \\ P'_{17} \\ \vdots \\ P'_{23} \end{Bmatrix} \begin{matrix} \left.\begin{matrix} \\ \\ \\ \\ \end{matrix}\right\} \text{external "loads"} \quad \{P'_a\} \\ \left.\begin{matrix} \\ \\ \\ \\ \end{matrix}\right\} \text{internal "loads"} \quad \{P'_b\} \end{matrix}$$

Partitioning Equation (3.35) into two equations, the following is obtained:

Table 1. Tezcan code numbers.

Element No.	Displacement or Moment Numbers											
	1	2	3	4	5	6	7	8	9	10	11	12
	u_1	v_1	w_1	M_{n_1}	u_2	v_2	w_2	M_{n_2}	u_3	v_3	w_3	M_{n_3}
1	1	2	3	4	5	6	7	21	17	18	19	20
2	5	6	7	8	9	10	11	22	17	18	19	21
3	9	10	11	12	13	14	15	23	17	18	19	22
4	13	14	15	16	1	2	3	20	17	18	19	23

Table 2. Tezcan code number algorithm.

```
      DO 150   L = 1,4
      DO 150   J = 1,12
      KA = ICODE (L, J)
      DO 150   N = J,12
      KB = ICODE (L, N)
150   TQEM (KA, KB) = TQEM (KA, KB) + TEMT (J, N)
```

TQEM	23 x 23 temporary quadrilateral element matrix.
TEMT	12 x 12 transferred triangular element matrix of the form in Equation (3.34).
ICODE	4 x 12 matrix of the code numbers in Table 1.

$$\left[\begin{array}{c|c} E'_{aa} & E'_{ab} \\ \hline E'_{ba} & E'_{bb} \end{array}\right] \left\{\begin{array}{c} \phi'_a \\ \hline \phi'_b \end{array}\right\} = \left\{\begin{array}{c} P'_a \\ \hline P'_b \end{array}\right\} \tag{3.36}$$

Taking the bottom equation of Equation (3.36) and solving for $\{\phi'_b\}$

$$\{\phi'_b\} = [E'_{bb}]^{-1}(\{P'_b\}-[E'_{ba}]\{\phi'_a\}) \tag{3.37}$$

The internal unknowns $\{\phi'_b\}$ are eliminated by substituting Equation (3.37) into the top equation of Equation (3.36). Thus

$$[E^*]\{\phi^*_a\} = \{P^*\} \tag{3.38}$$

where

$$\{\phi^*_a\} = \{\phi'_a\}$$

$$\{P^*\} = \{P'_a\} - [E'_{ab}][E'_{bb}]^{-1}\{P'_b\}$$

$$\{E^*\} = [E'_{aa}] - [E'_{ab}][E'_{bb}]^{-1}[E'_{ba}]$$

Inversion of the 7 x 7 matrix $[E'_{bb}]$ and multiplication of the indicated matrices of Equation (3.38) should be carried out in double precision. In the mixed method, the coefficient matrices can contain elements which differ widely in order of magnitude and result in ill-conditioned arrays.

3.5 System Equations and Solution Process

As the element matrices $[E^*]$ are generated, they are

appropriately superimposed into a system matrix [S]. This superimposition is accomplished in a manner similar to that in which the four triangular element matrices were combined into one quadrilateral element matrix. The code numbers this time, however, contain 16 entries corresponding to the 16 unknowns for each element.

A structural system that contains a large number of elements must necessarily involve a good deal of tedious input data preparation. This includes a code number for each element. In order to reduce preliminary work of this nature, a subroutine was written to generate the code numbers for each quadrilateral element. The information used by the subroutine is input information that ordinarily would be included for any matrix analysis of structures; the nodal point coordinates and the element connectivity. The latter includes for every element number the corresponding nodal point numbers.

When the system matrix [S] and system load vector {V} are generated using the code numbers and algorithm indicated in Table 2, the total system of simultaneous algebraic equations in the unknowns $\{\Phi\}$ is represented as

$$[S]\{\Phi\} = \{V\} . \tag{3.39}$$

The primary concern in the solution of this system is the conditioning of the system matrix. It is a symmetric matrix as a consequence of the symmetry of the triangular element matrix in Equation

(3.29) which is a result of conservation of energy. In addition, it is also a banded matrix where the band width is dependent on the direction of numbering the node points. They should be numbered in such a way as to minimize the difference between the largest and smallest nodal point number for any element. This is true in the mixed method just as in the more common displacement formulations. The band-width in this method is increased because of the existence of side nodal points which must also be numbered. Nevertheless, the system matrix is banded and advantage is taken thereof along with the symmetry when storing the coefficients in computer storage.

The solution process, contained in a single subroutine, is Gaussian elimination. The input system matrix is in the packed form; having a width of half the band-width plus one for diagonal terms and a length equal to the number of system unknowns. The band-width is automatically computed prior to solving the system as it is required input to the solution subroutine along with the system load vector. It is of course desirable to carry out the solution process in double precision especially in the mixed method for reasons mentioned in Section 3.4. This consideration must, however, be weighed with program size, desired accuracy and available computer storage.

IV. THE FINITE ELEMENT MODEL

The purpose of this chapter is to describe the finite element model and to describe its basic strengths and weaknesses. When interpreting results from the symmetrical penstock bifurcation model, a certain amount of judgement must be applied and it is hoped that this chapter will help cultivate that judgement. In order to accomplish this, two approaches to verifying the finite element model are taken. First, verification of the basic finite element is sought by comparing its results with those of known classical solutions. Second, verification of the symmetrical penstock bifurcation finite element solution is sought by comparing its results with experimental data from a hydrostatic test of a prototype penstock bifurcation.

4.1 Comparison with Classical Solutions

The basic finite element formulation of this investigation was applied to four different types of structures so that a feeling could be gained as to the behavior and validity of the formulation. The structures are relatively simple structures for which classical solutions are available. Even though the resulting finite element models are quite simple when compared to the complex model of the bifurcation, this type of verification has become traditional in finite element work.

Because the ring girder of the penstock bifurcation could

possibly contain flat plate bending, it is of interest to know how well the basic formulation approximates a flat plate structure. The thin, uniformly loaded, rectangular plate shown in Figure 4.1 is a good choice for comparison among classical plates because of its varied boundary conditions. A six by six element model was selected and the results are shown in Figures 4.2, 4.3, 4.4, and 4.5. It is seen that there is excellent agreement with the exact solution for the moments but that the displacements in Figure 4.5 are somewhat off on the high side. In general, however, the agreement is good. Reference (11) analyzed the same structure with an eight by eight element model of the same formulation and shows very similar results. The verification of the finite element formulation for the flat plate demonstrates its usefulness for what it was basically intended; analyze thin flat plates. It is of course another matter to use the flat plate element to model curved surfaces or shells.

The first shell structure to be considered in demonstrating the applicability of the formulation to curved surfaces is the open-ended cylinder. The cylinder is subjected to internal pressure and because the walls are unrestrained at the ends no moment should develop. Six elements were used to model a 90 degree portion of the wall as shown in Figure 4.6. The results for the membrane stress are shown in Figure 4.7 where it is seen that the agreement with the exact value is excellent. More interesting, however, are the moment results

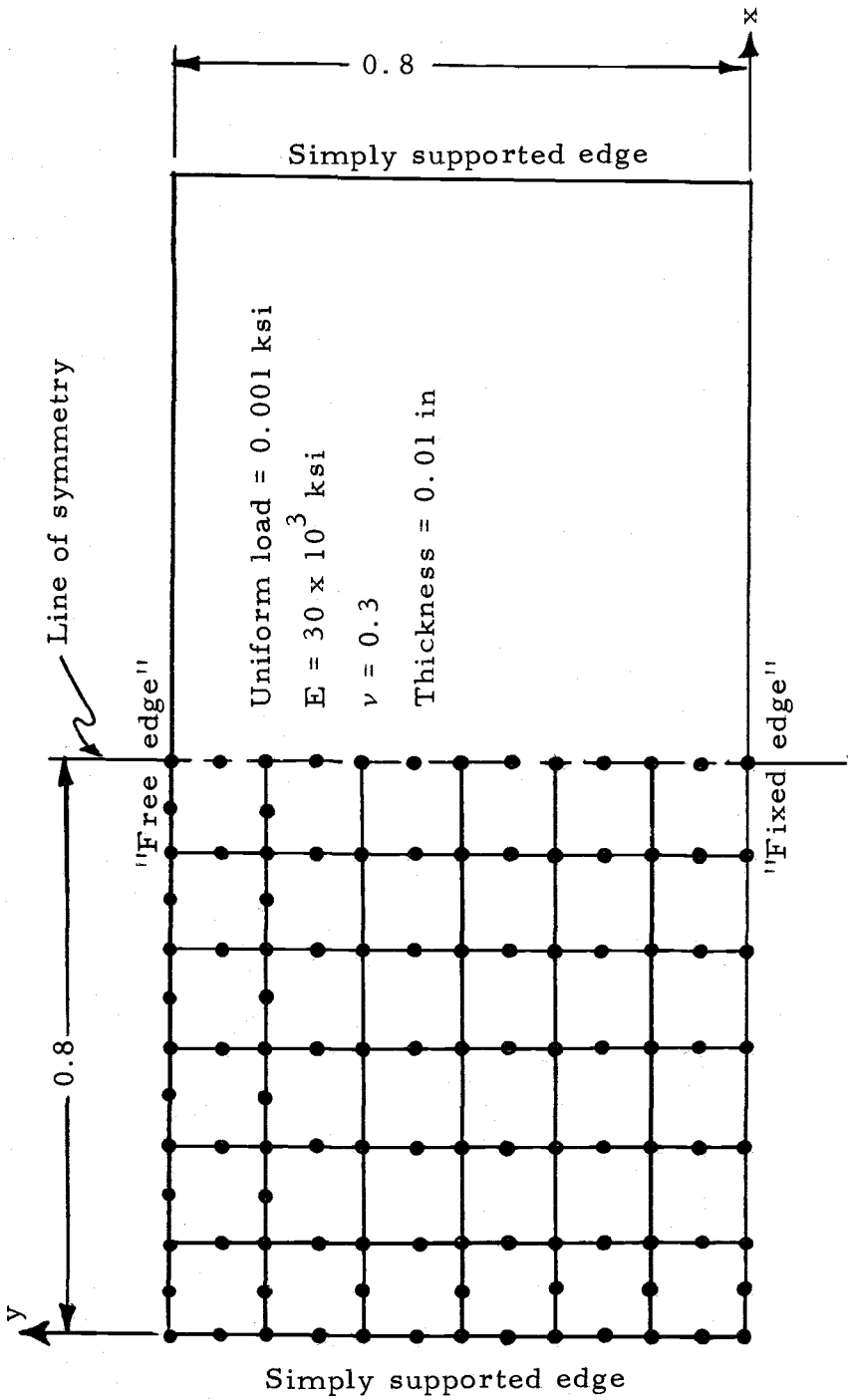

Figure 4.1. Thin rectangular plate modeled by a 6 x 6 finite element mesh.

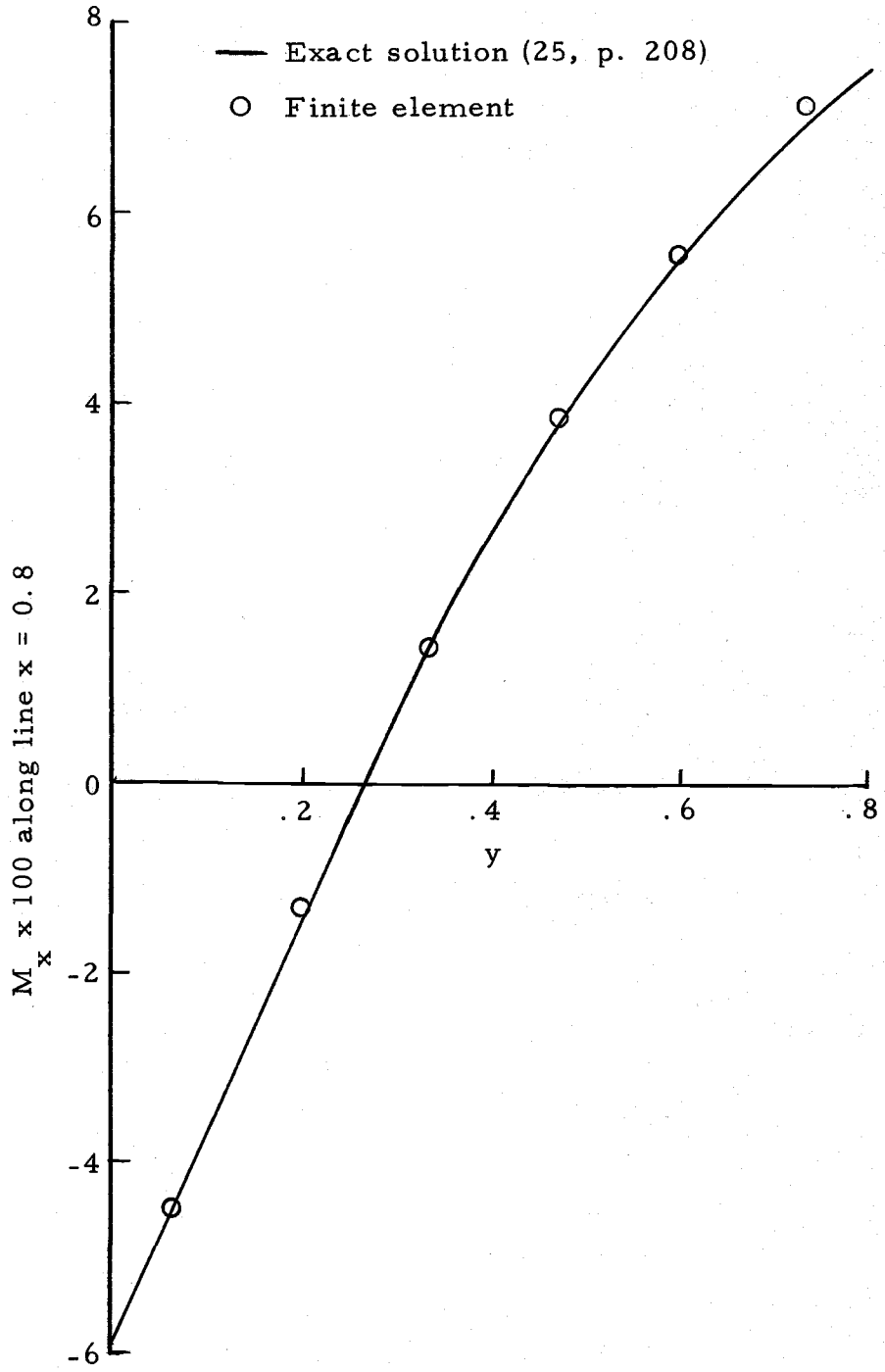

Figure 4.2. Moment (x component) in rectangular plate.

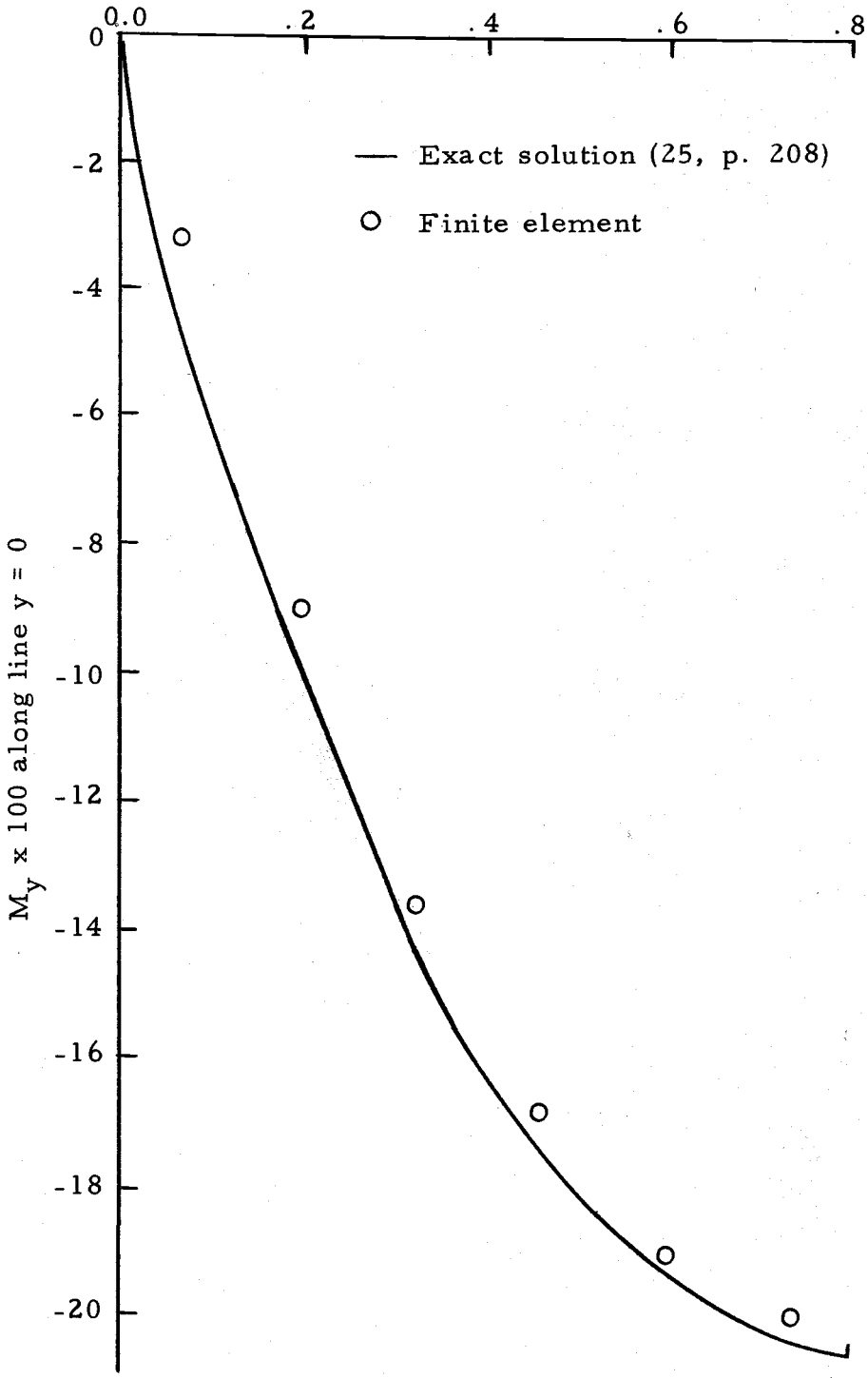

Figure 4.3. Moment (y component) in rectangular plate.

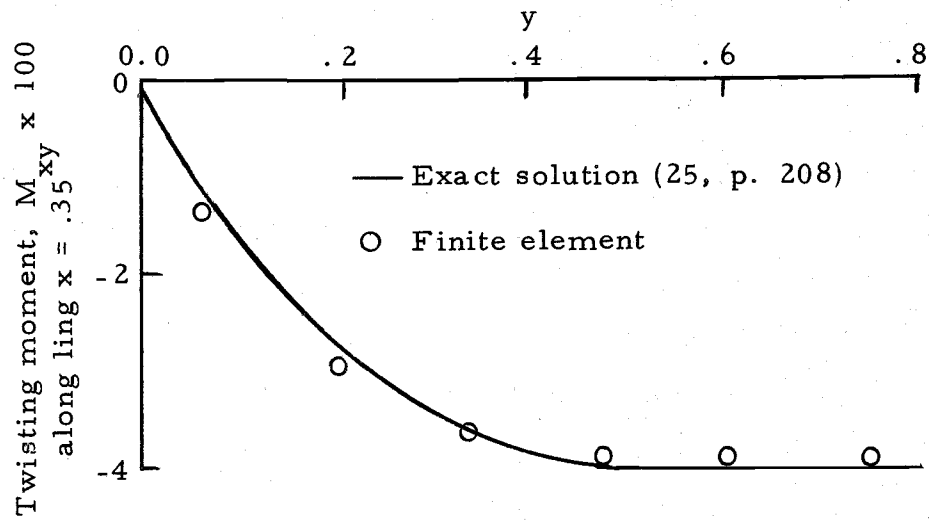

Figure 4.4. Twisting moment in rectangular plate.

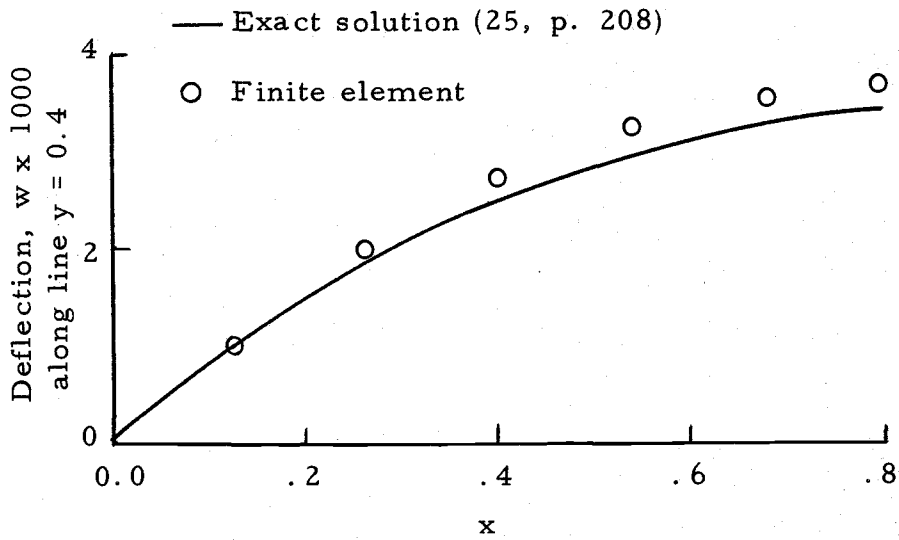

Figure 4.5. Transverse deflection in rectangular plate.

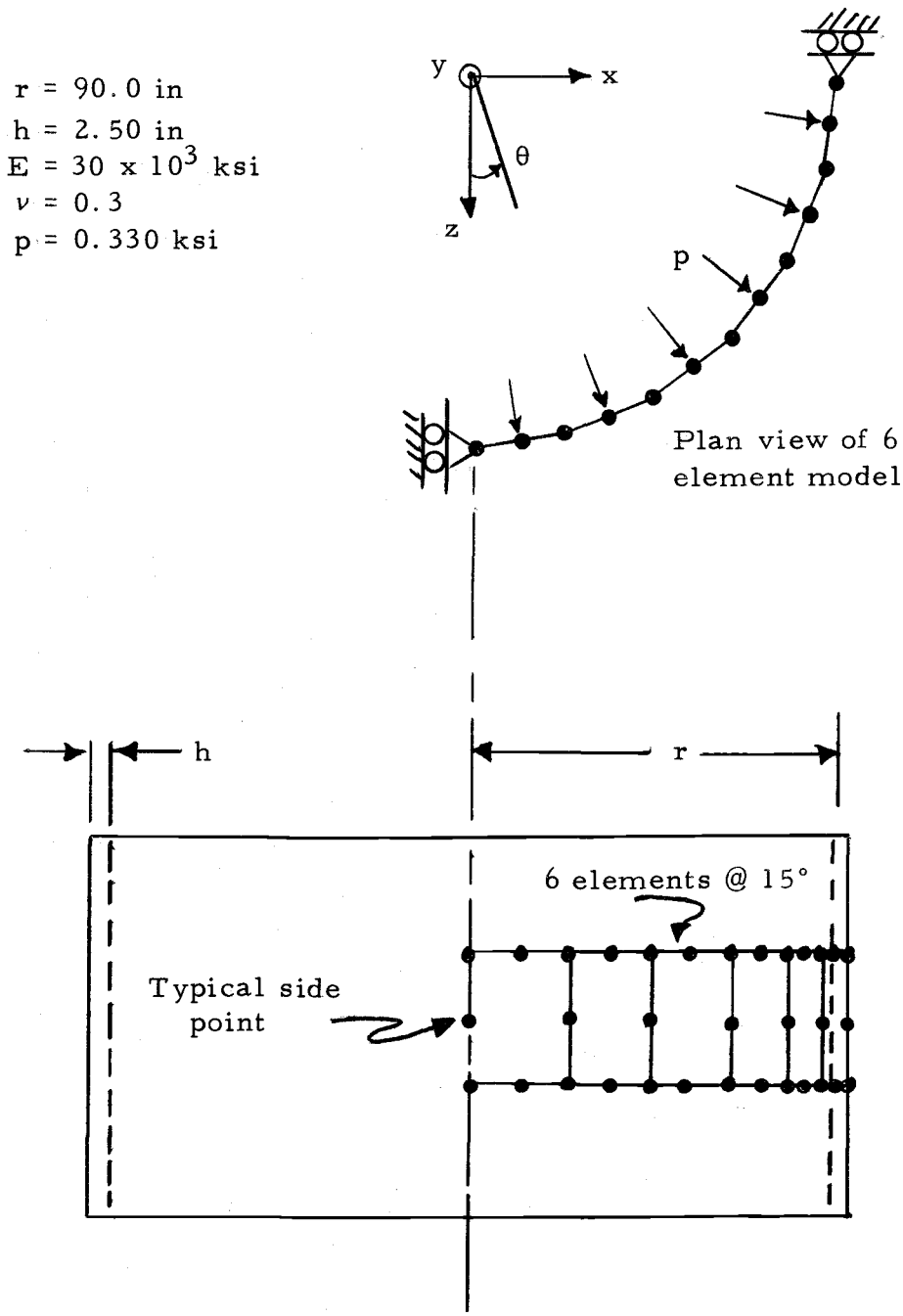

Figure 4.6. Finite element model of cylinder with unrestrained ends.

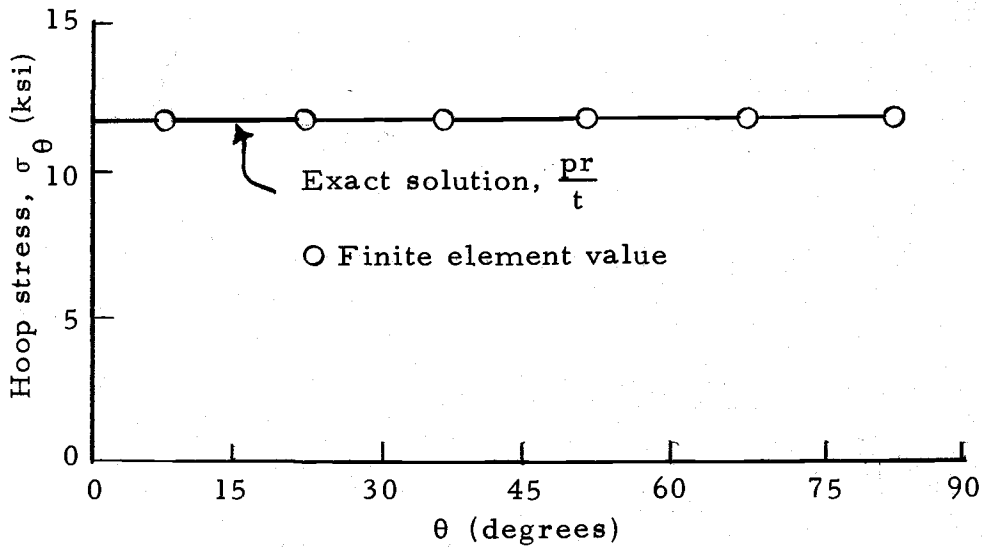

Figure 4.7. Hoop stress in cylinder wall.

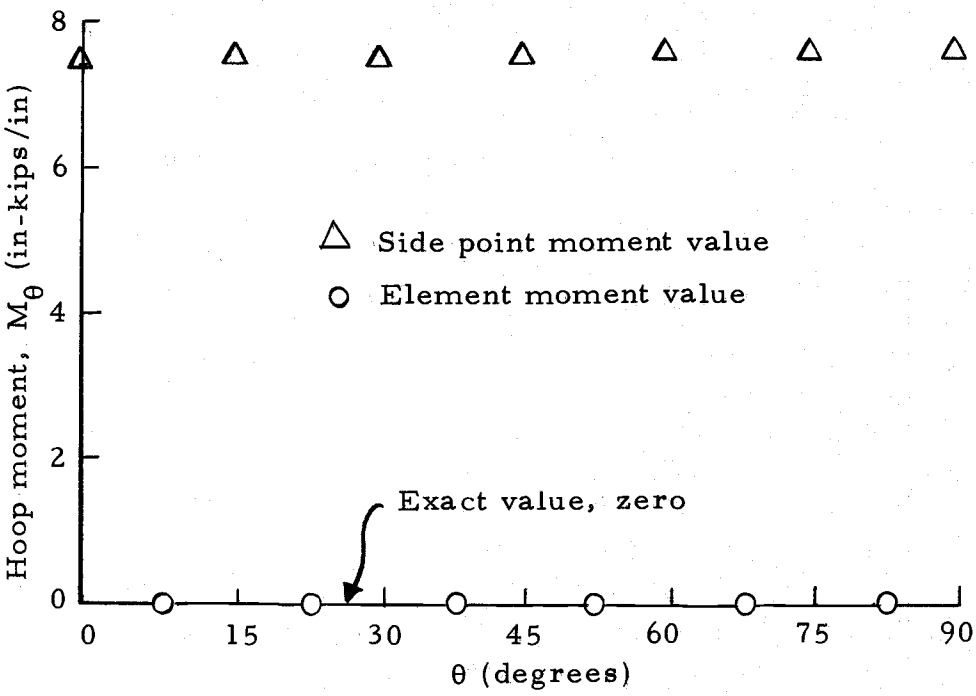

Figure 4.8. Comparison of side point moment values with element moment values.

shown in Figure 4.8. Here, the finite element results are shown in two forms; the side point moment values and the element moment values (moments at center of the element). The side point values are completely erroneous while the element moment values correctly show zero moment. The side point values reflect the slope discontinuity between elements and are naturally yielding moments that might be expected for an "equivalent folded plate structure." In the smooth shell, there are no such slope discontinuities and therefore the side point moment data should be ignored in favor of the element moment values.

The third structure to be analyzed is a circular cylindrical shell with both ends completely restrained against rotation and displacement. Under a uniform internal pressure the restrained ends will cause a vertical moment at the base of the cylinder to be developed. Characteristically this moment will be maximum at the base and will eventually decay to zero at some point above the base, provided the cylinder is sufficiently long. It is of interest to know how well the finite element formulation models this behavior because the penstock bifurcation contains a similar shell configuration with boundary conditions developing moment. The finite element model takes advantage of three planes of symmetry for the cylinder as shown in Figure 4.9. This figure shows six elements of 15 degrees each in the direction of curvature. A second model, not shown, with 12 elements

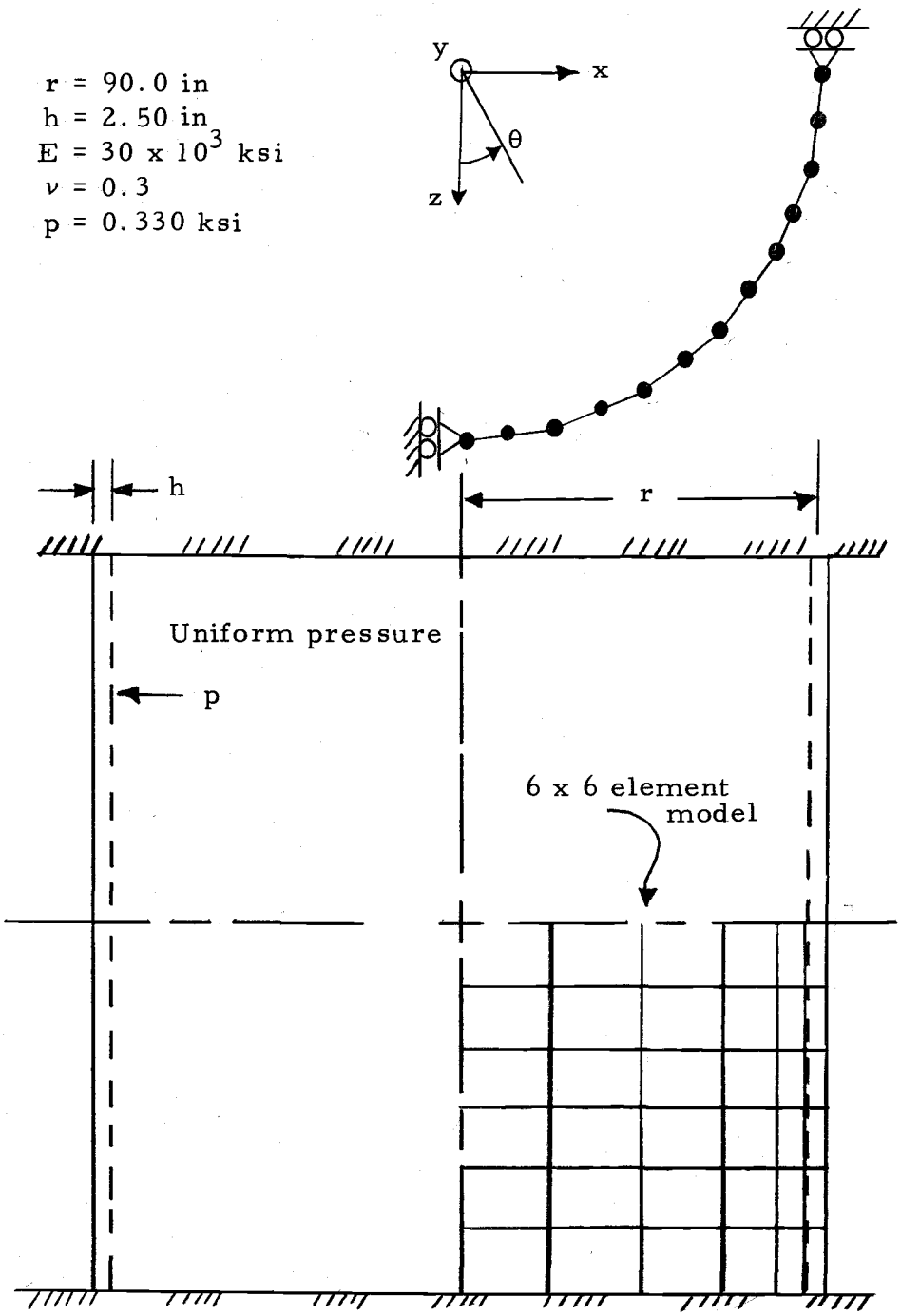

Figure 4.9. Finite element model of cylinder with restrained ends.

of 7.5 degrees each was also prepared because the first model proved very coarse. The results for both membrane hoop force and vertical moment are shown in Figures 4.10 and 4.11, respectively. The hoop force is on the high side near the base but achieves reasonably good accuracy with distance from the base. In Figure 4.11 it is seen that the six-element model yields moment which does not agree well with the exact results. A significant improvement is achieved with the 12 element model. Thus it is concluded that the results are very dependent on the number of elements in the direction of curvature.

The fourth structure is a spherical cap subjected to uniform internal pressure. It is included in this investigation because it is a doubly-curved shell and would seem a more difficult test for the formulation than the previous cylindrical shell. Two conditions are studied: the first has the outer edge of the shell restrained against vertical displacement only and the second has the outer edge completely restrained. Figure 4.12 shows the model configuration of seven elements in the meridian direction and six elements in the hoop direction. A second model was constructed with 13 elements in the meridian direction and six elements in the hoop direction. The results are shown in Figures 4.13 through 4.16.

From the results it can be seen that the second model with nearly twice the number of elements yielded little additional accuracy. It may be that the spherical cap's curvature was sufficiently mild to

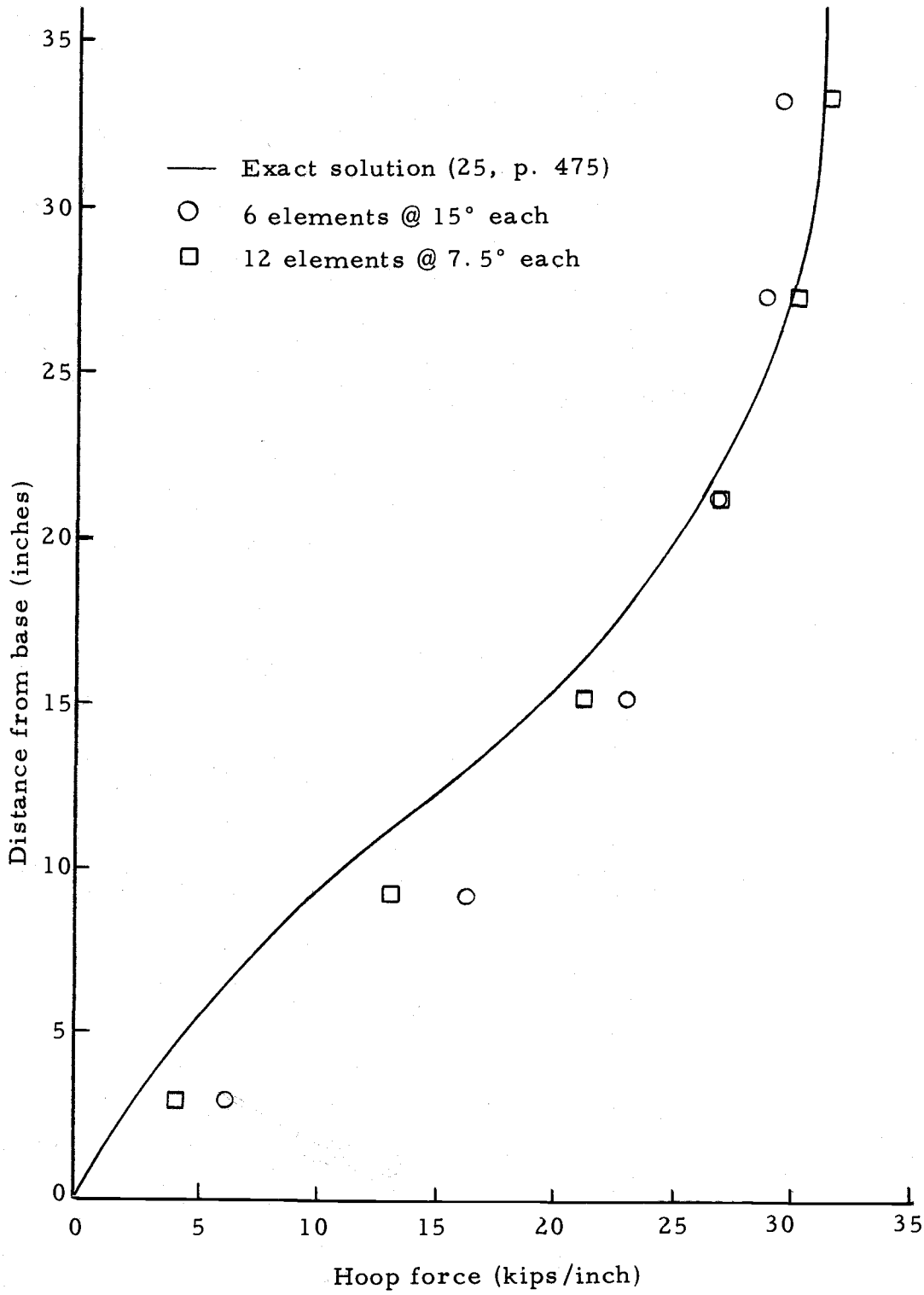

Figure 4.10. Membrane force for various element size.

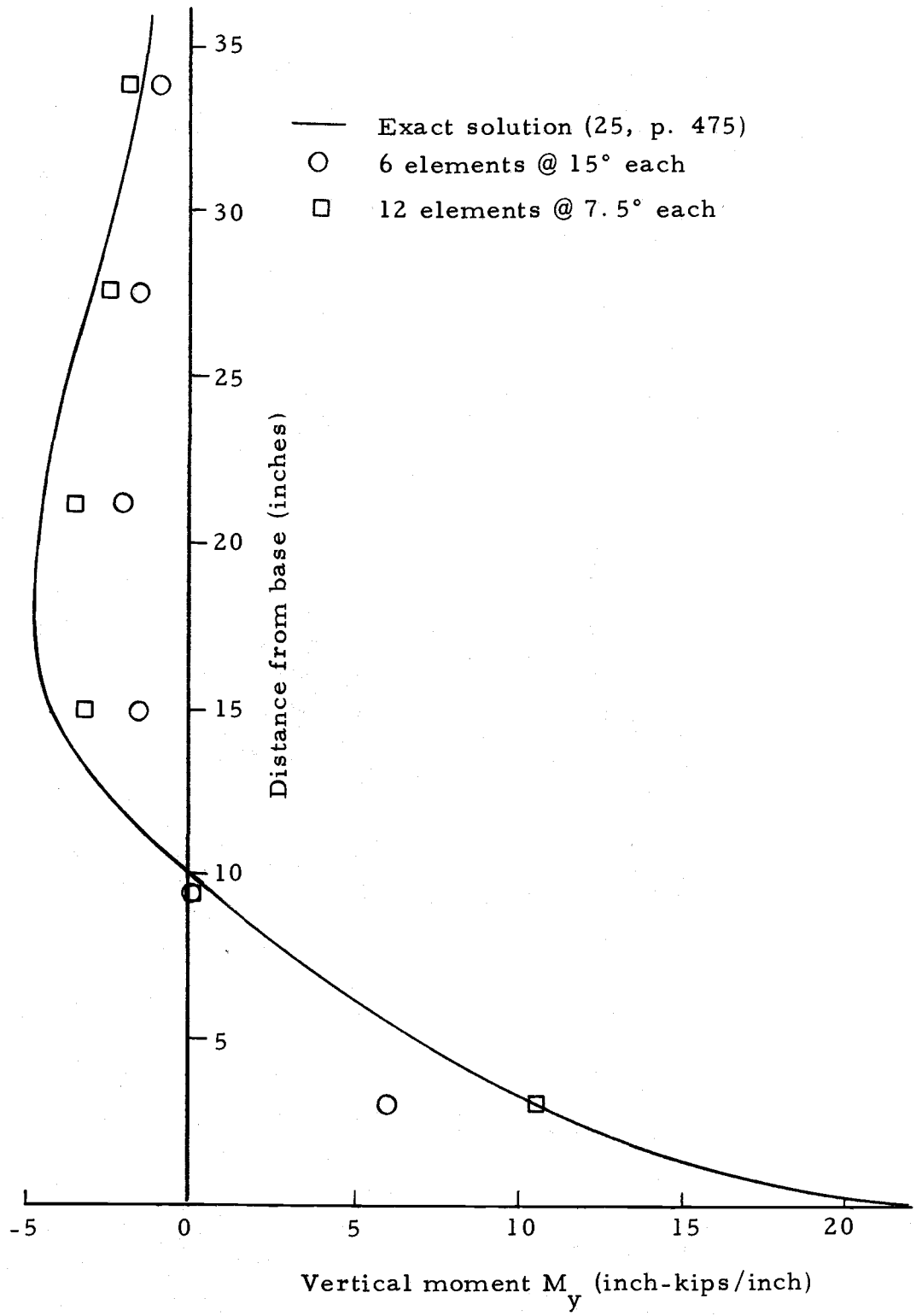

Figure 4.11. Moment for various element size.

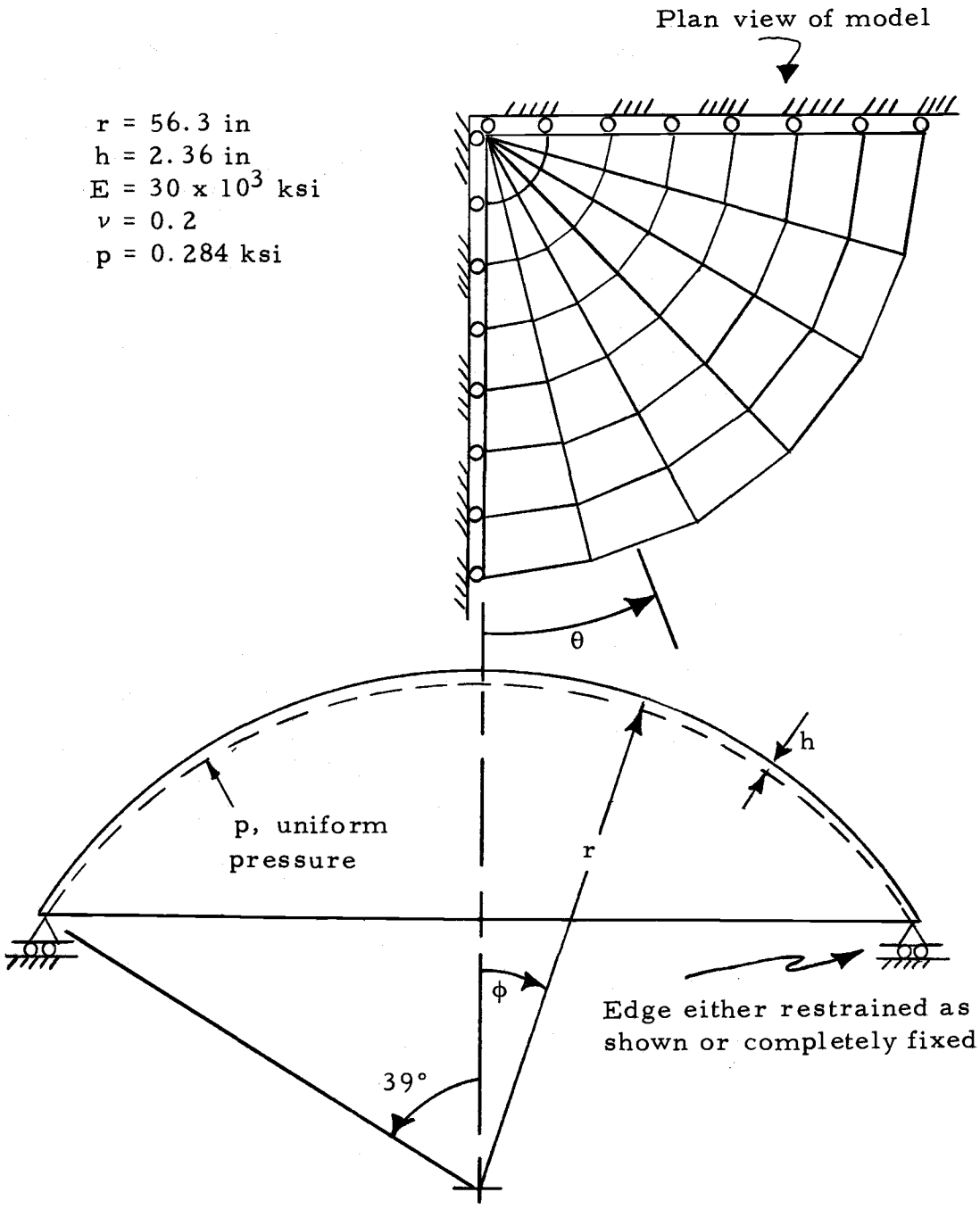

Figure 4.12. Finite element model of spherical cap.

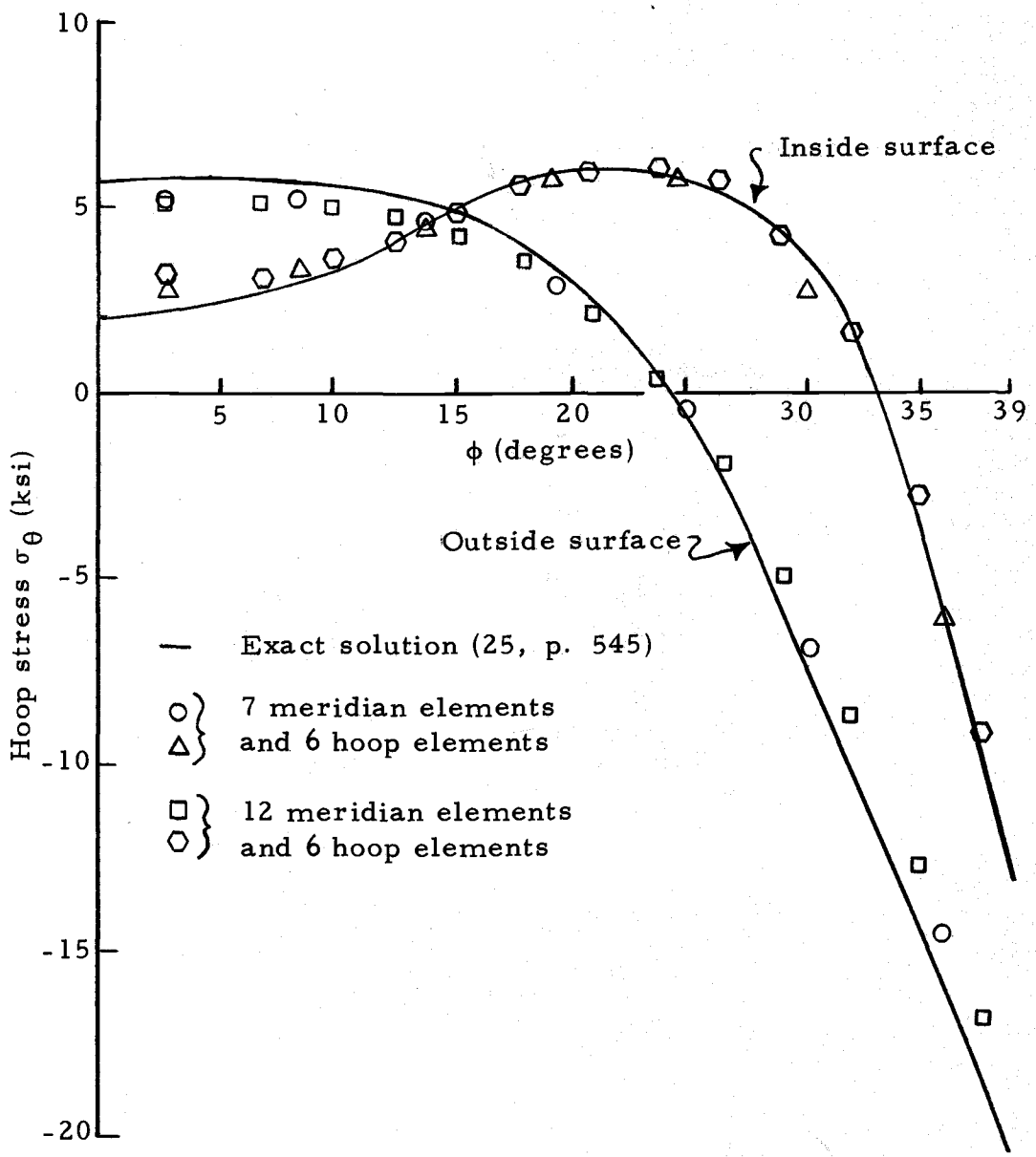

Figure 4.13. Hoop stresses for spherical cap with pinned edge.

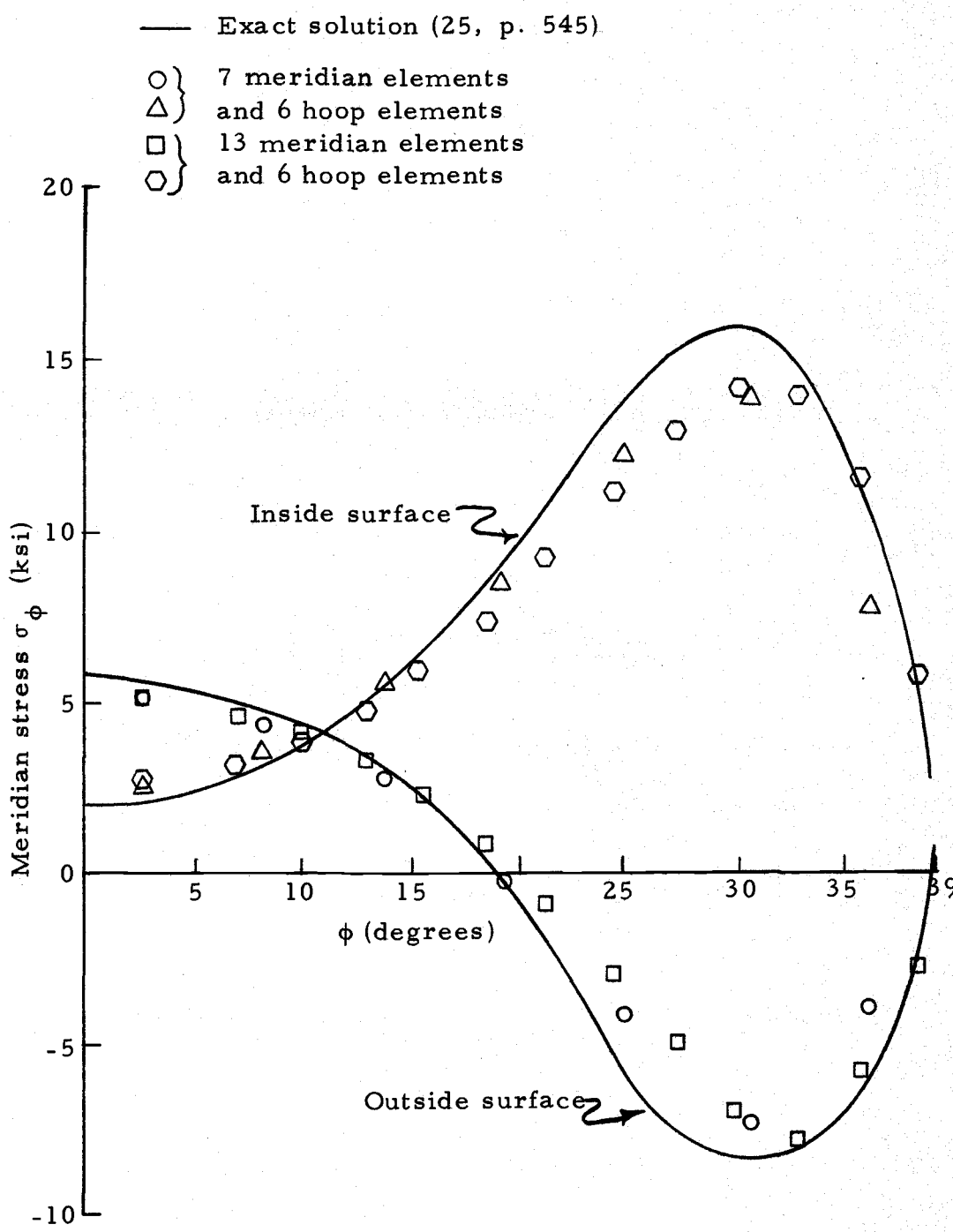

Figure 4.14. Meridian stress for spherical cap with pinned edge.

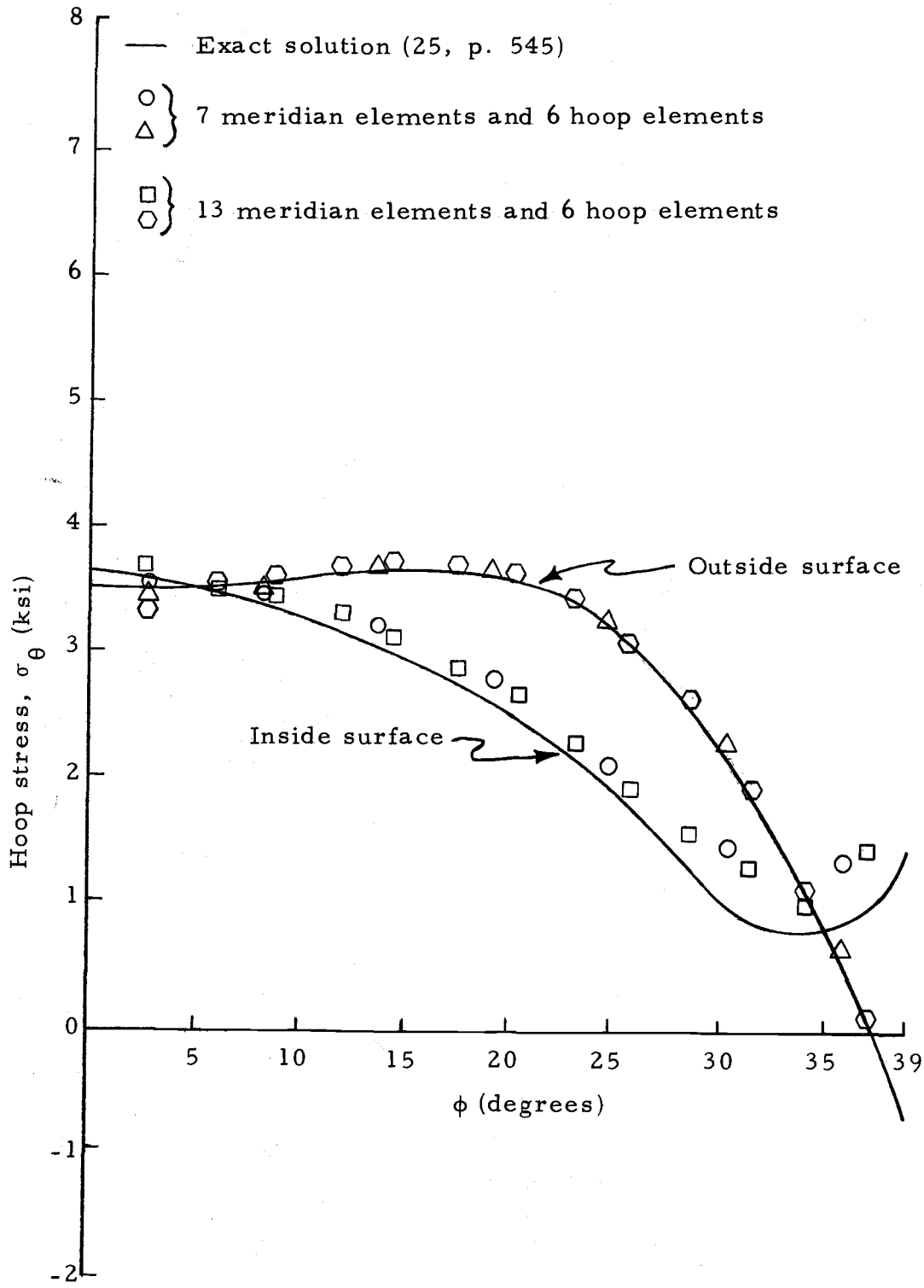

Figure 4.15. Hoop stress for spherical cap with fixed edge.

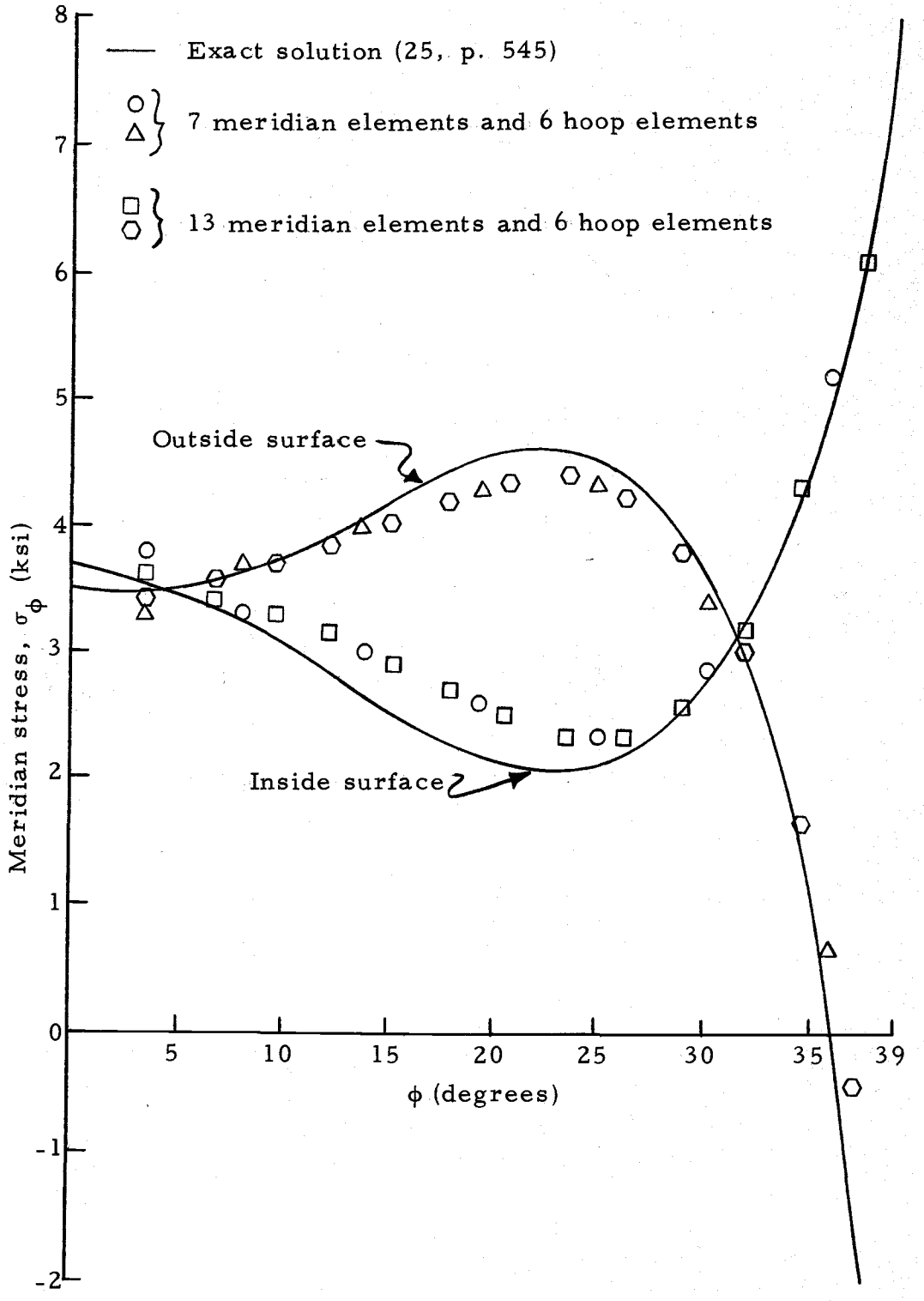

Figure 4.16. Meridian stress for spherical cap with fixed edge.

justify the smaller model only. The agreement is generally better for the hoop stresses than for the meridian stresses. The hoop stresses, at most points, are primarily due to membrane action whereas the larger meridian stresses are primarily due to bending action. It would seem, therefore, that the formulation will model membrane action better than bending action. Also it appears that the bending stresses, where agreement is poor, are on the small side.

4.2 Approximation of Curved Surfaces with Flat Plate Elements

As previously stated the basic unit of the finite element model used in this investigation is a flat plate element in which membrane action is superimposed on bending action. In the shell structures the flat plate representations resemble folded plate structures as can be seen in Figures 4.6, 4.9, and 4.12. The resulting slope discontinuities along the line of curvature will give rise to side point bending moments in the model where in the shell there are, in fact, none. This undesirable effect is inherent in this formulation and cannot be altered. It can be minimized by using a large number of elements in the direction of curvature so that the slope discontinuities are made less severe.

It has been noted, however, in (12) and at least partially demonstrated in Figure 4.8 that the quadrilateral element moments

(as opposed to the side point moments) give more reasonable results despite the fact that they are computed from the side point values. They are computed as follows: first, Equation (3.21) is used to obtain the rectangular cartesian components of the moment in a triangular element from the side point moments; second, the values for each of the four triangles making up a quadrilateral are referenced to a common set of axes for the quadrilateral; third, the four sets of values are then averaged to obtain the rectangular cartesian components of the moment within the quadrilateral.

The quadrilateral element moments then are to be treated as reasonable data while the side point values in the direction of curvature are to be treated as ficticious values and ignored. In addition, it has been shown (13) that the quadrilateral element moment data is adversely affected when the subtended angles of the elements in the direction of curvature are unequal. Thus it is advisable when developing the finite element model for the penstock bifurcation to make the elements uniform in the direction of curvature for the cylinder and cone.

Further comments on the appropriateness of modeling curved surfaces with flat plate elements can be found in (6, 9).

4.3 The Symmetrical Penstock Bifurcation Model

The symmetrical penstock bifurcation has two planes of

symmetry and these are used to advantage in the basic structure shown in Figure 1.3. It is this configuration that is discretized into flat plate elements resulting in the model shown in Figure 4.17.

The boundary conditions for the side points and corner points of the flat plate edges which lie in the $\bar{x}$-$\bar{y}$ and $\bar{x}$-$\bar{z}$ planes are dictated by symmetry; that is, the rotation of the side points are zero and the displacements perpendicular to the planes of symmetry are constrained to zero.

There are two load configurations studied in this investigation. They are the hydrostatic test condition and the operating load condition. Each requires a different set of boundary conditions along the inlet edge of the cylinder and the outlet edge of the cone.

The hydrostatic test configuration assumes the existence of bulkheads which constrain the displacements to zero in the plane of the inlet face and the outlet face; that is, the bulkheads are assumed infinitely rigid in their own plane. Displacements are allowed perpendicular to the planes in anticipation of the tensioning effect which is produced by equivalent static loads applied at the boundary nodes in the direction of these displacements. The infinitely rigid bulkheads are an idealization since in actual test conditions the bulkheads will most likely be hemispherical and will have a finite stiffness. Their stiffness cannot be determined in advance so the idealization is thought reasonable.

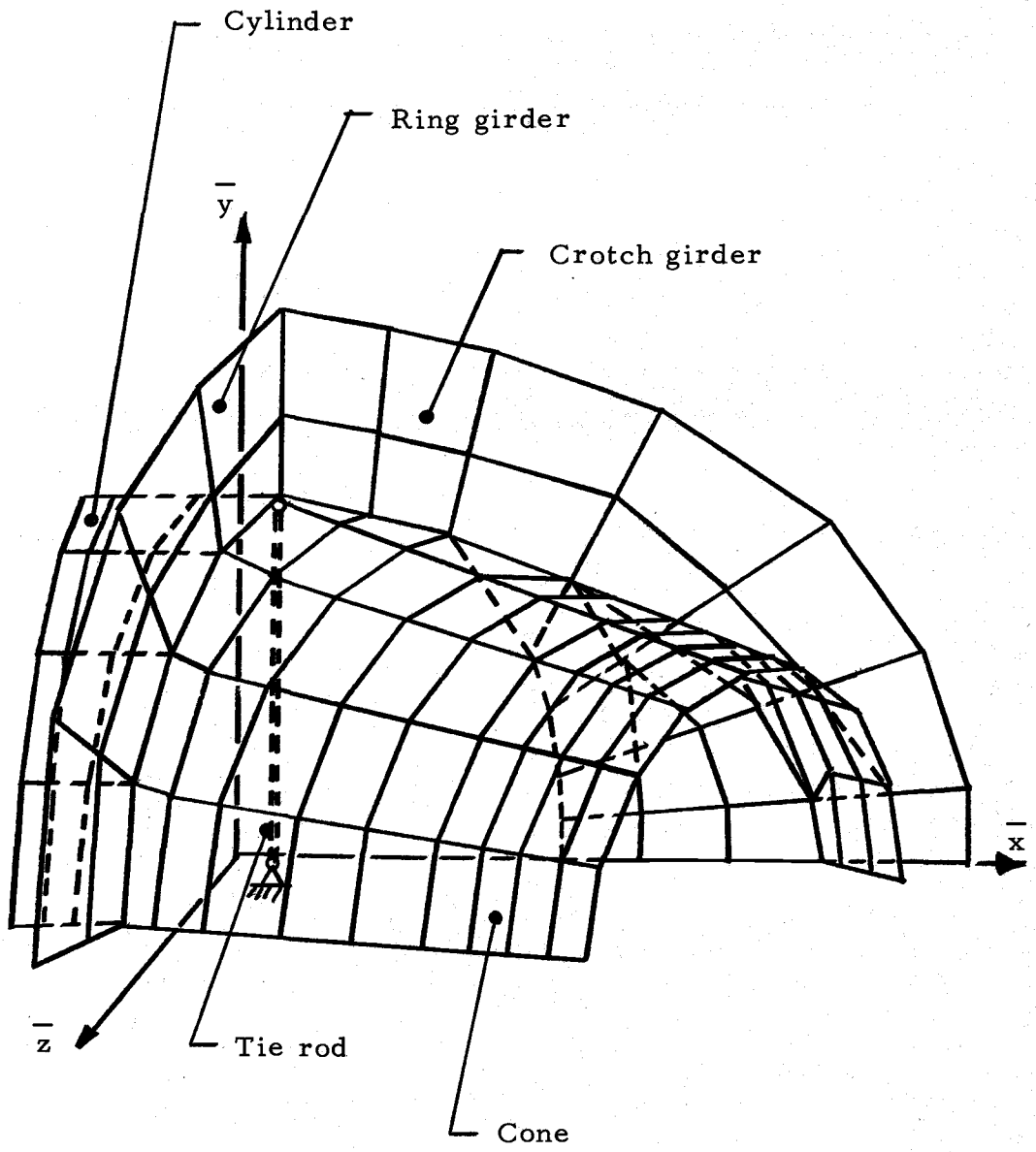

Figure 4.17. Finite element model of a symmetrical penstock bifurcation.

The operating load configuration assumes that no bulkheads exist and that displacements are constrained to zero in the direction of the longitudinal axes of symmetry for the cylinder and cone. Displacements are allowed in planes perpendicular to these axes.

For both load configurations the displacement boundary conditions on the inlet face of the cylinder coincide with the global reference system, thus there is no difficulty programming them. This is also true of the displacement boundary conditions mentioned previously.

The displacement boundary conditions for the cone outlet face, however, do not coincide with the global directions and therefore their inclusion requires more programming effort. There are two approaches to this problem (8). The first and more exact is to modify the method of generating the system of equations in terms of global unknowns to include some equations which are written for constraint-oriented axes. The second method is to remove the actual support and attach a ficticious axial member having an extremely large cross-sectional area so that its longitudinal axis is collinear with the constrained displacement. The opposite end of this member is restrained against displacement and therefore its boundary conditions can be conveniently cast in the global system. This method has the advantage of being more easily programmed. Even though more members are added to the structural system with one additional

unknown per member, the programming effort was significantly reduced and, for this reason, it is the method selected for the bifurcation model. Figure 4.18 illustrates the idealization of the boundary conditions on the outlet face of the cone.

4.4 Comparison with Experimental Data

Once verification of finite element formulations is achieved by comparisons with classical solutions it is assumed that the formulations can be applied to the analysis of more complex structures which defy classical methods. A need does exist, however, for experimental data to substantiate the use of finite element formulations for solving complex structures. In addition, such experimental investigations should be coordinated with the finite element investigation so that subsequent comparison of results will be meaningful. The experimental effort described herein was unfortunately not coordinated in this manner but it does offer valuable information where very little heretofore existed.

A symmetrical bifurcation prototype was constructed for the Snettisham project in southeastern Alaska. Its configuration and specific dimensions are shown in Figure 4.19. Hemispherical bulkheads were installed and the structure as shown in Figure 4.20, was hydrostatically tested in the shop at 900 psi internal pressure and was instrumented with 24 linear strain gages and 56 rosette strain gages.

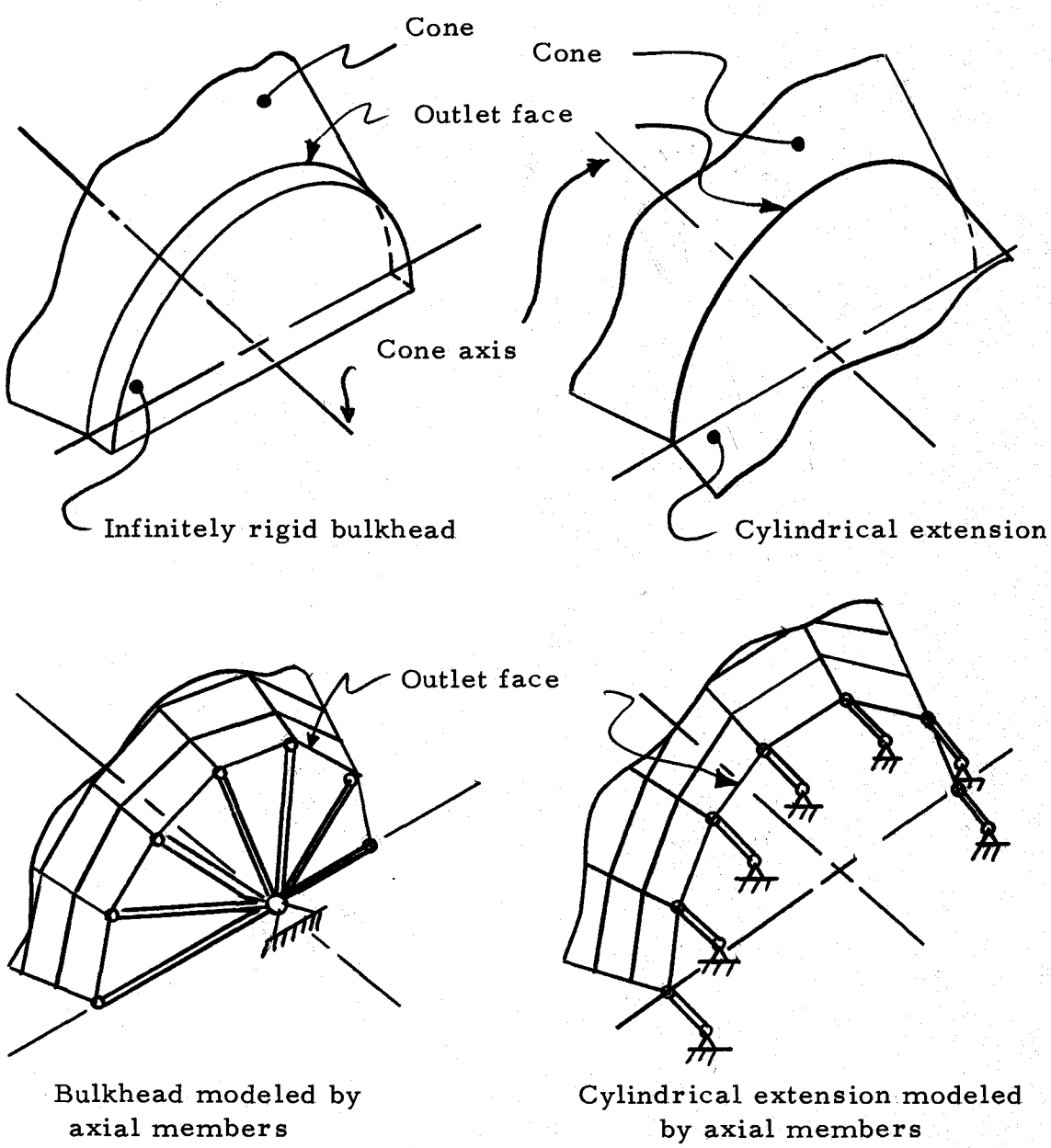

Figure 4.18. Cone outlet face boundary conditions as they are modeled.

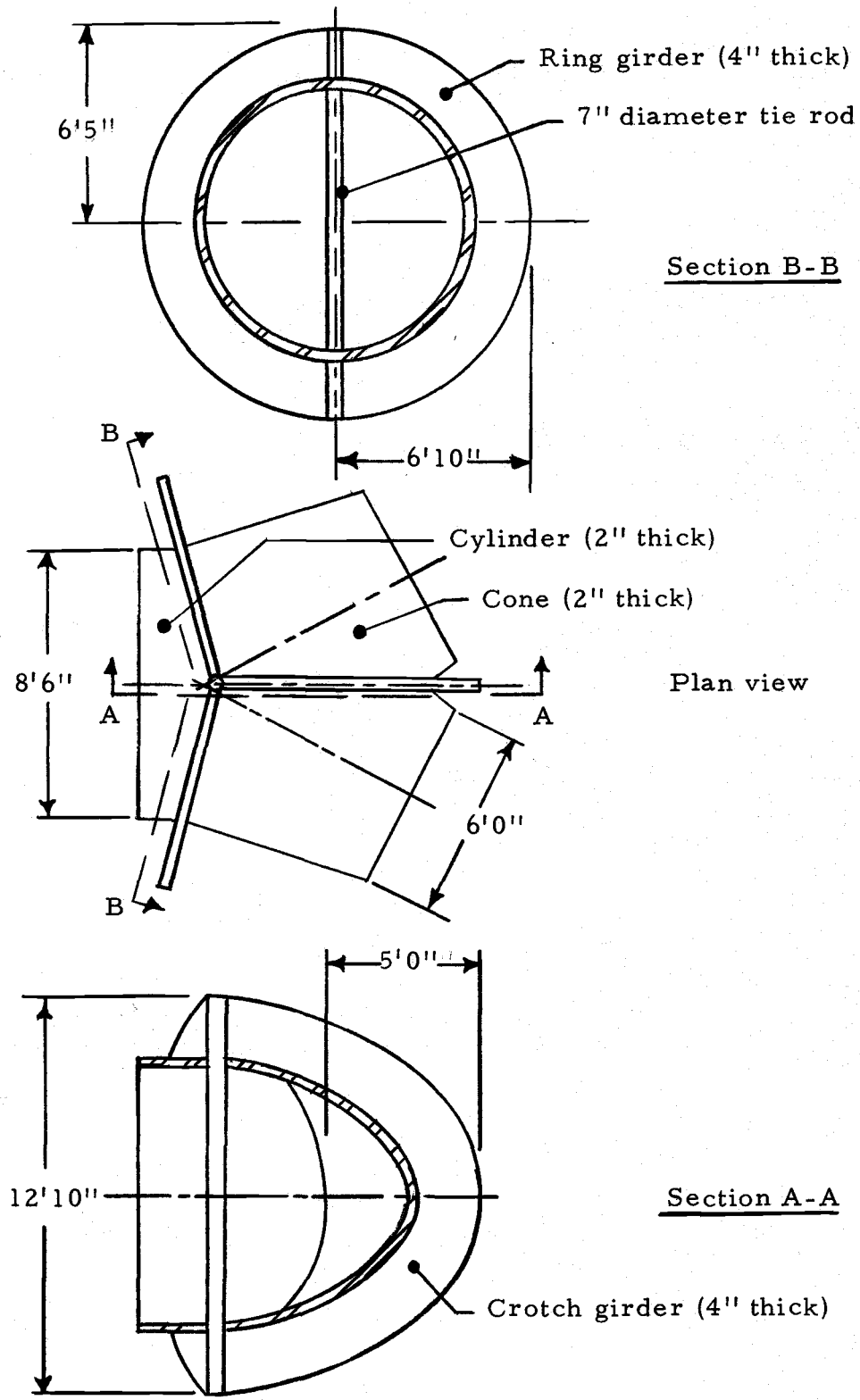

Figure 4.19. Snettisham penstock bifurcation.

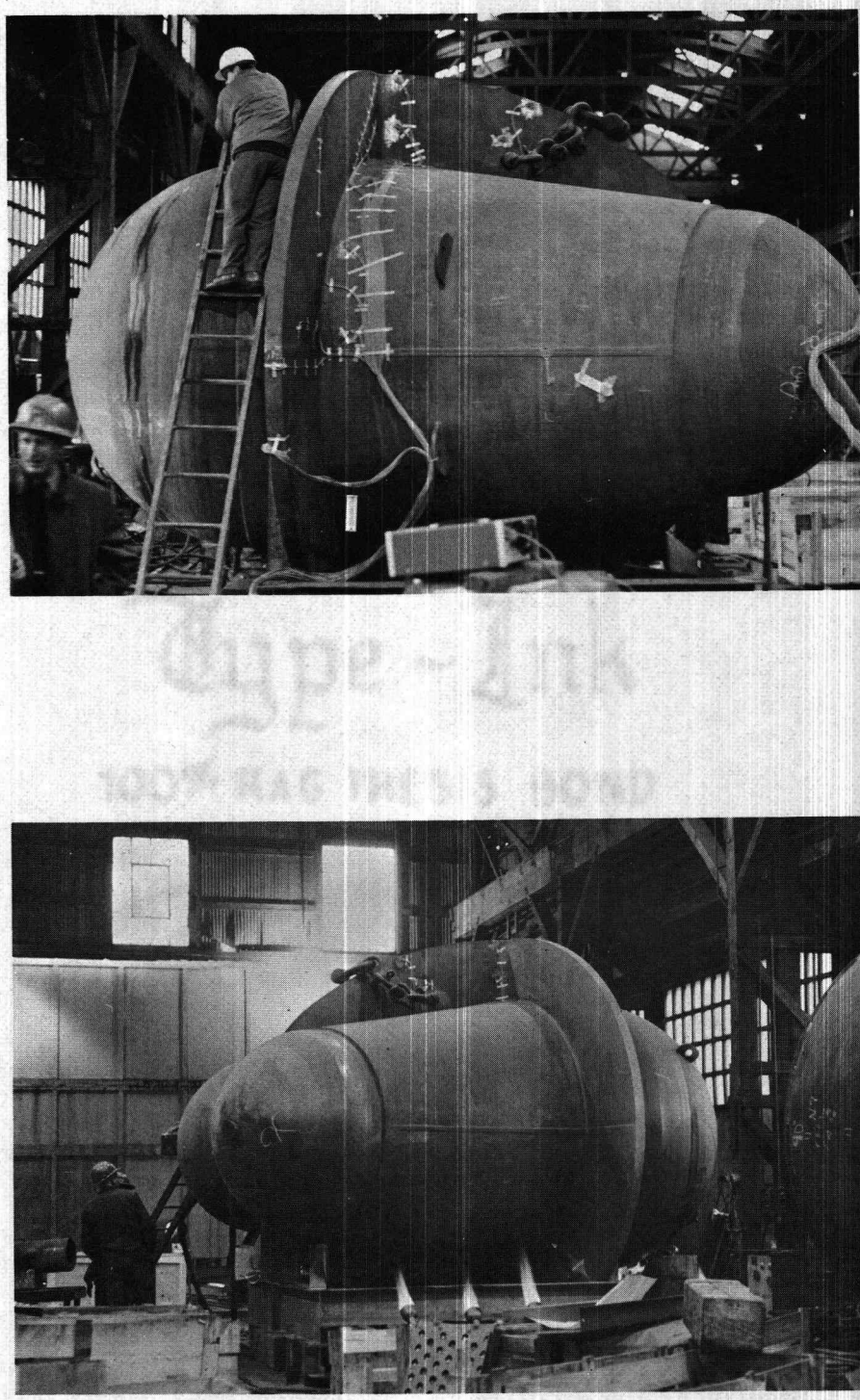

Figure 4. 20. Snettisham prototype bifurcation as tested in the shop.

The instrumentation was placed on the inside surface as well as the outside surface and arranged to measure bending stresses at isolated locations in the cone and cylinder and plane stresses in the ring girder and crotch girder.

A finite element model consisting of 116 elements was generated for the Snettisham configuration. This model is shown in Figure 4.17. The plane stress results for the crotch girder are shown in Figure 4.21 where the finite element principle stresses are shown along with the experimental stresses. The stresses along the horizontal line of symmetry are the more important data because they are maximum, as expected, at this location. It can be seen that finite element stresses agree very well with the experimental stresses both in magnitude and from a behavior point of view. To emphasize this, the finite element and experimental data are plotted at this location in Figure 4.22. A primary observation is that the maximum measured stress occurs just to the left of the cone attachment line. The finite element stress also shows this behavior but only in an approximate manner. The traditional analysis of penstock bifurcations (22) predicts the maximum stress to be on the inside edge as if the crotch girder were a curved beam in bending. While this may be true in other penstock bifurcations, the data clearly shows the Snettisham crotch girder behaves as a stretched plate instead.

The finite element model predicted the stress in the tie rod

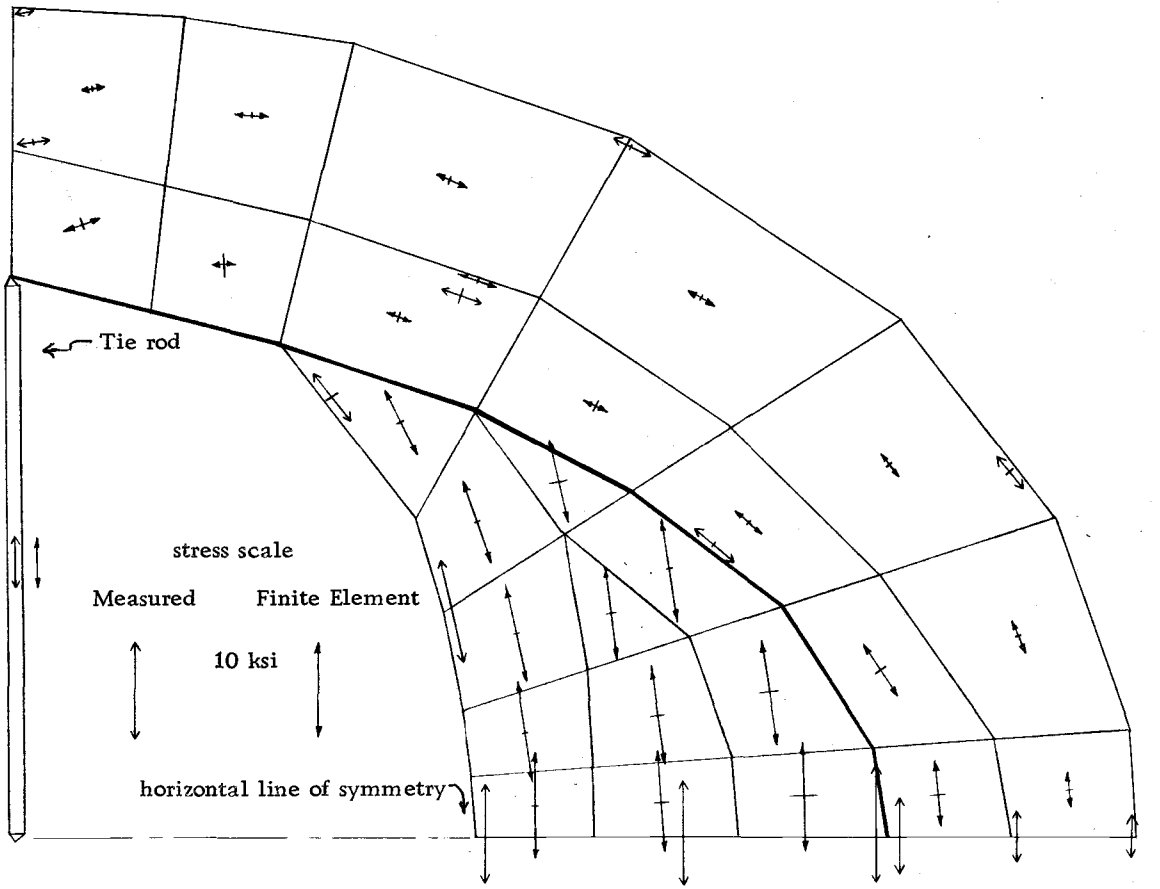

Figure 4.21. Comparison of stresses in the Snettisham crotch girder.

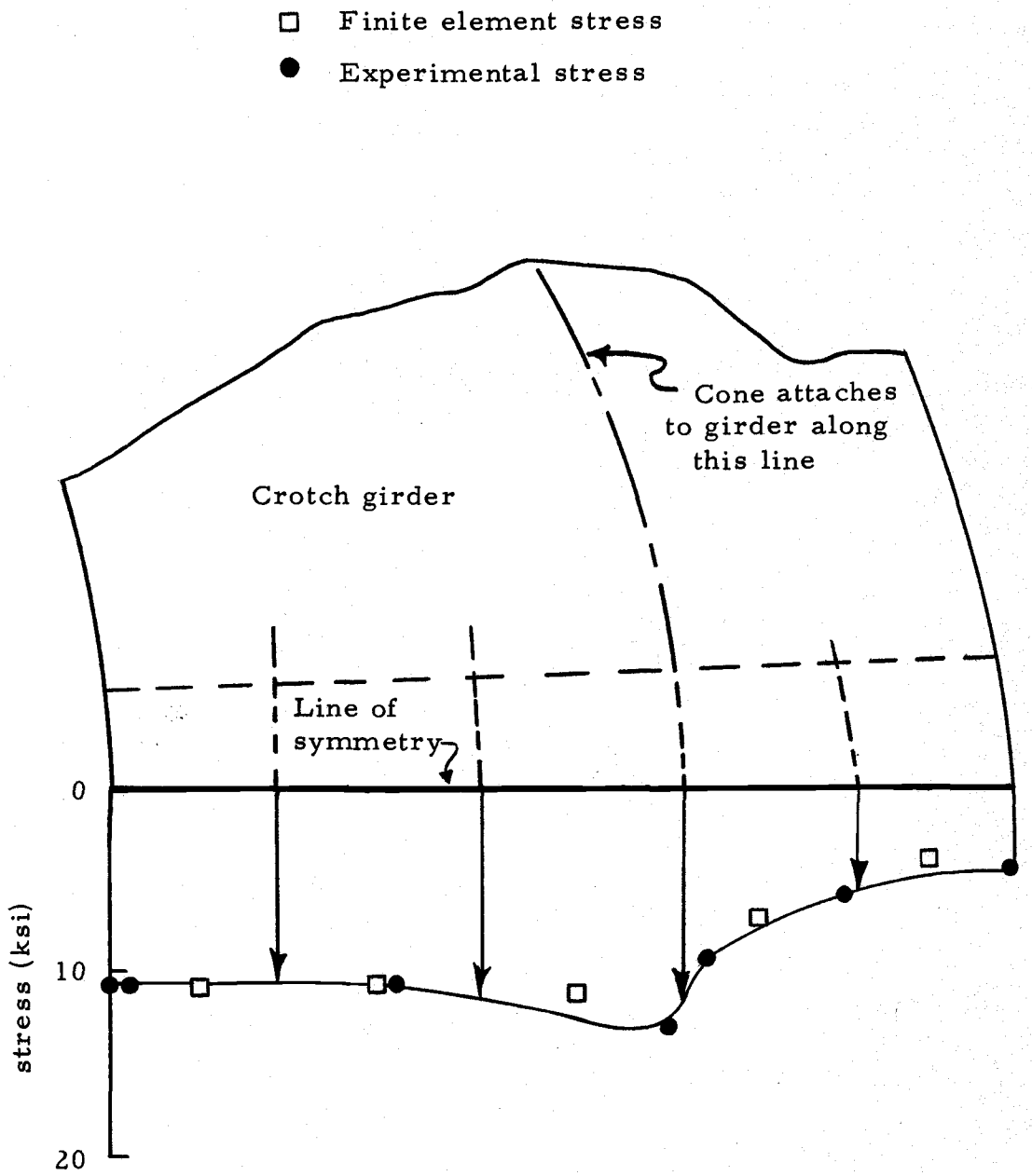

Figure 4.22. Comparison of finite element stresses with experimental stresses at crotch girder line of symmetry.

very well. The measured value was 5400 psi and the predicted value was 5457 psi.

Stresses in the ring girder are compared in Figure 4.23. Here the finite element stresses are plotted for each of the four triangles in a quadrilateral element because the elements are very coarse in comparison to the crotch girder elements. In this way the stress distribution or behavior can better be seen across the two rows of elements. The agreement is good but the finite element values are on the low side. This is probably attributable to the coarse mesh for the ring girder but it is doubtful that a finer mesh is warranted because the overall behavior is modeled and the maximum stresses in the crotch girder were predicted with sufficient accuracy. In addition, the computed stresses shown are plane stresses only and the ring girder does contain some bending stress. The maximum computed bending stress is about 2 ksi and that appears at the top near the intersection with the tie rod. This stress could account for some of the difference in Figure 4.23. Elsewhere in the ring girder, the bending stress varies from the maximum of 2 ksi to less than 1 ksi near the horizontal line of symmetry.

While a sufficient number of strain gages existed on the crotch girder and ring girder, insufficient experimental data was available on the shell portions of the bifurcation for an adequate comparison of data. Principal stresses were measured at 14 locations on the shell

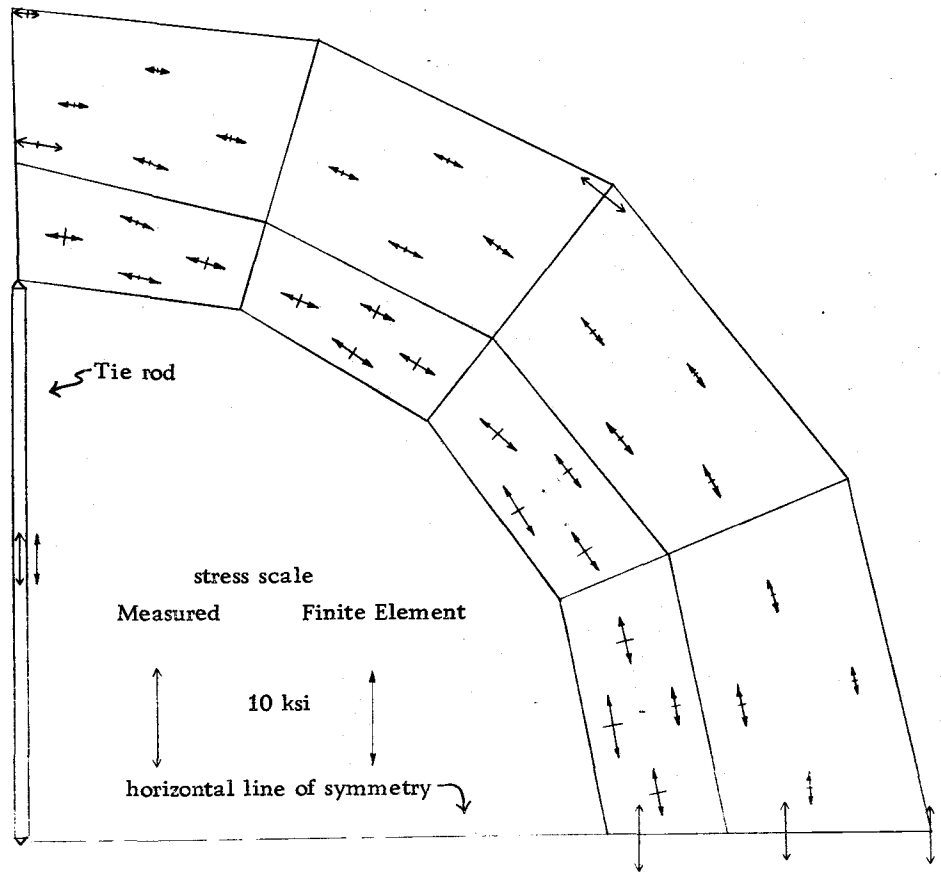

Figure 4.23. Comparison of stresses in the Snettisham ring girder.

as shown in Figure 4.24. Also unavailable was the information as to the strain gages' orientation thus precluding determination of the principal directions.

To facilitate comparison of the available data an "envelope" stress was computed. This "envelope" stress is a summation of the computed principal membrane stress and the computed principal bending stress without regard to their respective directions. The finite element data, in this form, will naturally be larger than the computed total principal stress and therefore is expected to be conservative in comparison with the experimental principal stress. Membrane stress values are also plotted so that the bending stress can be observed by noting the difference between the "envelope" stress and membrane stress. Comparison of stresses for the cylindrical shell are shown in Figure 4.25. The angle θ is measured from the horizontal plane of symmetry to top-center; that is, θ equals zero at points b and d and θ equals 90 degress at points a and c. The results for the cylinder show the actual and computed stresses to be less than the stresses for an equivalently loaded thick-walled cylinder. The hemispherical bulkhead constraint and the ring girder constraint account for this behavior. But the finite element data, it must be concluded, reflects a modeled bulkhead that is too stiff. If the bulkhead were correctly modeled, the envelope stress would be conservative, as mentioned above, and it is not. However, it does

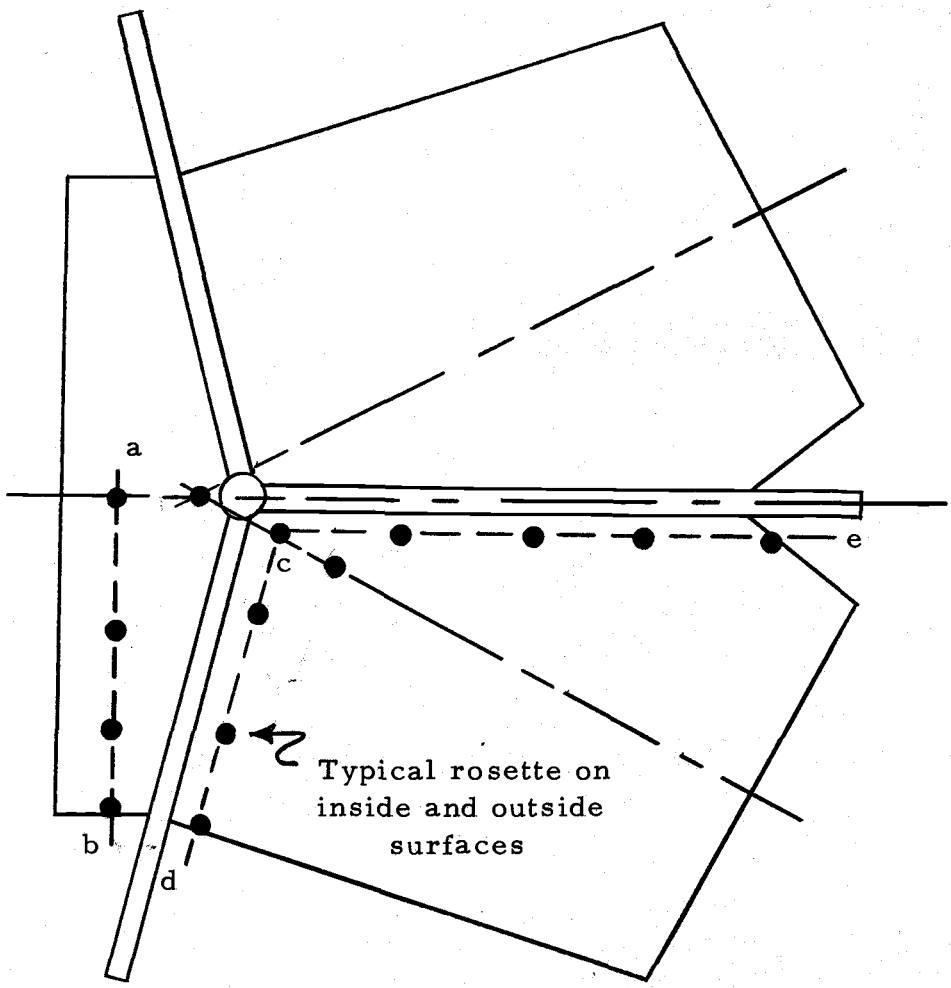

All rosetts are equally spaced along shell curvatures

Figure 4.24. Strain gage rosette locations on Snettisham penstock bifurcation.

appear that the finite element data behaves more rationally than does the experimental data. The effect of the ring girder constraint decreases from point b to point a, gradually allowing the membrane stress to develop. This gradual increase is shown in the finite element data.

The comparison of stresses for the cone along line c-d is shown in Figure 4.26. The finite element "envelope" stress values are conservative for the most part. However, for good agreement, the curve of experimental values should be somewhere between the "envelope" and membrane stress values.

Comparison of stresses for the cone along line c-e is shown in Figure 4.27. The computed values here, except for the data at 4 feet, show better agreement than before. Again, however, where the computed data does not surround the experimental curve it is high and therefore too conservative. The data at 4 feet was taken from an unusually large element in the model and therefore is suspect.

The finite element model from which the above data has been taken can be considered coarse with regard to the stresses near lines c-d and c-e in the conical shell. As can be seen in Figure 4.17, only four elements are used in the direction of curvature to model the 90 degree cylindrical surface and eight elements are used to model the 180 degree cone surface. However, with respect to the crotch girder stresses, the model is adequate.

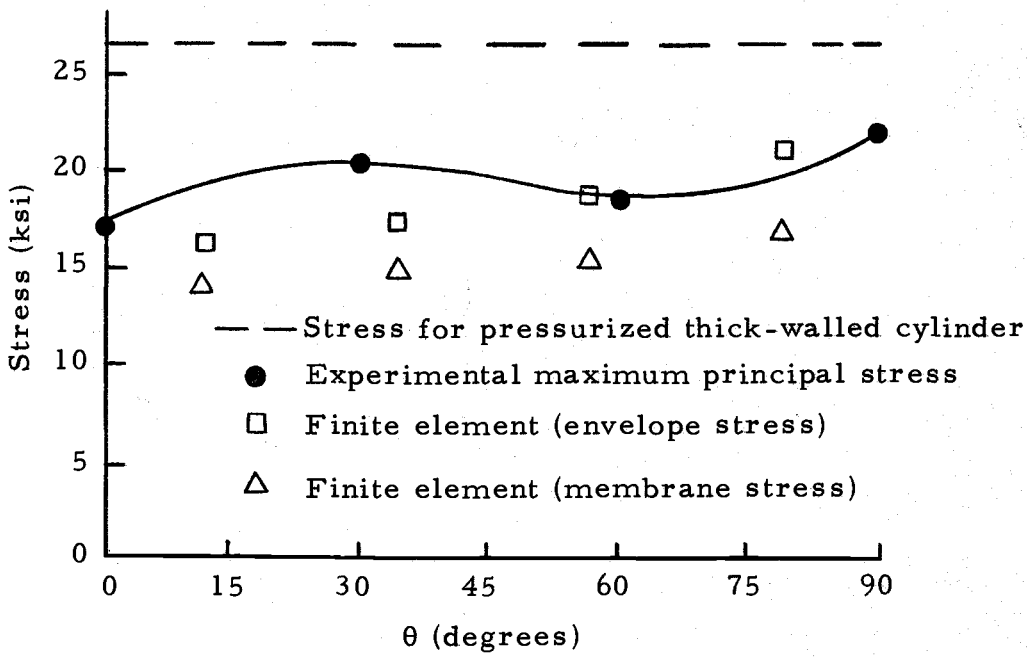

Figure 4. 25. Stress in cylinder along line a-b.

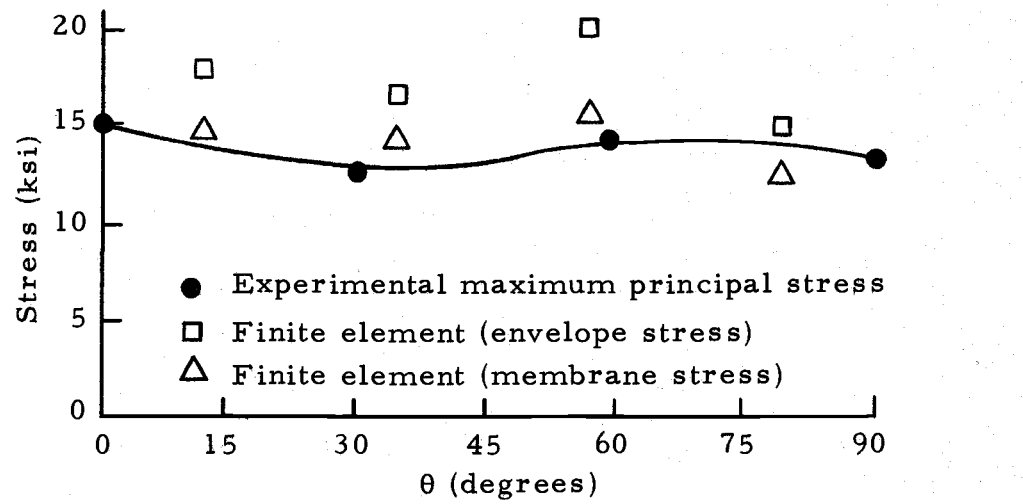

Figure 4. 26. Stress in cone along line c-d.

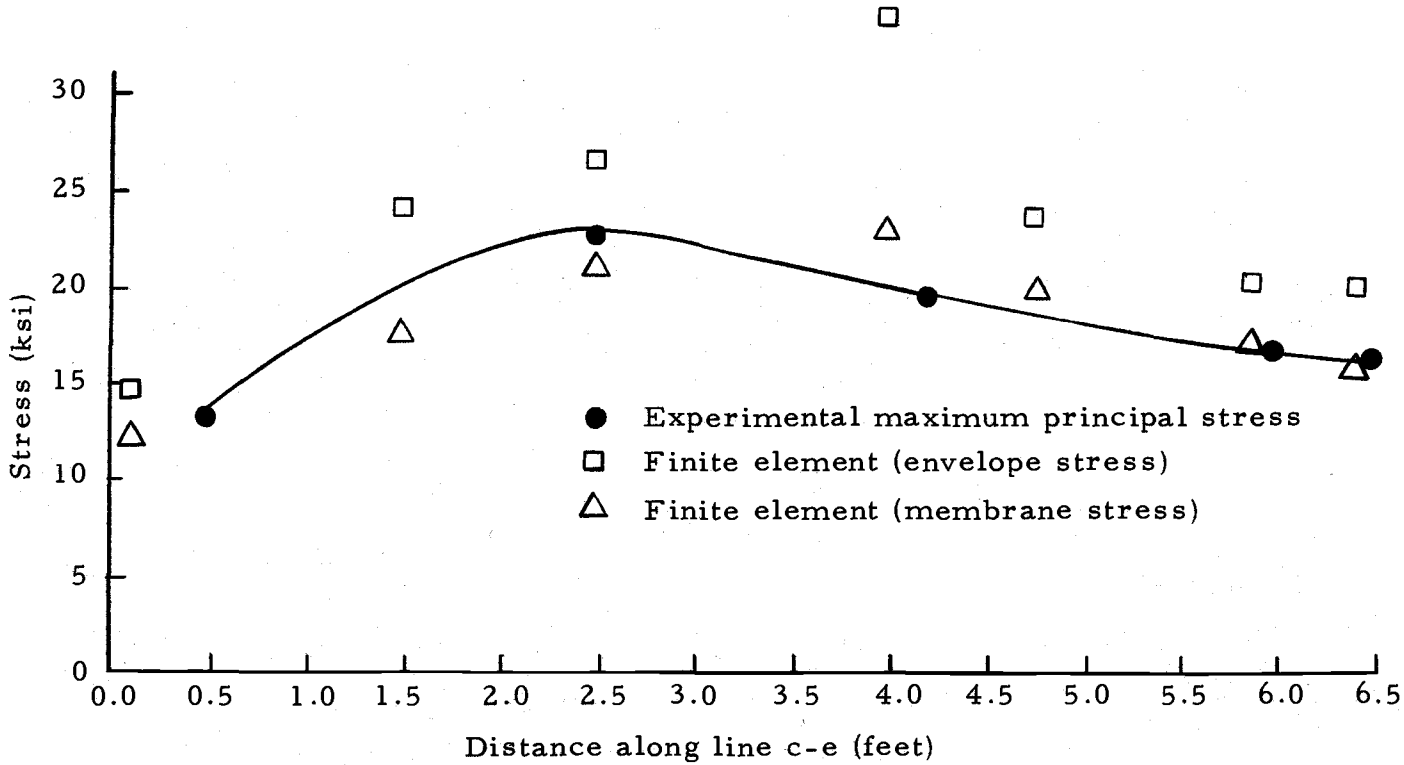

Figure 4.27. Stress in cone along line c-e.

It was noticed that the triangular elements on the conical surface near the crotch girder gave unusually high bending stresses but accurate membrane stresses. The bending stress data for such elements, which are few in number, was ignored in favor of the bending stress data for the quadrilateral elements.

The stresses in the cylinder were unconservative (too small) due to the assumption of infinitely rigid bulkheads. This is also likely to be true for the stresses near the outlet face of the cone, although there is no experimental verification.

V. FINITE ELEMENT STRESS ANALYSIS OF LOST CREEK BIFURCATION

As mentioned in the beginning of this dissertation, the results of the computer program development are applied to the analysis of the penstock bifurcation for the Lost Creek project. The proposed design configuration for the structure is illustrated in Figure 5.1. It is considerably larger than the Snettisham bifurcation (Figure 4.19) but the design load is considerably less; 220 psi internal pressure for the operating load configuration and 330 psi for the hydrostatic test configuration. The design differs noticeably in two respects. First, the crotch girder, for all practical purposes, is entirely external and second, the tie rod is much larger and placed differently.

Because the computer program was written to handle symmetrical bifurcations whose configurations are of the Lost Creek format, no difficulty was experienced in generating the necessary input data. A user's manual for the program, which describes all necessary operations for generating the data, is included as Appendix B. Appendix C describes the function of the primary subroutines and Appendix D is a listing of the program. An 82-element model was generated for the structure and is shown in Figure 5.2. The modulus of elasticity of the steel was assumed to be 30×10^3 ksi and Poisson's ratio was assumed to be 0.3.

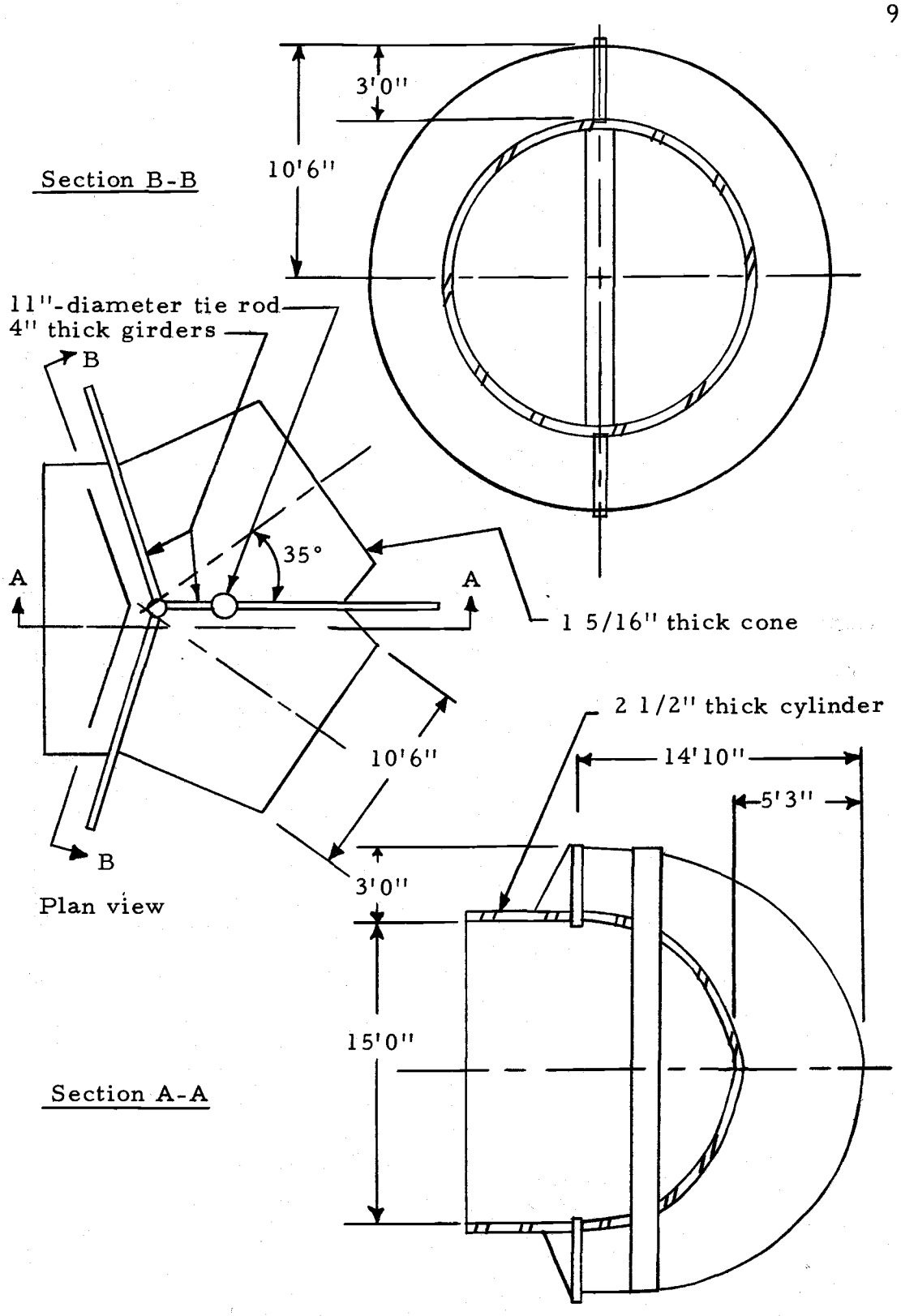

Figure 5.1. Lost Creek penstock bifurcation.

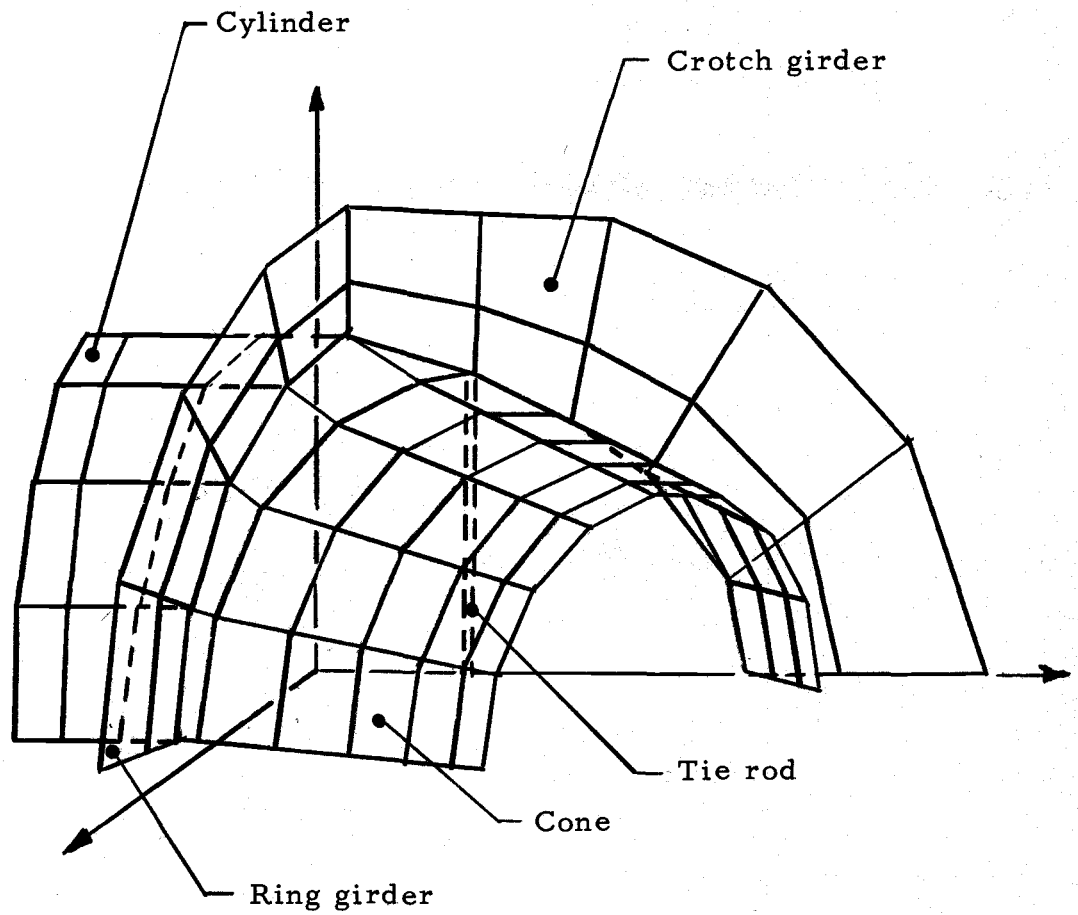

Figure 5. 2. Lost Creek finite element model.

Once the basic input data is generated, the computer program can be used as a design tool by varying the member thicknesses and/or the input geometry in a trial and error fashion. However, no attempt will be made in this investigation to design the Lost Creek bifurcation as this was not an objective of this investigation. An analysis of the present design configuration is undertaken with the added goal of analyzing the effect and structural participation of the tie rod. Two basic configurations are therefore studied. The first contains the tie rod (11 in. in diameter) and the second has a negligibly small tie rod (.0001 in. in diameter). Both of these structures are subjected to the hydrostatic and operating load configurations.

An extensive amount of data is naturally obtained (see Appendix B) from the computer output for each run. It is not possible to present all the data and therefore the data to be discussed is limited to stresses only. In order to present it clearly, it will be discussed in two separate categories. First, the data pertaining to the stiffening members, the crotch girder, the ring girder, and the tie rod, will be presented. This data includes plane stress and axial stress. Second, the data pertaining to the shell portions of the structure, the cylindrical shell and the conical shell, will be presented. This information includes membrane stress and bending stress data.

5.1 Analysis of the Stiffening Members in the Prototype Configuration

With regard to the stiffening members the crotch girder contains the largest stress and it exists, as expected on the inside edge near the horizontal line of symmetry as shown in Figure 5.3. This location is very different from the location of the largest stress for the Snettisham configuration (see Figure 4.22). Moreover, in the Lost Creek configuration, the stresses decrease more rapidly from the maximum on the inside edge of the crotch girder to the minimum stress on the outside edge of the crotch girder along the horizontal line of symmetry and are everywhere tensile. These differences are due to the difference in the locations of the conical shell-crotch girder attachement line or the "load line" for the crotch girder.

Figure 5.4 shows the finite element stresses in the crotch girder for the operating load configuration. It is obvious that the hydrostatic load condition is more severe with regard to the crotch girder stresses. Further comparison of Figures 5.3 and 5.4 reveals, however, that the 11 in.-diameter tie rod is more severely stressed in the operating load configuration. This reflects the existence of the bulkheads in the hydrostatic case which produce a constraining effect on the structure similar to the tie rod. Since the bulkheads are absent in the operating load configuration, the tie rod is allowed to participate structurally to a greater extent, in spite of the reduced

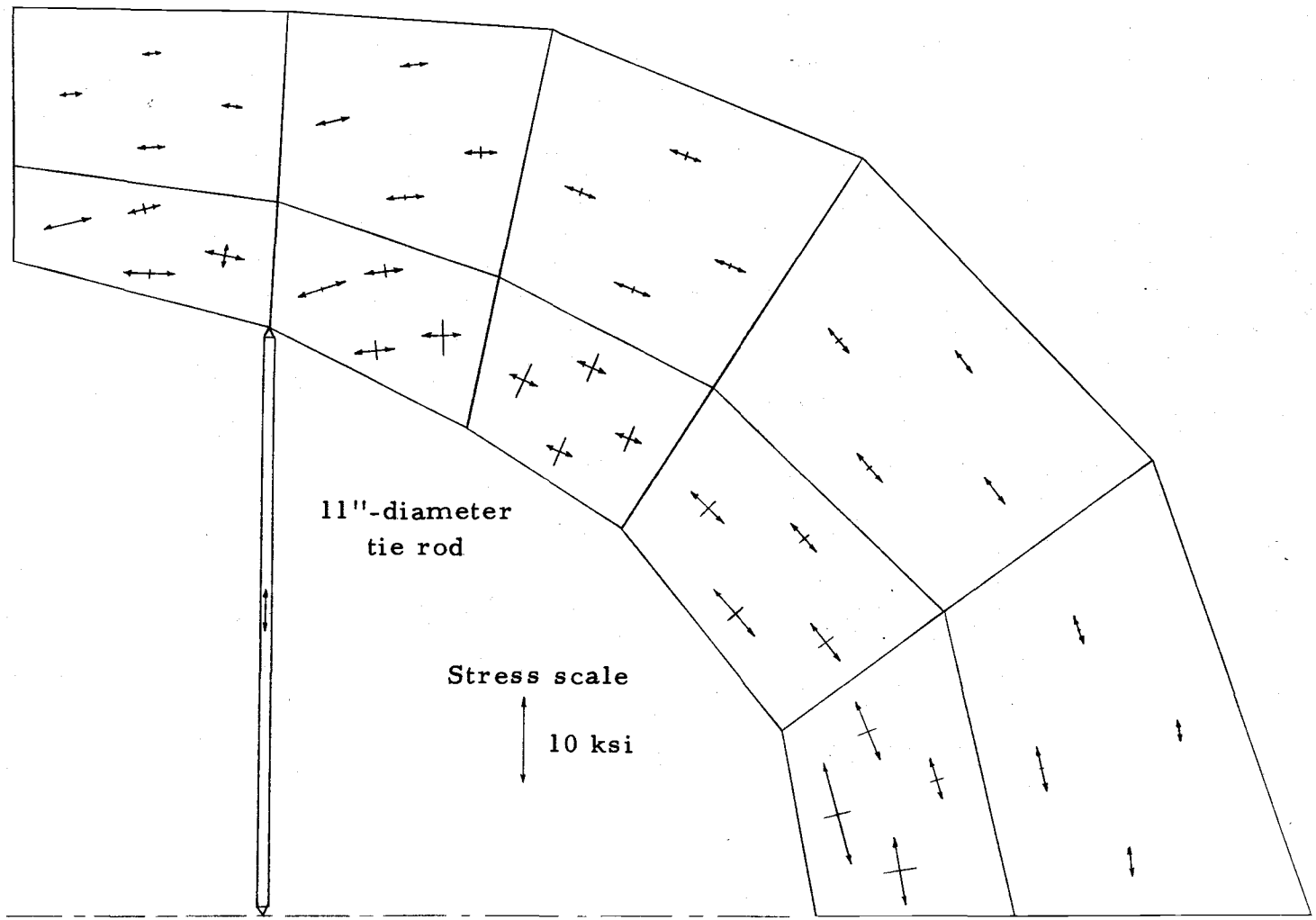

Figure 5.3. Principal stresses in crotch girder and tie rod for hydrostatic test condition.

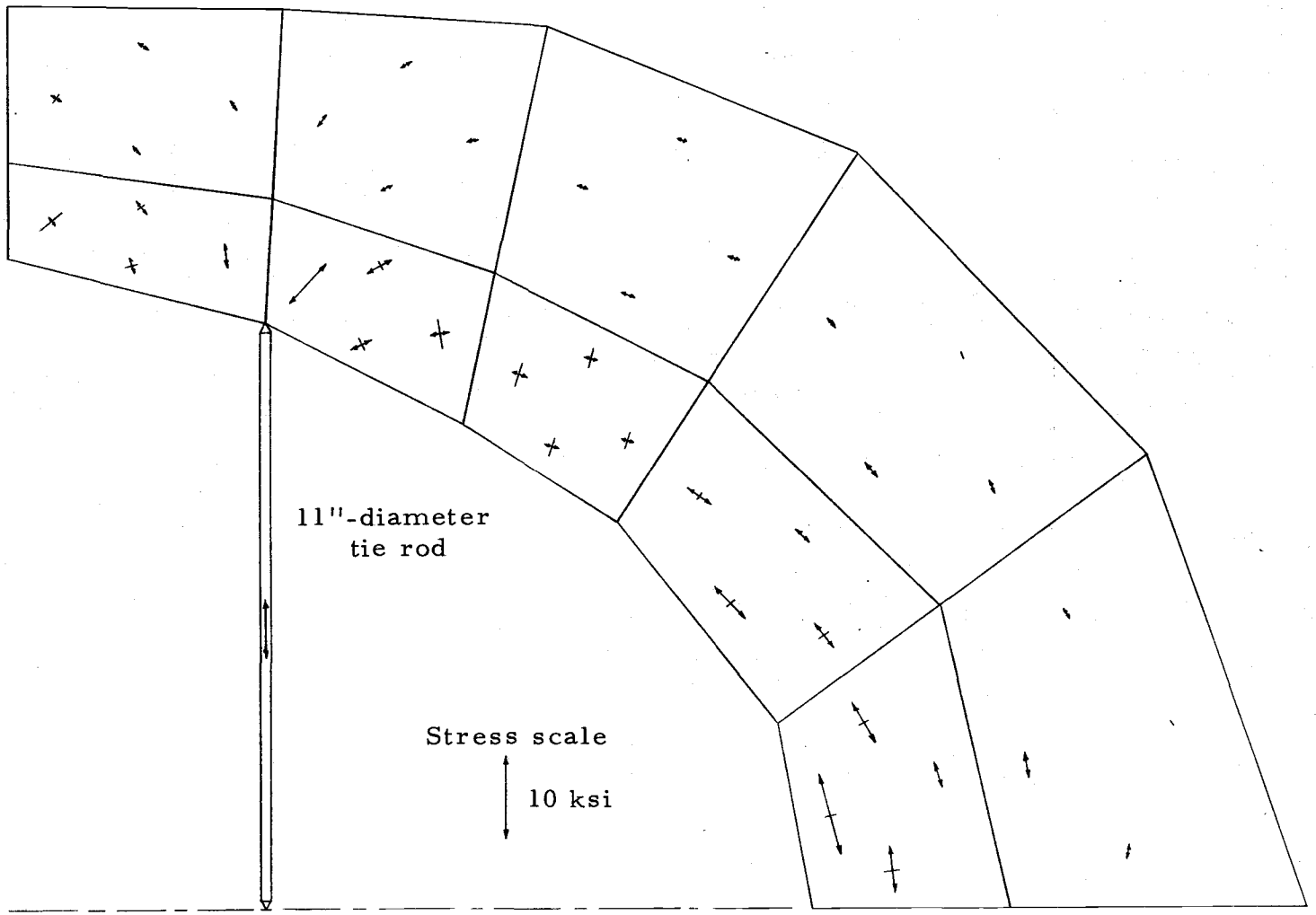

Figure 5.4. Principal stresses in crotch girder and tie rod for operating load condition.

loading. This greater tie rod force is also evident in comparing the principal stress directions at the point where the tie rod attaches to the crotch girder. The changes in principal directions are more pronounced near the point of attachment in the operating load configuration.

The stresses in the ring girder are shown for the hydrostatic load configuration in Figure 5.5 and the operating load configuration in Figure 5.6. They are rather small in each case. Even though the maximum stress occurs for the operating configuration, they are slightly larger for the hydrostatic load configuration from an overall point of view. The stress distribution along the horizontal plane of symmetry is similar to that in the crotch girder except the magnitudes are smaller, that is, the stresses vary from a maximum on the inside edge to a minimum on the outside edge and are everywhere tensile. This behavior is not duplicated on a cross-section near the top. Instead, the stresses across the ring girder are fairly constant (tensile) for the hydrostatic configuration. For the operating load configuration they vary from a minimum on the inside edge to a maximum on the outside edge; just the reverse of the stress distribution along the horizontal plane of symmetry. This tendency is present in the hydrostatic configuration but is only barely discernible.

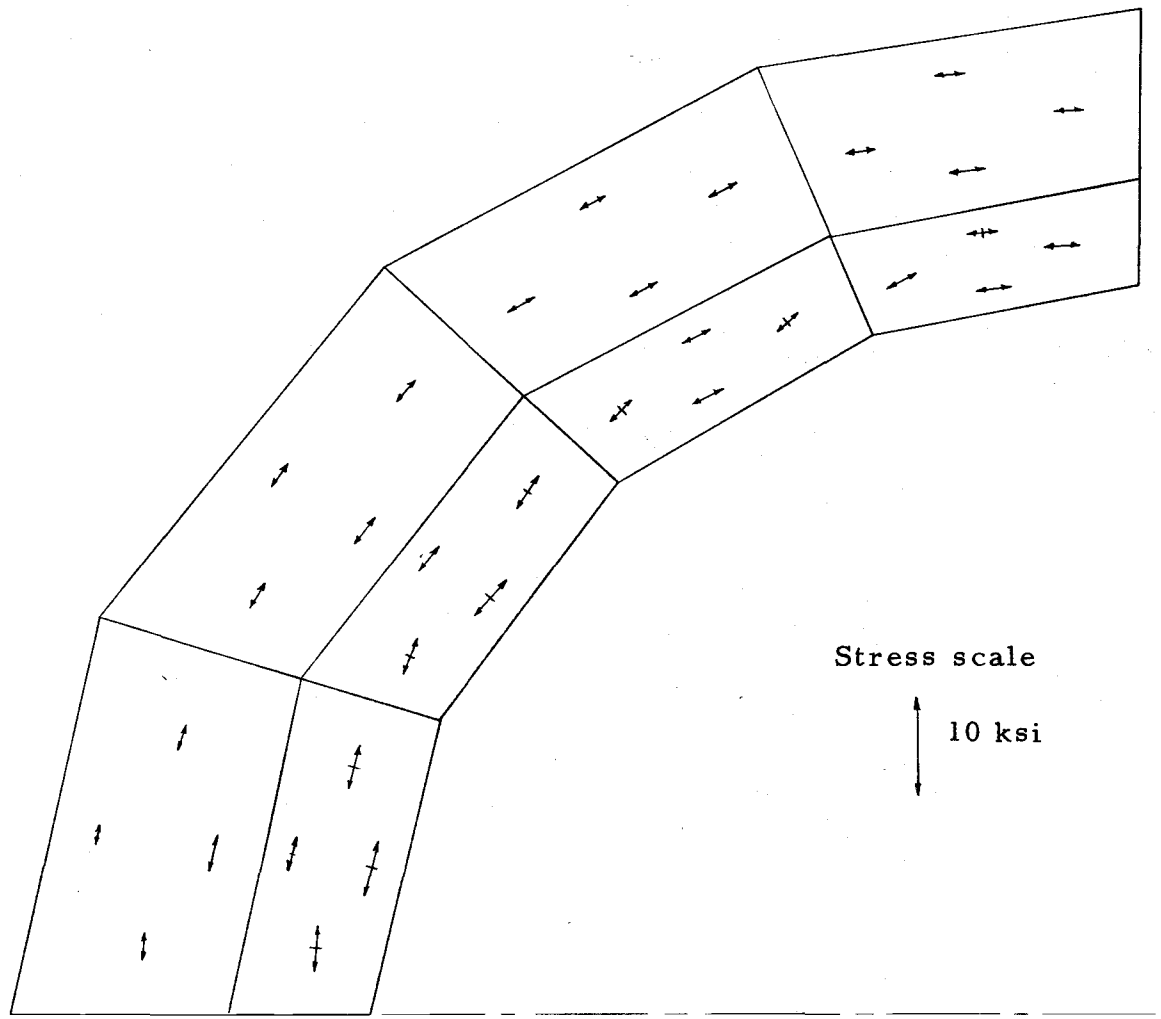

Figure 5.5. Principal stresses in ring girder for hydrostatic test configuration.

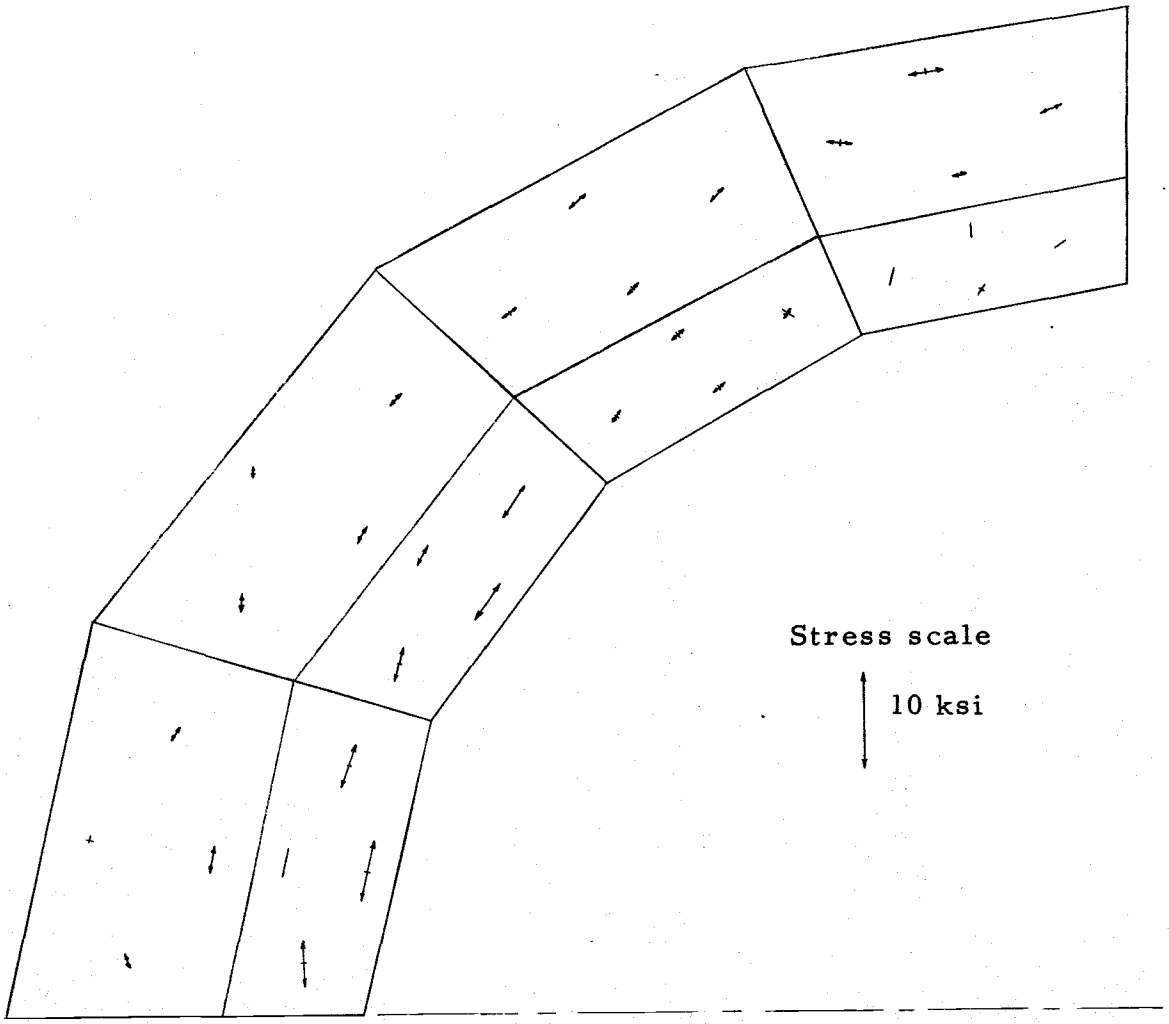

Figure 5.6. Principal stresses in ring girder for operating condition.

5.2 Analysis of the Stiffening Members Without the Tie Rod

The study of the behavior of the stiffening members without the tie rod was effected by assigning a rod diameter value of 0.0001 in. in the input data and repeating the computer run for both loading conditions. Figure 5.7 shows the stresses that result in the crotch girder for the hydrostatic load configuration. The maximum stress occurs at the same location but is increased by about 25%. The stress variation along the horizontal line of symmetry can be seen to be more pronounced when compared with the data for the 11 in-diameter tie rod (Figure 5.3). While the stress on the inside edge is greater the stress on the outside edge is smaller. Also it can be seen that no concentrated stresses are induced in the proximity of the tie rod attachment point. The stress-flow bypasses this area exhibiting little change in principal direction. The reduced magnitudes just to the right of the attachment point reflect the tendency of the stress distribution across the crotch girder to gradually change to a maximum stress on the outside edge and a minimum stress on the inside edge. This tendency is not fully developed at the top of the crotch girder in the hydrostatic configuration. However, the data for the crotch girder in the operating condition shown in Figure 5.8 better illustrates this reversal in stress distribution. This behavior is the same as that mentioned in Section 5.1 for the ring girder. Thus, without the tie

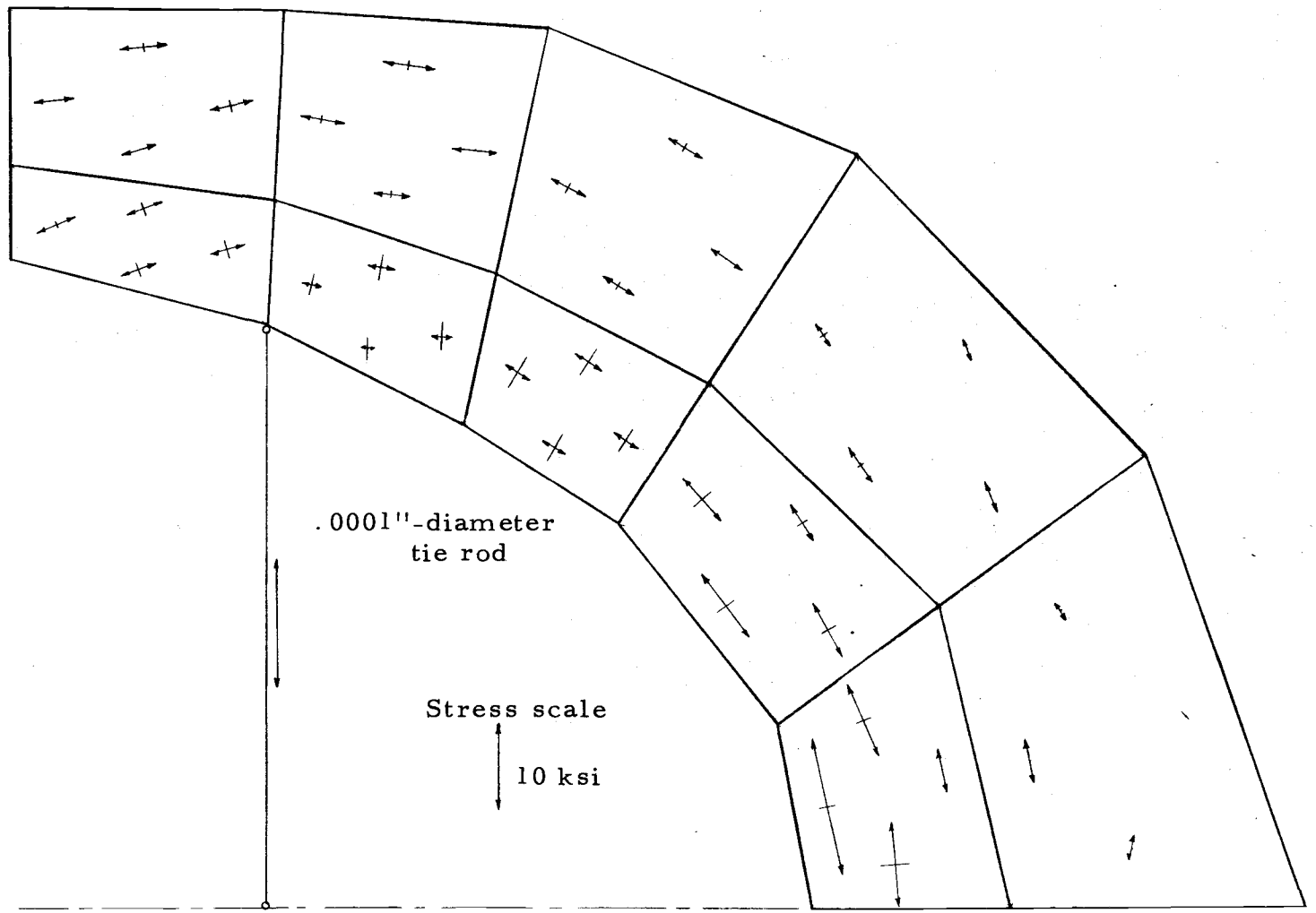

Figure 5.7. Principal stresses in crotch girder and small tie rod for hydrostatic test condition.

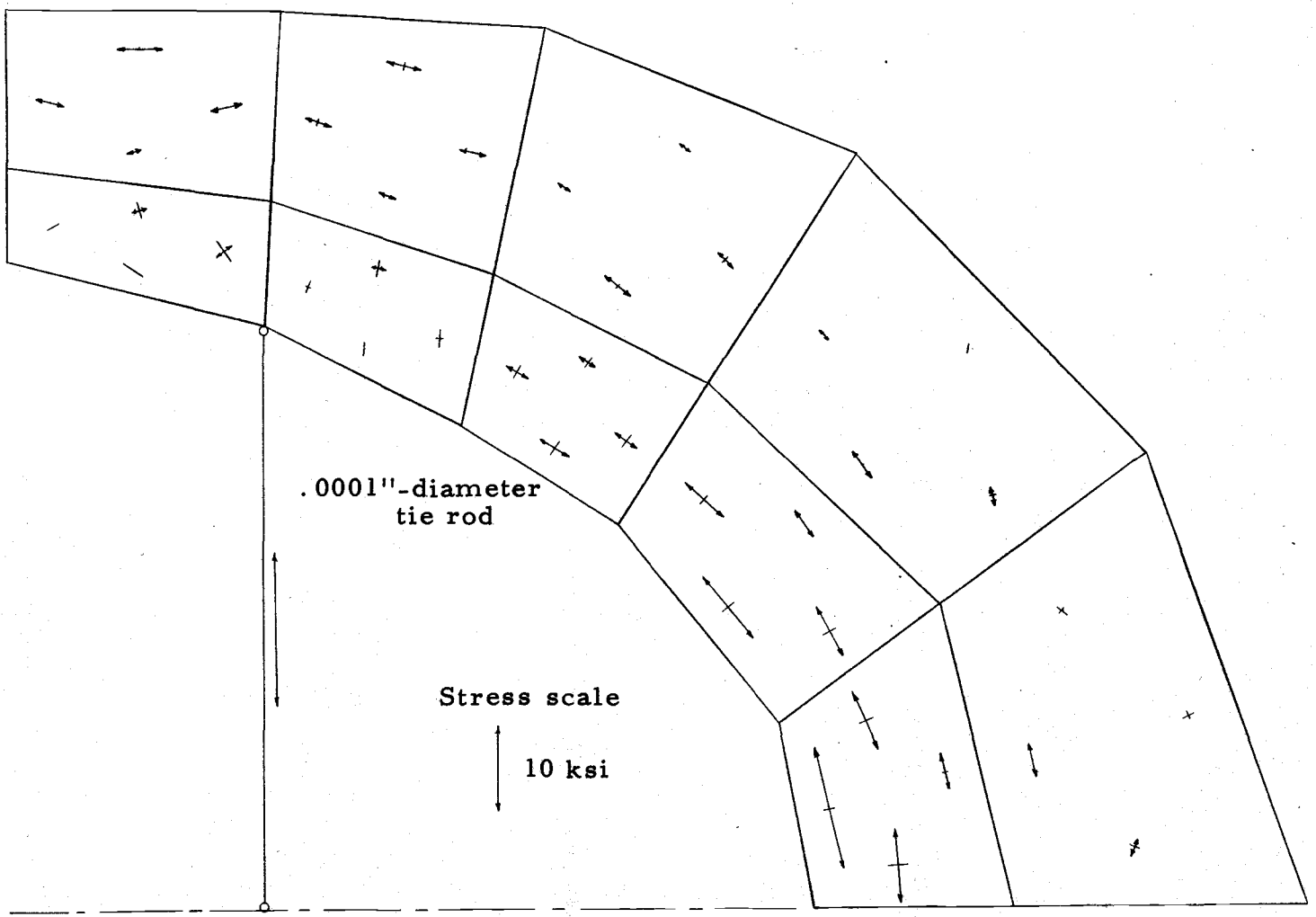

Figure 5.8. Principal stresses in crotch girder and small tie rod for operating condition.

rod, the crotch girder participates structurally in the same manner as the ring girder. In addition, it participates to a greater extent; the stress levels being generally larger and the stress flow being less disturbed.

It is also of interest in regard to Figure 5.8 that the maximum stress in the crotch girder for the operating condition increases by about 45% (compare with Figure 5.4) due to the absence of the tie rod. Nevertheless, the largest stress occurs for the hydrostatic case as it did in the tie rod configuration.

The effect of the tie rod's absence on the ring girder is to increase the stress levels everywhere in a fairly proportionate manner. Figures 5.9 and 5.10 represent the data for the hydrostatic and operating load configurations, respectively. When this data is compared with that of the prototype data (Figures 5.5 and 5.6), this proportionate increase can be seen. In addition, the maximum stress is increased by about 20% for the hydrostatic configuration and about 27% for the operating load configuration.

5.3 Analysis of the Shell Members in the Prototype Configuration

The stress data for the cylindrical shell and conical shell is presented in graphs as opposed to plotting stresses on the member configuration as was done for the stiffening members. Such a

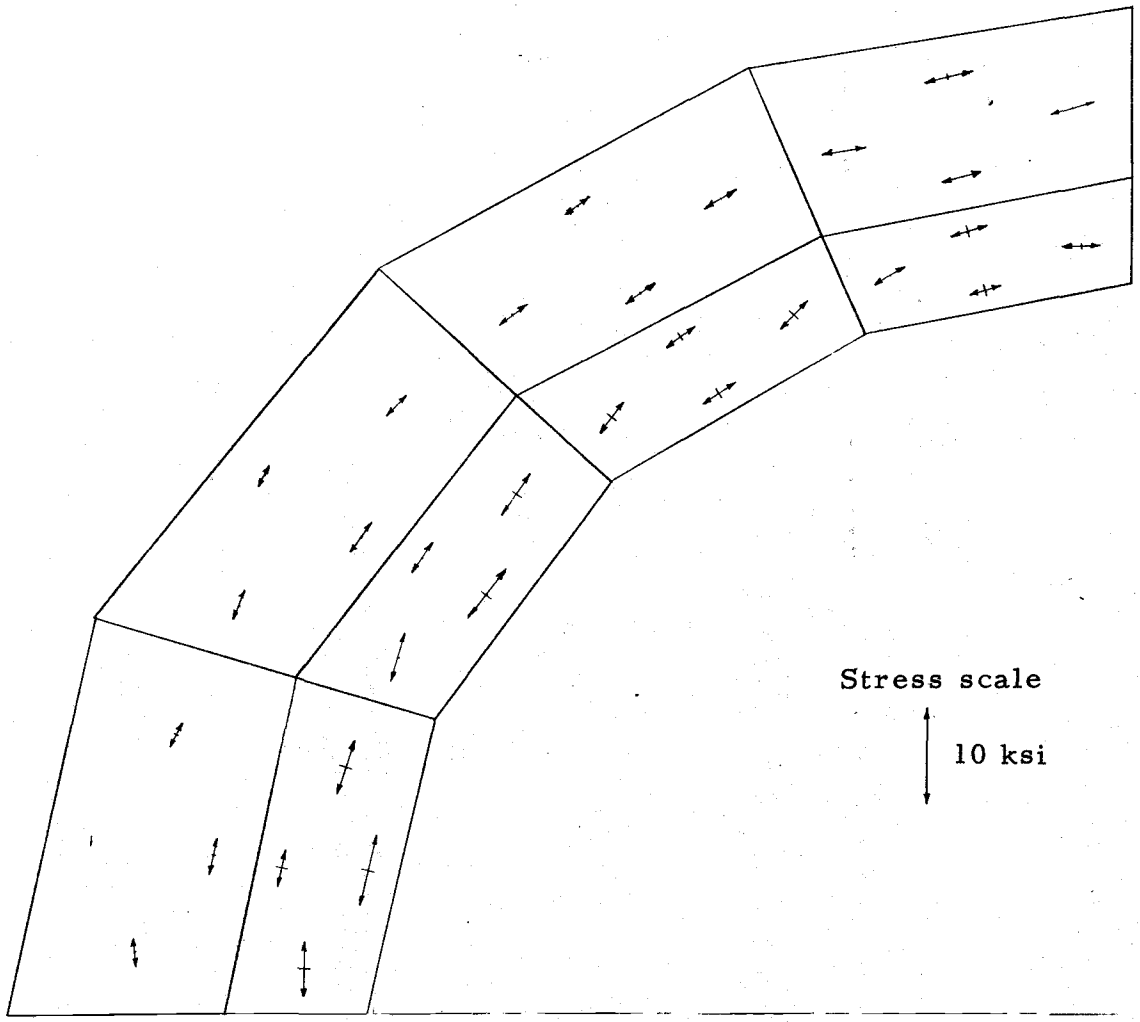

Figure 5.9. Principal stresses in ring girder as affected by small tie rod for hydrostatic condition.

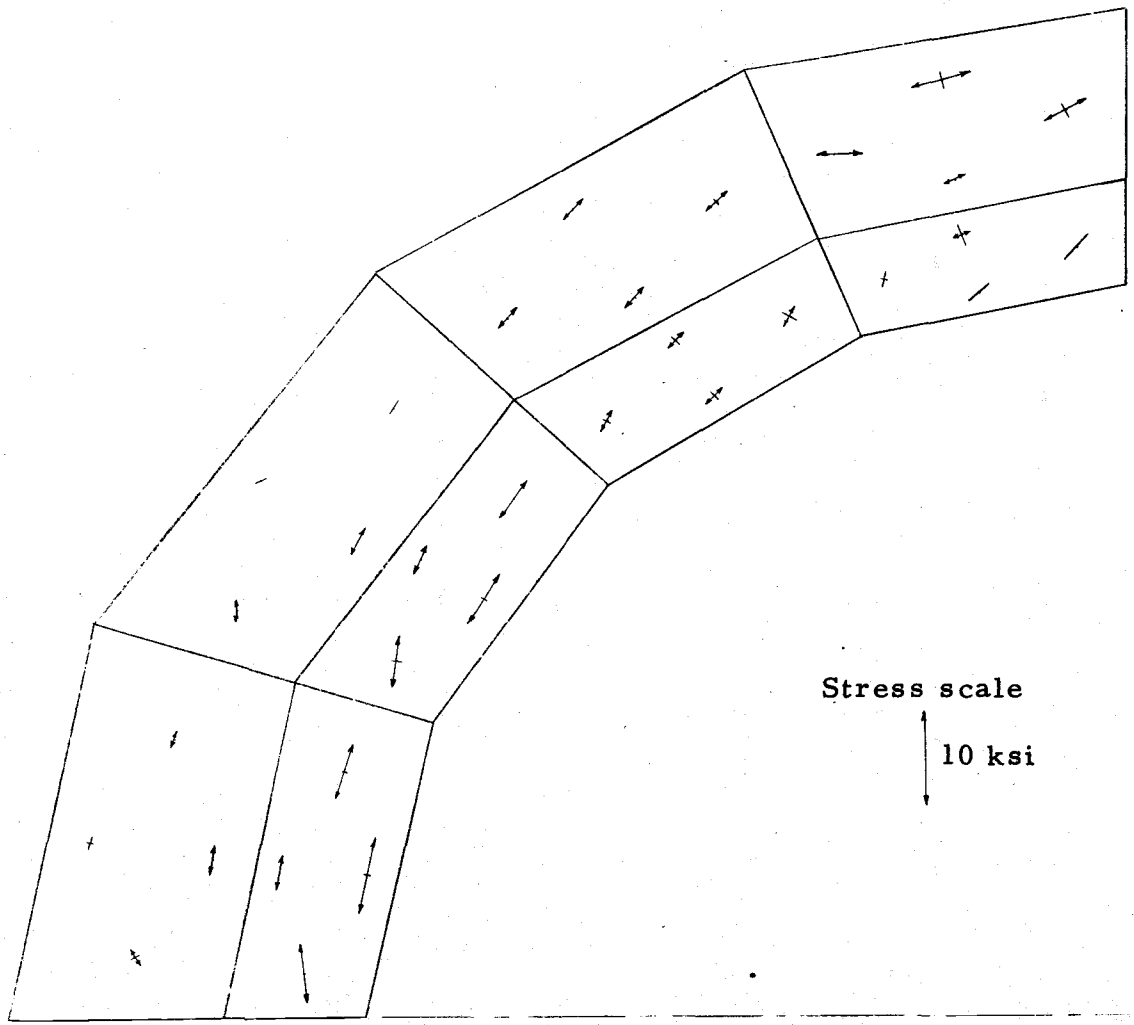

Figure 5.10. Principal stresses in ring girder as affected by small tie rod for operating condition.

procedure for the shell surfaces, though perhaps more revealing from an overall standpoint, does not permit sufficient scale to emphasize the relative amount of bending stress as compared to membrane stress. The distinction between these two types of stress is paramount because the bending stresses in the shells have been heretofore generally ignored in the analysis of penstock bifurcations.

A reference diagram for subsequent graphs is given in Figure 5.11. A preliminary survey of the shell stress data revealed the locations which were most highly stressed and, based on that survey, the sections shown in Figure 5.11 were chosen. In addition, the locations in the shell immediately adjacent to the girders are of interest because they are likely to contain significant bending stresses. Unless otherwise noted in the graphs to follow, the membrane stress and the total stress are both plotted. The bending stress is observed by noting the difference between these two stresses. The total stress is plotted for one surface, either inside or outside, whichever is more severely stressed.

The data for the cylinder is shown in Figures 5.12a and 5.12b. The angle θ is referenced to point a and has a value of 90 degrees at point b. The hoop stresses in Figure 5.12a are compared with the hoop stress in a pressurized thick-walled cylinder. The data for the hydrostatic case is similar to the data for the Snettisham bifurcation (Figure 4.25) in that they are both conservative

when compared to the thick-walled cylinder, though the Lost Creek data is less so. Again this must be attributed to the constraint of the bulkhead attached to the cylinder in the hydrostatic configuration. With the bulkhead removed (the operating configuration), the hoop stresses are seen to approximate more closely the thick-walled cylinder stress. The bending stresses, as expected, are very small in the hoop direction.

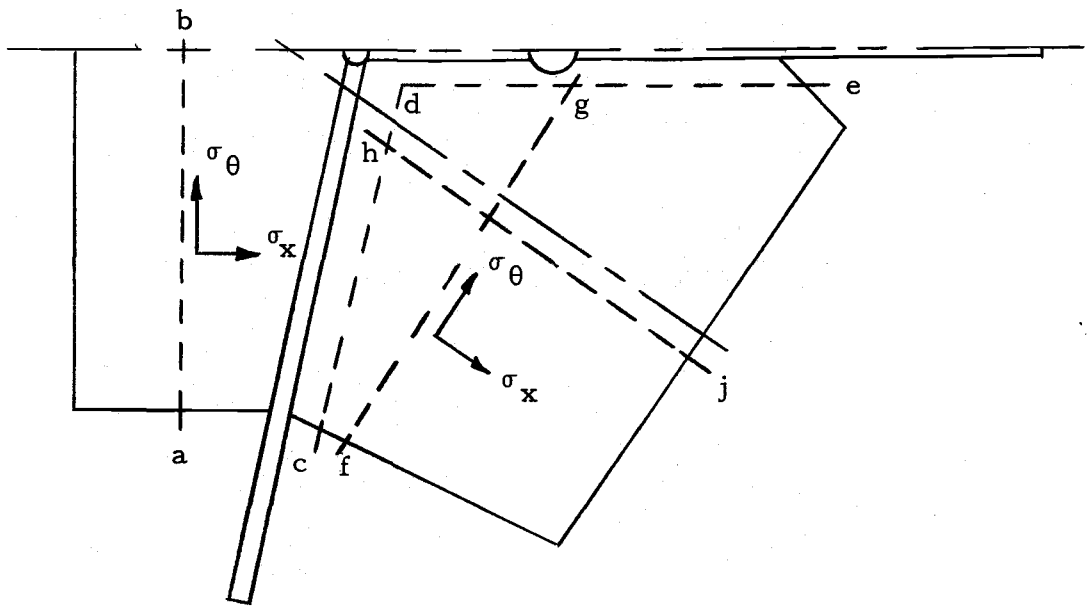

Figure 5.11. Reference diagram for shell stresses.

The longitudinal stresses in the cylinder are shown in Figure 5.12b as they vary along line a-b. The membrane stresses for the hydrostatic condition approximates closely the longitudinal stresses for a closed cylinder. In the operating condition these stresses, of

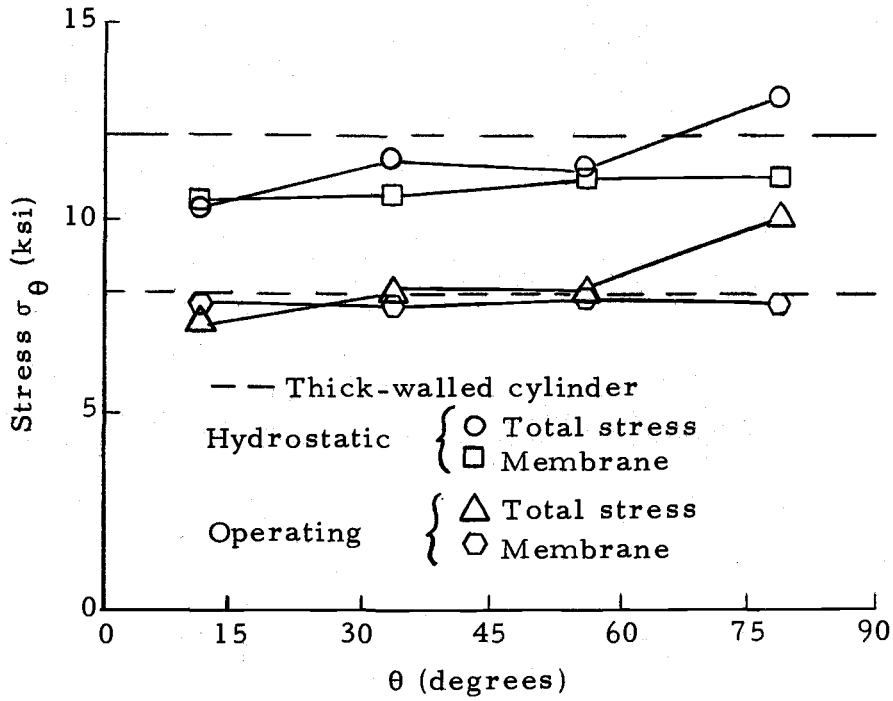

Figure 5.12a. Hoop stress on outside surface along line a-b.

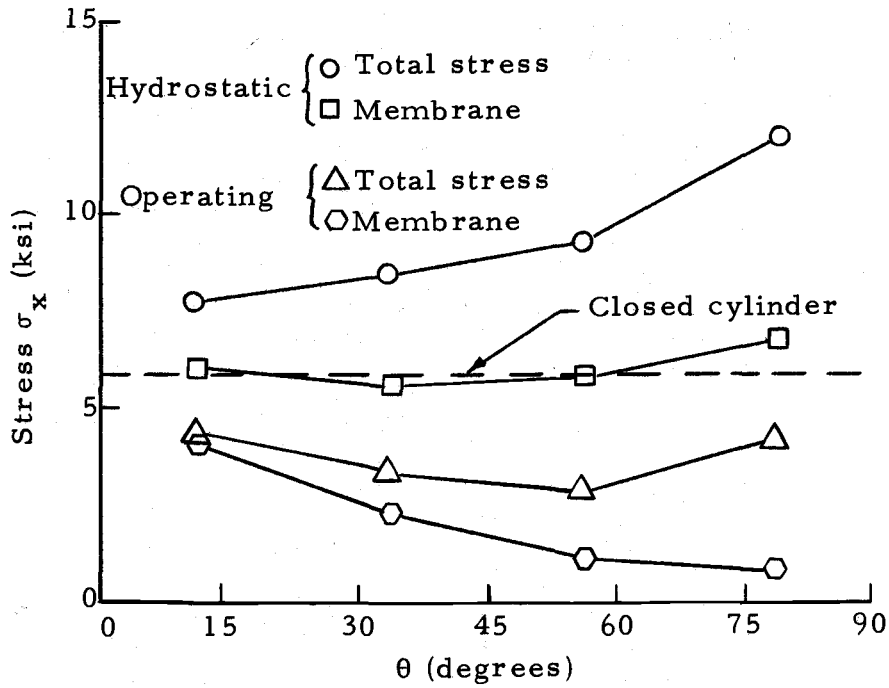

Figure 5.12b. Longitudinal stress on outside surface along line a-b.

course, drop off markedly because the cylinder is not closed at its end. The bending stresses are more significant in the longitudinal direction than in the hoop direction. They appear to increase from point a to point b to a maximum at the top of the cylinder. Nevertheless, the maximum stresses in the cylinder are in the hoop direction as can be seen by comparing Figures 5.12a and 5.12b.

The stresses in the cone along lines c-d and d-e are plotted in the same manner as the finite element data in Section 4.4. That is, the principal membrane stress and the principal bending stress are superimposed without regard to their respective directions. The sum that results is termed the "envelope" stress. Plotted with this stress is the maximum principal membrane stress. By noting the difference between the two, the maximum principal bending stress is observed. In this manner the bending stress along lines c-d and d-e is emphasized. However the computed total stress (true maximum stress) along these lines most probably lies between the two data points at each station where data is plotted.

The stress data for Figure 5.13 was taken from the row of four quadrilateral elements on the cone which border the ring girder (see Figure 5.2). The angle θ is referenced to point c and has a value of 90 degrees at point d. It can be seen that the principal bending stress is considerable when compared to the principal membrane stress, especially at the smaller angles. There is a reversal in

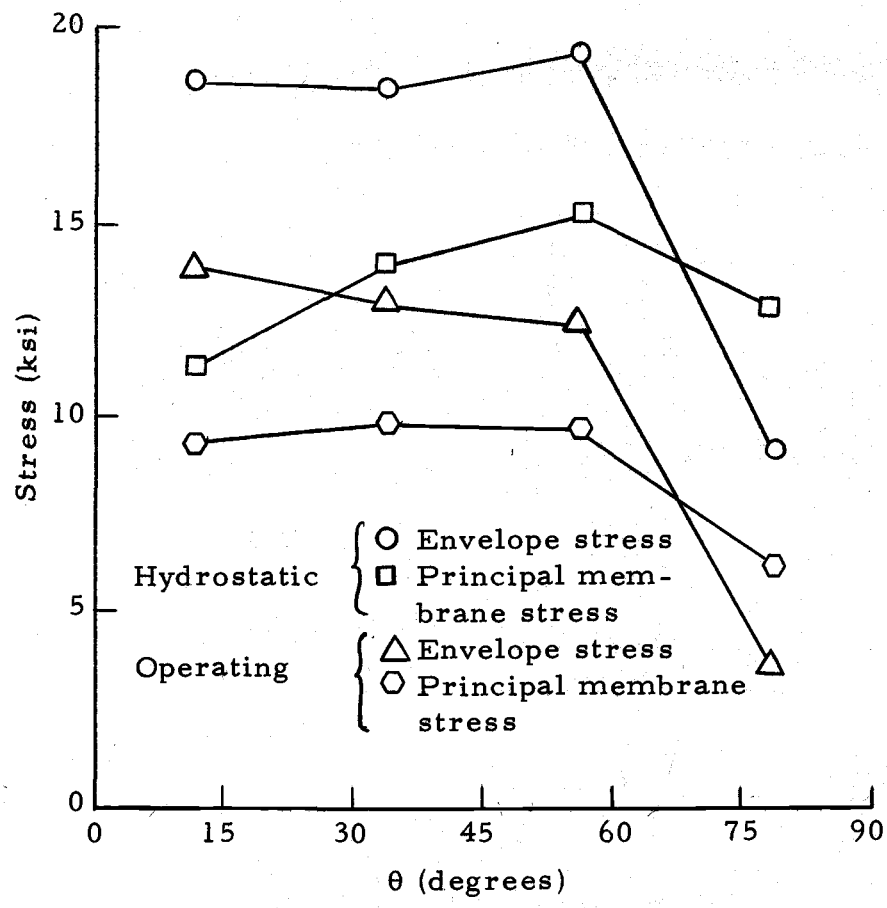

Figure 5.13. Stress on inside surface along line c-d.

the sign of the moment at about 70 degrees.

The data for the stresses along line d-e in Figure 5.14 was taken from the quadrilateral elements on the cone nearest the crotch girder. Triangular-element moment data was found suspect in the experimental verification study of Section 4.4 and therefore this data was purposely avoided. Because there are four triangular elements bordering the girder the data plotted does not represent stresses in the cone immediately adjacent to the crotch girder, but instead about 1.5 to 2 feet away. The bending stresses are significant in the region of the tie rod, but drop off toward point e where a reversal in the sign of the moment takes place. It is suspected, though no data is available for support, that the moment in the cone closer to the crotch girder is even larger than that shown. Combining this suspected moment with the large membrane stresses (18-19 ksi in the hydrostatic configuration) computed for the triangular elements (triangular element membrane stresses are believed reliable) a potentially localized high stress could exist in the cone near the tie rod for the hydrostatic configuration.

The hoop stresses in the cone along line f-g are plotted in Figure 5.15a. The angle θ is referenced to point f and has a value of 112.5 degrees at point g. This data and that of the following graph were taken from the five quadrilateral elements, two rows out from the ring girder (see Figure 5.2). The membrane stresses in

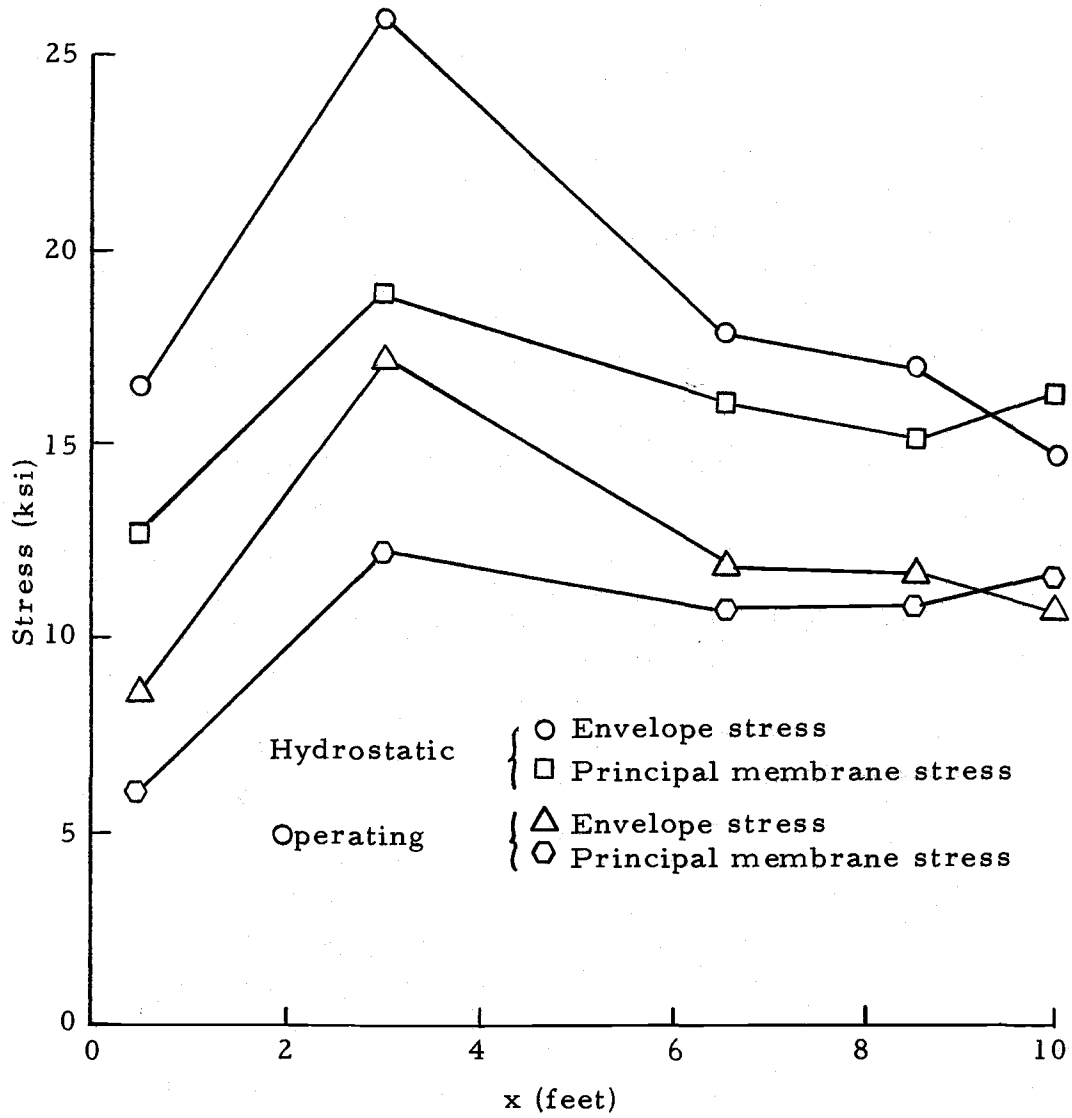

Figure 5.14. Stress on outside surface along line d-e.

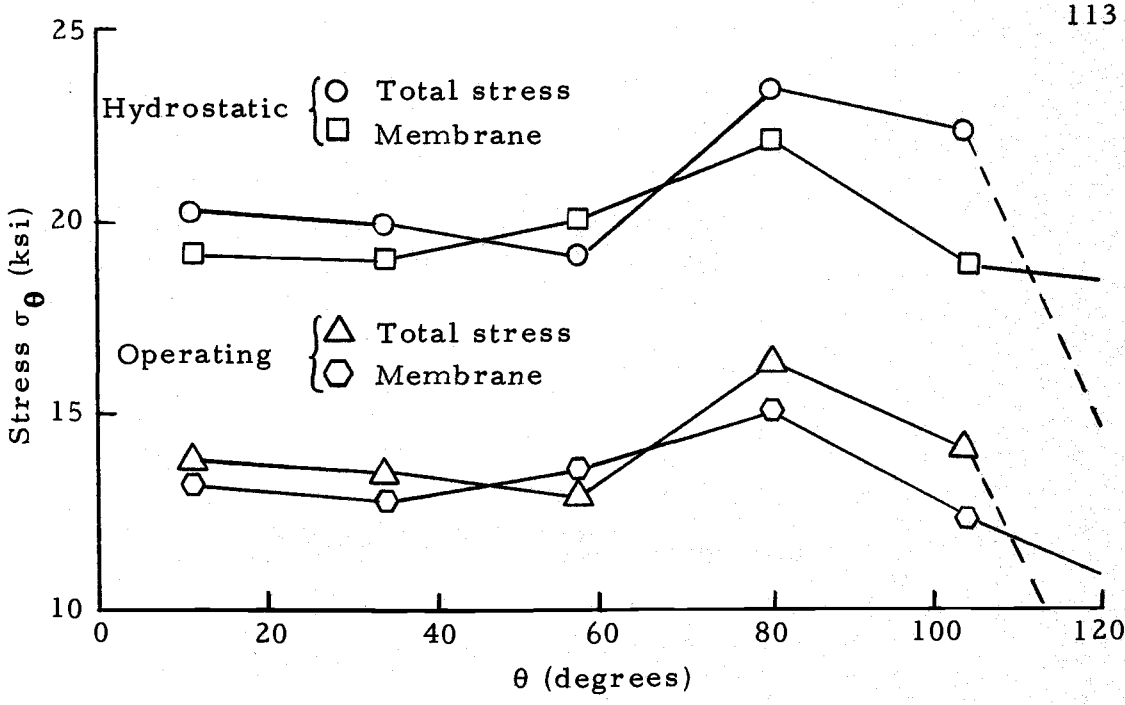

Figure 5.15a. Hoop stress on outside surface along line f-g.

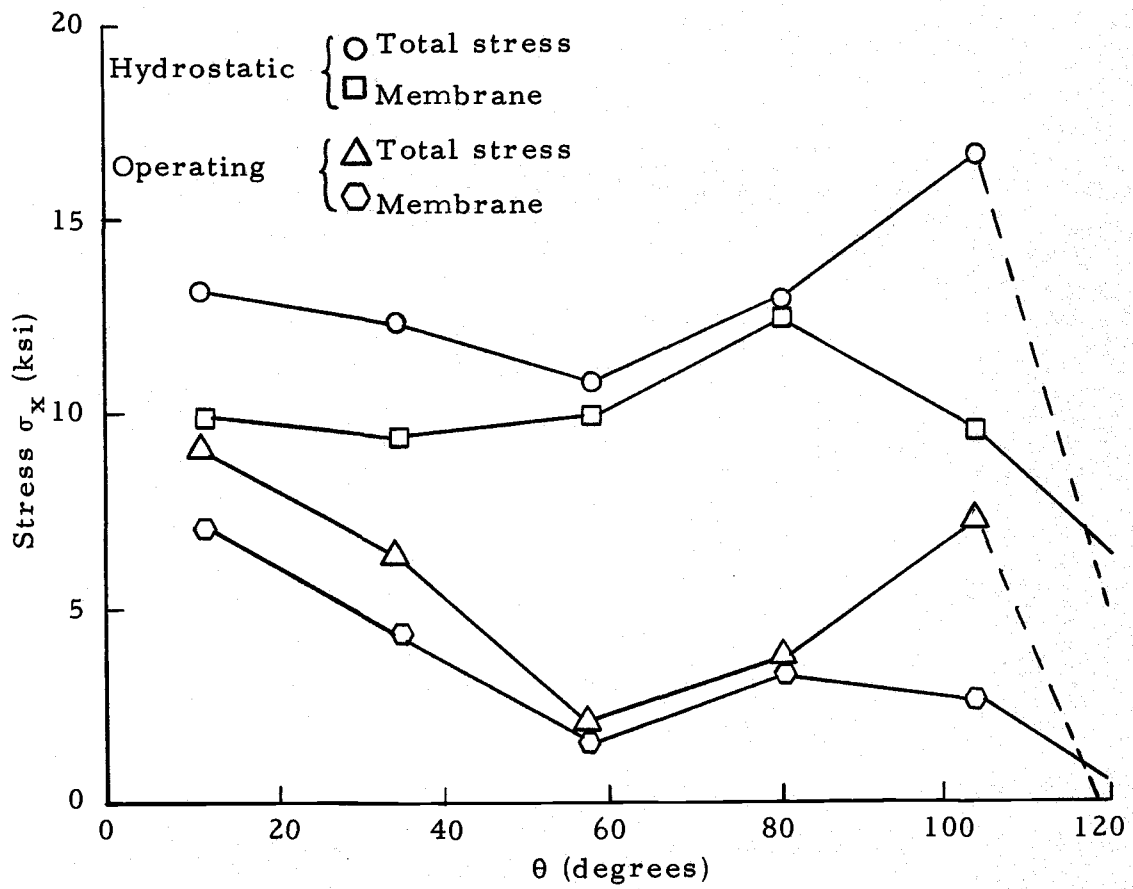

Figure 5.15b. Longitudinal stress on outside surface along line f-g.

Figure 5.15a for the hydrostatic case with $\theta \approx 80$ degrees is the highest computed membrane stress in the structure. This is to be expected because line f-g is near the largest circumference on the cone which is sufficiently removed from the constraining ring girder. The influence of the ring girder gradually diminishes as θ is increased from zero to 80 degrees allowing this hoop stress to gradually develop. Fortunately, the accompanying bending stress is rather small up to 80 degrees. The bending stress thereafter increases before it undergoes a reversal in sign. The dotted line is an extrapolation of the bending stress which is only suspected as was discussed above in connection with the stresses along line d-e.

The bending stress variation in Figure 5.15b reflects the ring girder constraint. It is large near point f which is nearest the ring girder. Thereafter, the moment decreases to its minimum value at about 80 degrees as the line f-g diverges from the ring girder. At angles greater than 80 degrees, the moment increases and then reverses due to the proximity of the constraining crotch girder. The stresses in the longitudinal direction, however, are smaller than the hoop stresses along line f-g.

Stress data for line h-j is taken from a row of quadrilateral elements along top-center of the cone. The cone is approximately 10 feet long at this location and this distance is measured from point h to point j along the abscissa in the next two graphs. Figure

5.16a shows the hoop stresses as they are constrained by the girders near point h and as they rapidly increase to their maximum value at about 4 feet. This value is the same maximum stress discussed for the stresses along line f-g (see Figure 5.15a). Beyond the 4-foot station the hoop stresses for both load conditions decrease gradually as the circumference of the cone decreases. The obvious difference in behavior near point j is due to the constraining effect of the bulkhead at the outlet face of the cone in the hydrostatic configuration. The data for the operating configuration continues the gradual decrease in hoop stress to the end of the cone. Bending stresses along this line are fairly small and decrease to zero near the end of the cone.

The longitudinal stresses along line h-j are shown in Figure 5.16b. The membrane stresses behave similar to the membrane stresses in the hoop direction although not as pronounced. The bending stresses are largest near the extremities of line h-j. This is due to the ring girder constraint near point h and the bulkhead constraint near point j. It is also interesting to note that the longitudinal stresses near point j are in compression for the operating condition. This compression zone is localized and the stress magnitudes are small. By comparing Figures 5.16a and 5.16b it is seen that the hoop stresses are again the larger of the two stress components.

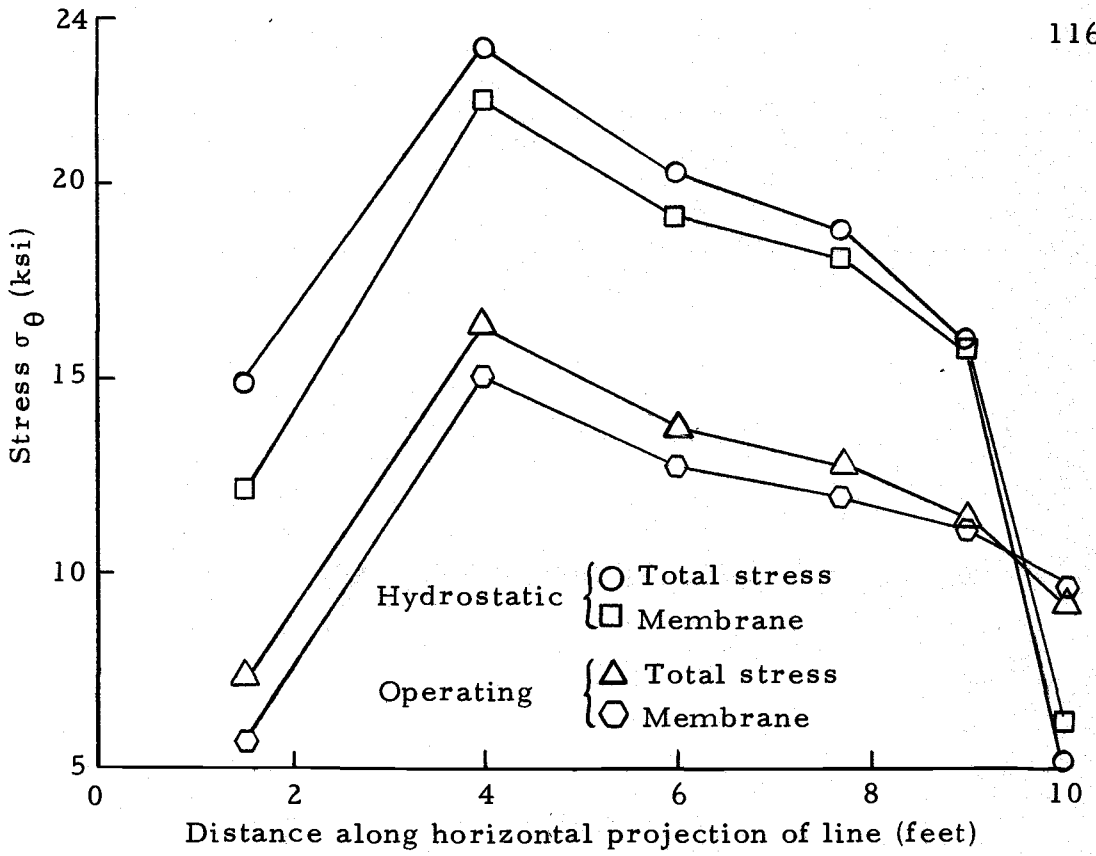

Figure 5.16a. Hoop stresses on outside surface along line h-j.

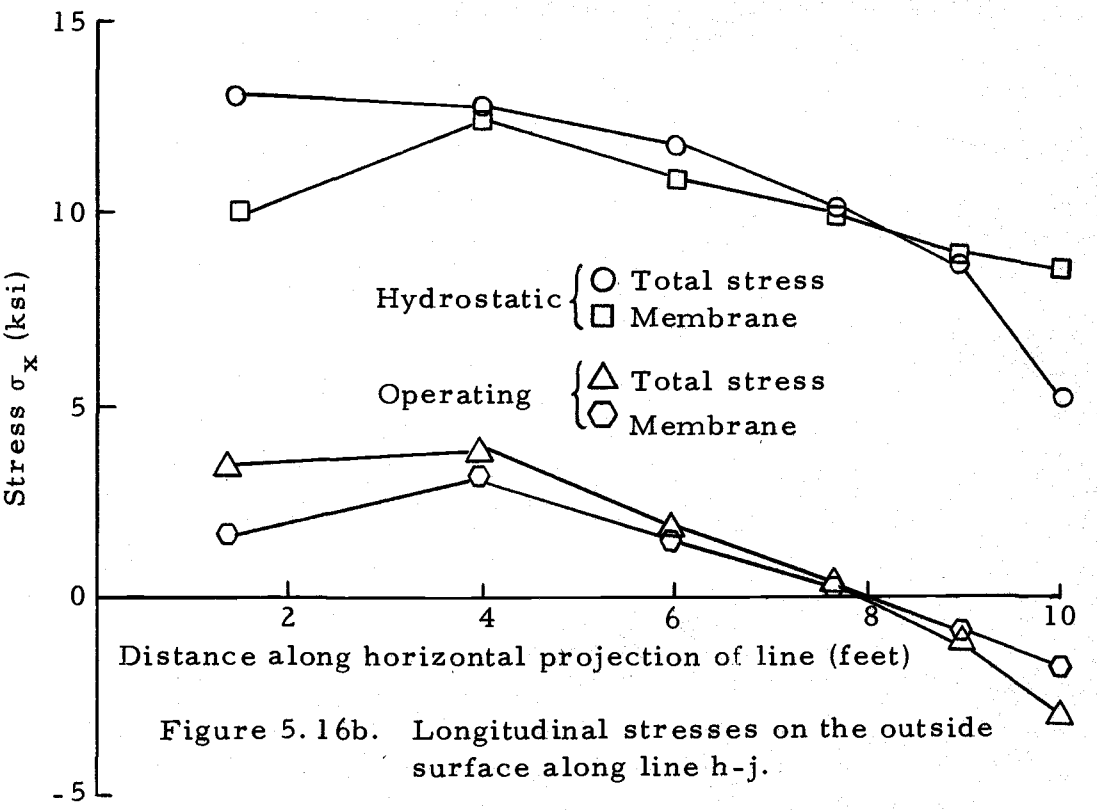

Figure 5.16b. Longitudinal stresses on the outside surface along line h-j.

5.4 Analysis of the Shell Members Without the Tie Rod

The stress magnitudes in the cylindrical shell are very similar (in either loading condition), with or without the tie rod. It therefore appears that the cylinder is sufficiently removed from the tie rod that it is not influenced by the tie rod's size.

A more noticeable effect on stress magnitude appears in the cone. In some locations the stresses are actually smaller but for the most part the cone membrane stresses have increased. Bending stresses remained basically unchanged. This effect was more noticeable in the operating condition than in the hydrostatic condition. The largest increase in membrane stress occurred near the outlet face of the cone and this was about a 10% increase.

VI. SUMMARY AND CONCLUSIONS

This dissertation was initiated by a need for an in-depth investigation into the structural behavior of symmetrical penstock bifurcations. Heretofore, analyses generally had been based on classical indeterminate methods of analysis where the structure was conveniently reduced to a tractable form. As a result of the inherent assumptions of this procedure, the design basis was compromised and a very conservative approach had to be taken.

The current level of development in structural analysis by matrix methods using the digital computer offered an alternative approach to analysis of these structures. The basic advantage of such an approach is that the structure need not be reduced in form to such a great extent. Thus the structure can be treated as a continuous entity with the degree of continuity being limited only by the computer's capacity to solve simultaneous equations. The results of this approach are a more accurate model of the structure and a more complete picture of its structural behavior on which to base the design. This is not to say that the resulting design will be less conservative but that, whatever the degree of conservatism, it will be better realized.

6.1 Discussion of the Method of Solution

For about ten years the finite element method has been in a rapid

state of development and as a consequence there are many different types of elements available for use. In the selection of the basic element used in this investigation, two considerations were most important. First, the element must be capable of modeling the plane stress situation in the crotch girder and the membrane and bending stress occurring in the ring girder and shell portions of the structure. A single finite element formulation with the flexibility of modeling both stress conditions would seem more advantageous than using two different finite elements. Second, the finite element formulation should be capable of convergence with decreasing element size while containing a minimum number of unknowns. The geometry of the penstock bifurcation is complex and a large number of elements would seem necessary and therefore the basic element must contain as few unknowns as possible. The convergence requirement is best studied by deriving the finite element formulation from a valid variational functional such as the potential energy functional or the Hellinger-Reissner functional. If the conditions on the variables of the finite element formulation are sufficient to insure the existence of the functional, then the compatibility requirement is satisfied and convergence with vanishing element size is expected.

The finite element formulation chosen is a flat plate element which superimposes plane stress action and bending action. It is derived from the Hellinger-Reissner principle and is shown to satisfy the

requirement of convergence. Its variables are, in the most general case, the in-plane displacement, the transverse displacement, and the normal moment. It is termed a mixed method as opposed, for example, to a pure displacement method. In addition, the finite element formulation selected for use had been applied with good results to an intersecting shell problem. Whereas the penstock bifurcation partially resembles an intersecting shell, the formulation was thought a good choice from this point of view also.

6.2 Discussion of the Development of the Finite Element Model

After the basic finite element was selected, a finite element model of the penstock bifurcation was constructed. Element matrices for elements appearing on the crotch girder are formed by generating only those stiffness coefficients which correspond to in-plane displacements. Elsewhere on the structure the element matrices are formed by generating the coefficients corresponding to all the variables. No difficulty was experienced in compatibly connecting these two elements together along their common boundary; the crotch girder-cone attachement line. This is because they are basically the same element with the same number and types of unknowns at corner node points. Along the common boundary between the ring girder and shell, three elements share the same side point node, commonly called a branch point. Here it was necessary to assign two unknown

moments to each branch point. The third moment was computed by virtue of moment equilibrium of the branch point after solution of the system of simultaneous equations yielded values for both of the other moments. This equilibrium condition or constraint is applied at each branch point.

Displacement boundary conditions for the finite element model were dictated by symmetry and the type of loading condition selected. Difficulty was experienced in applying the correct boundary conditions to the outlet face of the cone. These boundary conditions are not expressible in terms of global coordinate directions as were all other boundary conditions. Linear elements were added to the structure along the outlet face of the cone to solve this problem. These elements were given an extremely large axial stiffness and were geometrically oriented so that their axes were collinear with the direction of the constrained displacement. The resulting displacements in these directions were not zero but were several orders of magnitude less than typical displacements in the structure and the desired effect was achieved.

6.3 Discussion of Verification of the Finite Element Model

Verification of the finite element formulation was sought by comparing the finite element solutions of several simple structures for which classical solutions were available. Very good agreement

was achieved for membrane stresses in shells and bending moments in flat plates. Bending moments in shells were found to be less accurate and required a greater number of elements in the direction of curvature for good accuracy. The side point moments in the direction of curvature were found unreliable and should be ignored in favor of the moments computed for the center of the elements. The compromise in moment data was not unexpected because a flat plate element is being used to model the behavior of a smooth shell. The need here is for a curved shell element with a reasonably small number of unknowns, but this is only in the developmental stage at present.

In addition to the above verification, a finite element model for a prototype penstock bifurcation was constructed and the results were compared with experimental data obtained from a hydrostatic test of that prototype structure. Very good agreement was achieved for stresses in the crotch girder and tie rod. Moreover, the stress distribution along the critical section of the crotch girder was accurately predicted and the crotch girder behaved as a stretched plate instead of a curved beam as presumed by previous methods of analysis. Elsewhere in the structure the finite element data was consistent from a behavior standpoint but the accuracy was not as good as that achieved in the crotch girder and tie rod. The difficulty could well have been the very coarse model that was used, but experimental data was

unfortunately too scarce to justify a second model with a greater number of elements. The agreement with the available experimental data, on the whole, was good and served to verify the capability of the finite element model to analyze reasonably well a symmetrical penstock bifurcation.

Additional experimental verification of the basic formulation used in this study may be found in a report (9) on an experimental model study of structures similar to symmetrical penstock bifurcations.

It was also found that the element moment data for the triangular elements in the model was abnormally high and suspect. It is believed the triangular elements are influenced by the side point moments to too great an extent. It is therefore recommended that the triangular element moment data be ignored along with the side point moment data and that the use of triangular elements on the shell be kept to a minimum.

6.4 Discussion and Recommendations for the Lost Creek Bifurcation

The data indicates that the structure as designed would not be subject to failure under either the hydrostatic test condition or the operating load condition. There is some evidence that a localized elastic failure might occur between the top-center area of the cone

and the tie rod during hydrostatic testing. The data definitely shows the stresses in this localized area of the structure to be maximum and that they could equal 80% of yield stress (based on a yield stress of 30 ksi) which is the upper limit according to current design specification.

Elsewhere in the structure the stresses are much lower. The maximum computed stress in the crotch girder is about 12 ksi for the hydrostatic condition. The maximum computed tie rod stress is about 6.7 ksi and it occurs in the operating load configuration. The maximum stress in the ring girder is about 6.4 ksi and it too occurs in the operating load configuration. The maximum stress in the cylindrical shell is about 15 ksi in the hydrostatic configuration. Generally, the data for the Lost Creek bifurcation indicates an under-stressed condition except for a localized area in the cone.

The results for the structure with the negligibly small tie rod indicate that the 11 in. diameter tie rod affects the stresses in the girders to a greater extent than in the shell where little significant difference in stress level was indicated. The stress flow in the crotch girder is substantially improved allowing the crotch girder to participate structurally in the manner in which it was intended. The results indicate that the tie rod could be deleted or relocated to the weld point between the girders where it would double as a weld post and stiffening member. On the whole, the deletion of the tie rod does increase the stresses in the structure but the maximum stresses in the crotch girder and ring girder remain at a safe level.

BIBLIOGRAPHY

1. Bogner, F.K., R.L. Fox and L.A. Schmit. A cylindrical shell element. American Institute of Aeronautics and Astronautics Journal 5:745-750. April, 1967.

2. Cantin, Giles and Ray W. Clough. A curved cylindrical shell finite element. American Institute of Aeronautics and Astronautics Journal 6:1057-1062. June, 1968.

3. Connor, Jerome, Jr. and Carlos Brebbia. Stiffness matrix for a shallow rectangular shell element. Proceedings of the American Society of Civil Engineers, Journal of the Engineering Mechanics Division 93:43-65. October, 1967.

4. Crandell, Stephen H. Engineering analysis. New York, McGraw-Hill 1956. 417 p.

5. Ferrante, A.J. The generalization of a computer system for structural analysis. Doctoral dissertation. Cambridge, Massachusetts Institute of Technology, 1969. 408 numb. leaves. (Microfilm)

6. Gallagher, Richard H. Analysis of plate and shell structures. In: Application of Finite Element Methods in Civil Engineering, ed. by William H. Rowan, Jr. and Robert M. Hackett. School of Engineering, Vanderbilt University and the American Society of Civil Engineers, 1969. p. 184-185.

7. Gere, James M. and William Weaver, Jr. Matrix algebra for engineers. Princeton, Van Nostrand 1965. 168 p.

8. Gere, James M. and William Weaver, Jr. Analysis of framed structures. Princeton, Van Nostrand 1965. 475 p.

9. Godden, W.G. and A.R. Griffith. Model analysis of the A.D. Edmonston pumping plant discharge line manifolds. Berkeley, 1969. 115 numb. leaves. (University of California, Dept. of Civil Engineering, Division of Structural Engineering and Structural Mechanics, Structures and Materials Research. Report no. 69-25 on the Dept. of Water Resources, State of California, Contract no. 355974)

10. Herrmann, L.R. A bending analysis for plates. In: Proceedings of the First Conference on Matrix Methods in Structural Mechanics, Report no. AFFDL-TR-66-80, Wright-Patterson Air Force Base, 1965. p. 577-604.

11. Herrmann, L.R. Finite element bending analysis for plates. Proceedings of the American Society of Civil Engineers, Journal of the Engineering Mechanics Division 93:13-26. October, 1967.

12. Herrmann, L.R. and D.M. Campbell. A finite element analysis of thin shells. American Institute of Aeronautics and Astronautics Journal 6:1842-1847. October, 1968.

13. Herrmann, L.R., Professor of Civil Engineering, University of California. Personal communication. Davis, California, September 30, 1970.

14. Johnson, M.W. and R.W. McLay. Convergence of the finite element method in the theory of elasticity. Transactions of the American Society of Mechanical Engineers, Journal of Applied Mechanics 90:274-278. June, 1968.

15. Jones, R.E. A generalization of the direct-stiffness method of structural analysis. American Institute of Aeronautics and Astronautics Journal 6:821-826. May, 1964.

16. Laursen, Harold I. Structural analysis. New York, McGraw-Hill, 1969. 486 p.

17. Pian, T.H.H. and Pin Tong. Basis of finite element methods for solid continua. International Journal for Numerical Methods in Engineering 1:3-28. January-March, 1969.

18. Prager, William. Variational principles for elastic plates with relaxed continuity requirements. International Journal of Solids and Structures 4:837-844. September, 1968.

19. Prato, Carlos. A mixed finite element method for thin shell analysis. Doctoral dissertation. Cambridge, Massachusetts Institute of Technology, 1969. 225 numb. leaves. (Microfilm)

20. Prato, Carlos. Shell finite element method via Reissner's principle. International Journal of Solids and Structures 5:1119-1134. October, 1969.

21. Reissner, E. On a variational theorem in elasticity. Journal of Mathematics and Physics 29:90-95. July, 1950.

22. Rudd, R.O. Stress analysis of wye branches. U.S. Bureau of Reclamation, Engineering Monograph No. 32. 1964.

23. Sokolnikoff, I.S. Mathematical theory of elasticity. 2d ed. New York, McGraw-Hill, 1956. 476 p.

24. Tezcan, Semih, S. Computer analysis of plane and space structures. Proceedings of the American Society of Civil Engineering, Journal of the Structural Division 92:143-173. April, 1966.

25. Timoshenko, Stephen P. and S. Woinowsky-Krieger. Theory of plates and shells. 2d ed. New York, McGraw-Hill, 1959. 580 p.

26. Washizu, Kyuichiro. Variational methods in elasticity and plasticity. Oxford, Pergamon Press, 1968. 349 p.

27. Wilson, Edward L. Structural analysis of axisymmetric solids. American Institute of Aeronautics and Astronautics Journal 3:2269-2274. December, 1965.

28. Zienchiewicz, O. D. The finite element method in structural and continuum mechanics. London, McGraw-Hill, 1967. 272 p.

APPENDICES

APPENDIX A

DERIVATION OF DIRECTION COSINES IN TERMS OF GLOBAL COORDINATES

The 3 x 3 orthogonal rotation matrix [R] mentioned in Section 3.3 is composed of the nine direction cosines R_{ij} relating the local unknowns (u, v, w) to the global unknowns $(\bar{u}, \bar{v}, \bar{w})$ for a triangular element (see Figure A.1).

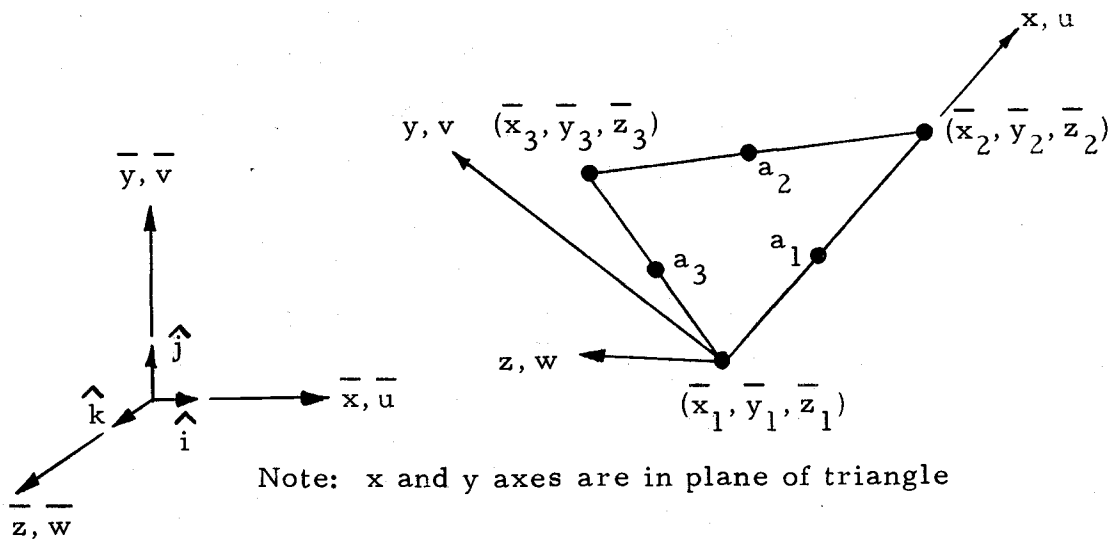

Note: x and y axes are in plane of triangle

Figure A.1. Global and local coordinate systems.

In terms of the global coordinates of the three corner nodes the side lengths a_i become

$$a_i = [(\bar{x}_j - \bar{x}_i)^2 + (\bar{y}_j - \bar{y}_i)^2 + (\bar{z}_j - \bar{z}_i)^2]^{1/2}$$

where

$$j = \begin{cases} i+1 & i = 1, 2 \\ 1 & i = 3 \end{cases}$$

Unit vectors $\hat{x}$ and $\hat{n}_3$ which are collinear with the x axis and side 3, respectively, are written as

$$\hat{x} = \frac{1}{a_1}[(\bar{x}_2 - \bar{x}_1)\hat{i} + (\bar{y}_2 - \bar{y}_1)\hat{j} + (\bar{z}_2 - \bar{z}_1)\hat{k}]$$

$$\hat{n}_3 = \frac{1}{a_3}[(\bar{x}_3 - \bar{x}_1)\hat{i} + (\bar{y}_3 - \bar{y}_1)\hat{j} + (\bar{z}_3 - \bar{z}_1)\hat{k}]$$

where $\hat{i}$, $\hat{j}$, and $\hat{k}$ are unit vectors in the global system.

The direction cosines for the x axis, R_{11}, R_{12}, and R_{13}, are found by the following scalar products

$$R_{11} = \hat{i} \cdot \hat{x} = \frac{\bar{x}_2 - \bar{x}_1}{a_1}$$

$$R_{12} = \hat{j} \cdot \hat{x} = \frac{\bar{y}_2 - \bar{y}_1}{a_1}$$

$$R_{13} = \hat{k} \cdot \hat{x} = \frac{\bar{z}_2 - \bar{z}_1}{a_1}$$

The following scalar products will be of use in computing the remaining direction cosines.

$$C_1 = \hat{i} \cdot \hat{n}_3 = \frac{\bar{x}_3 - \bar{x}_1}{a_3}$$

$$C_2 = \hat{j} \cdot \hat{n}_3 = \frac{\bar{y}_3 - \bar{y}_1}{a_3}$$

$$C_3 = \hat{k} \cdot \hat{n}_3 = \frac{\bar{z}_3 - \bar{z}_1}{a_3}$$

The C_i are direction cosines for an axis along side 3.

The angle ψ between sides 1 and 3 is defined by the vector product

$$\hat{x} \wedge \hat{n}_3 = \sin\psi \, \hat{z}$$

where $\hat{z}$ is a unit vector along the z axis. Therefore, the sine of the angle ψ can be written as

$$\sin\psi = [(R_{12}C_1 - R_{13}C_2)^2 + (R_{13}C_1 - R_{11}C_3)^2 + (R_{11}C_2 - R_{12}C_1)^2]^{1/2}$$

The direction cosines for the z axis, R_{31}, R_{32}, and R_{33}, are found by the following scalar products

$$R_{31} = \hat{i} \cdot \hat{z} = \frac{R_{12}C_3 - R_{13}C_2}{\sin\psi}$$

$$R_{32} = \hat{j} \cdot \hat{z} = \frac{R_{13}C_1 - R_{11}C_3}{\sin \psi}$$

$$R_{33} = \hat{k} \cdot \hat{z} = \frac{R_{11}C_2 - R_{12}C_1}{\sin \psi}$$

A unit vector $\hat{y}$ in the direction of the y axis is created by performing the vector product $\hat{z} \wedge \hat{x}$. Then the direction cosines for the y axis, R_{21}, R_{22}, and R_{33} are found, as above, by the following scalar products.

$$R_{21} = \hat{i} \cdot \hat{y} = R_{32}R_{13} - R_{33}R_{12}$$

$$R_{22} = \hat{j} \cdot \hat{y} = R_{33}R_{11} - R_{31}R_{13}$$

$$R_{23} = \hat{k} \cdot \hat{y} = R_{31}R_{12} - R_{32}R_{11}$$

APPENDIX B

USER'S MANUAL FOR GENERAL SYMMETRIC PENSTOCK BIFURCATION PROGRAM

This appendix is included in order to encourage the use of the developed computer program to analyze and design symmetrical penstock bifurcations. While the subsequent descriptions are thought sufficient by themselves to operate the computer program, users are encouraged to read the dissertation to which this manual is appended for general information.

Initially, generating input data for a preliminarily designed bifurcation may be tedious. Thereafter, the design effort can be greatly reduced by modifying member sizes and geometry with only slight variations in the input data. Such a trial and error procedure of analysis and design can result in an optimum final design in which each component is stressed to the desired level.

B. 1 Program Capability

The FORTRAN IV program written for an IBM 360 computer described herein computes principal membrane strains, principal membrane stresses, principal bending moments, and displacements for a symmetrical penstock bifurcation, subjected to internal hydrostatic pressure. Use of the program with other computers should be

possible with additional setup effort. The structure may or may not contain a tie rod and/or an internal crotch girder. The method of analysis is the finite element method using a triangular plate element based on a mixed formulation. The analysis is a static, linear elastic analysis and does not include the effects of concrete encasement or thermal loads. Two load configurations can be analyzed; the hydrostatic test configuration and the operating load configuration. The test configuration assumes infinitely rigid bulkheads are placed over the bifurcation apertures and the operating configuration assumes the apertures free to deflect in the radial direction and that the bulkheads do not exist. The program does not provide for unsymmetrical loads in the operating configuration.

Present limitations on the finite element model's size are as follows; 315 node points, 116 elements, 47 constrained nodal points, and 5 branch points. If the user wishes to increase these limits the following named common areas must accordingly be changed in the program; common A1, common A4, common B1, common BCD, common C2, and common E1. In addition the number of unknowns and the band width, presently specified as 486 and 87 respectively, must also be expanded. To accomplish this the following must be changed; common F1, common SLOW, the indices on both DO LOOPS in subroutine INTABC, and the dimension statement in subroutine SYMSOL.

B. 2 Preparation of the Finite Element Mesh

After taking advantage of the bifurcations two planes of symmetry, only one-fourth of the structure (see Figure 1.3) is to be discretized. Three shapes of elements are used to construct the model; quadrilateral, triangular, and linear as shown in Figure B. 1. The model shown in this figure is also shown in perspective in the dissertation (see Figure 4. 17). The majority will be quadrilateral elements as they are the most efficient; that is, the quadrilateral element is sub-divided by the program into four triangles. Moreover, the number of equations in the final system of simultaneous equations associated with one quadrilateral is less than the number for four triangles with no corresponding loss in accuracy. Since the system of equations requires a large amount of core storage, the use of quadrilaterals should be encouraged wherever possible.

In some areas of the structure the geometry is such that the use of quadrilaterals may be impossible. Such areas sometimes may occur along the conical shell at its intersection with the crotch girder. When this happens the mesh generation can be expedited by using triangular elements, but it should be mentioned that moment data is suspect for these elements. In addition, the use of triangles is advisable where the layers of quadrilateral elements need increasing because the structure gradually widens; see, for example, Section

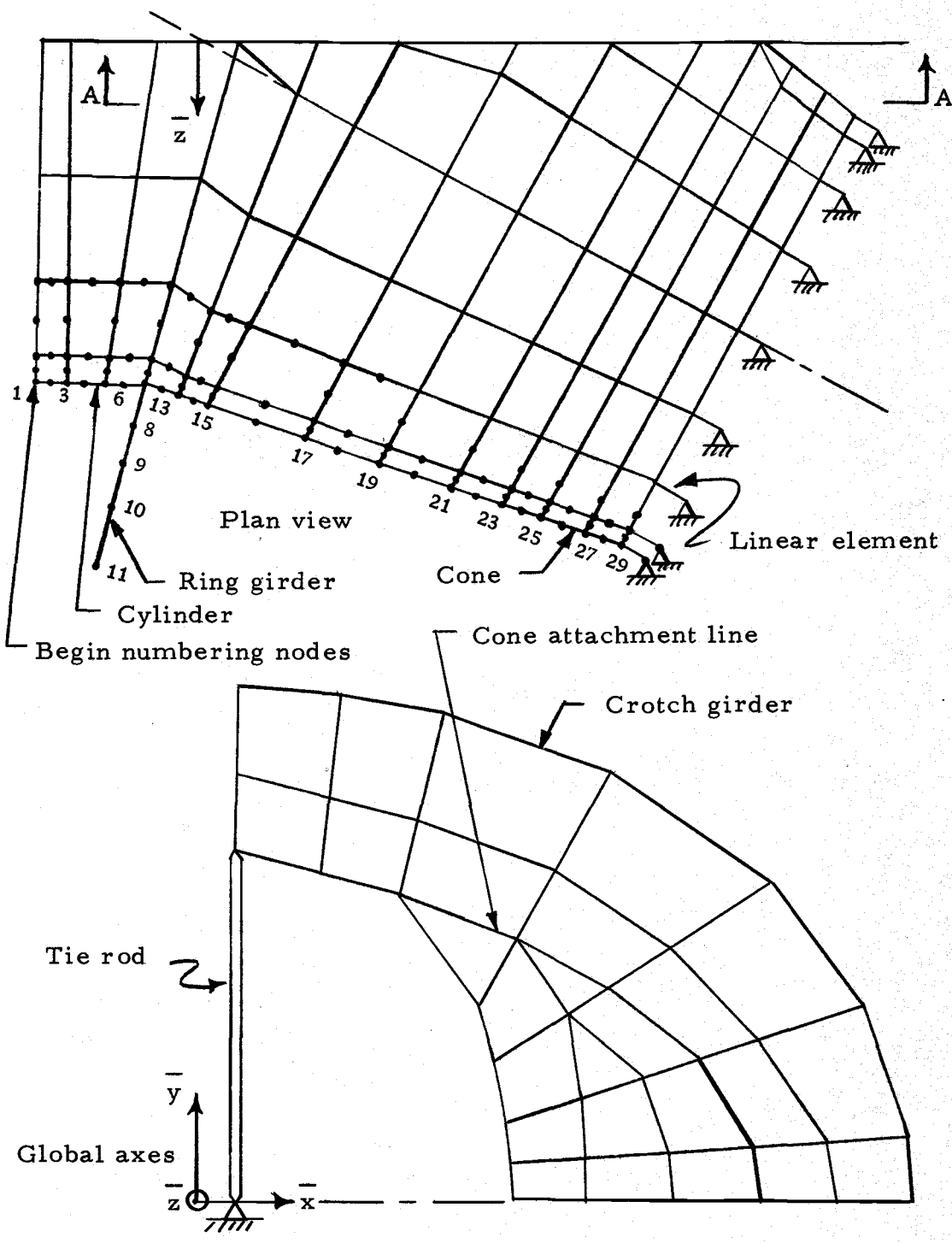

Figure B. 1. Example finite element mesh showing beginning of node numbering scheme.

A-A in Figure B. 1.

The linear elements are actually axial members and they are provided for two reasons: First, in the event of an inside tie rod as seen in Section A-A of Figure B. 1, a linear member will model the axial stiffness of the tie rod. Second, the boundary conditions along the outlet face of the cone are modeled by linear members having a very large axial rigidity as shown in the Plan View of Figure B. 1. In the second instance, the linear elements can be termed fictious, but nevertheless should be shown in the finite element mesh to facilitate subsequent numbering and geometry definition. Their length is not important as long as it is reasonably similar to adjacent quadrilateral element dimensions.

On the shell portions of the bifurcation, quadrilateral shell elements should be constructed so that each subtends the same angle in the direction of curvature. That is, if four elements are to be used over a 90° arc, each should subtend a 22. 5° arc. This will allow for easy data input, but moreover, there is evidence that the elements will model more closely the actual shell behavior. This procedure, however, must be abandoned in the area of the intersections with stiffening girders where, as mentioned above, the complex geometry prohibits uniform mesh development.

Numbering the node points should begin after the finite element mesh has been decided upon. In general, two types of node points are

assumed to exist for the elements; a corner point node at each corner and a side point node at the half-way point along each side of the element. Numbering of these nodes should begin where shown in Figure B. 1 and proceed in the axial direction of the cylinder and then the cone in a layered manner. When the ring girder is encountered, the numbering proceeds up the side of the girder and continues again at its base along the cone. Generally, the nodes of the crotch girder are numbered from top to bottom and then along the cone again. But the primary objective of the numbering scheme is to minimize the numerical difference between node point numbers associated with the elements. This technique minimizes the computer storage requirement for a given number of elements.

The numbering scheme should be sequential up to the largest numbered node, and naturally no node points should remain without a number. The elements of the crotch girder and linear elements do not receive side point numbers because there is no moment, thus no side point node, associated with these elements. Side point nodes will occur where the crotch girder intersects the ring girder and cone, but these nodes belong to the elements of the ring girder and cone and not to the crotch girder elements. Once the numbering has been accomplished, it should be checked so that no points have been missed, and no numbers have been repeated or left out and that no side point numbers have been assigned to elements of the crotch girder or

linear elements. An error at this point will nullify any further effort.

Next, all elements should be numbered sequentially and in a layered manner following as closely as possible the scheme for numbering the nodes.

B.3 Sign Conventions

Global displacement and load components are positive when in the direction of the positive global coordinates $(\bar{x}, \bar{y}, \bar{z})$ shown in Figure B. 1. Local displacement and load components are positive when in the direction of the positive local coordinates. The local coordinate systems for the various elements are shown in Figure B.2 as they relate to side one of the elements. Side one is defined by the first two or three, as the case may be, nodal point numbers associated with the element (see Section B. 5. 7). Note that the quadrilateral has a different local coordinate system for each corner point while the triangle and linear elements have only one coordinate system per element. Positive moments cause compressive stress on the top surface of the element (see Section B. 5. 7 for a definition of top surface). The normal load on an element is positive when acting as a pressure on the bottom surface.

The above description of local coordinate systems is not necessary for constructing the input data but only in interpreting the output data.

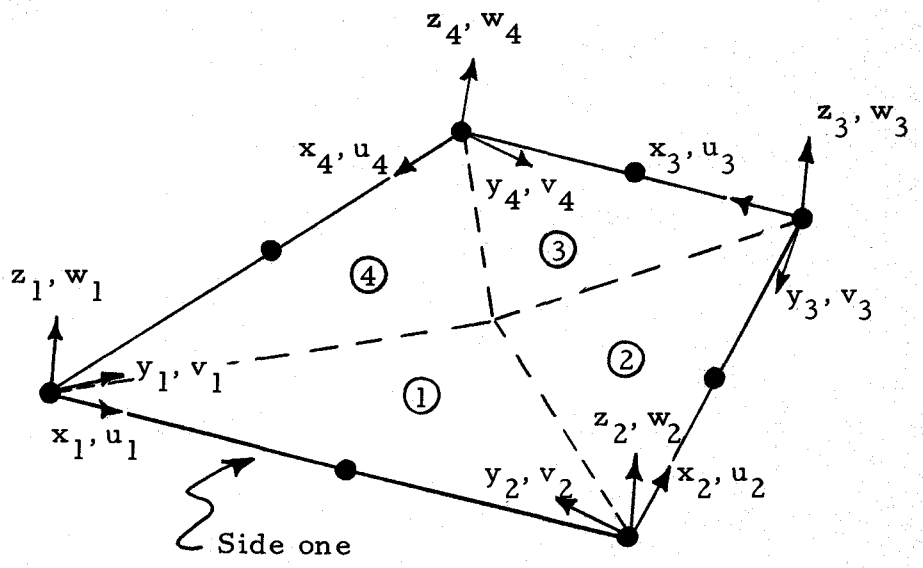

Quadrilateral element

Note: x and y axes lie in plane of the element

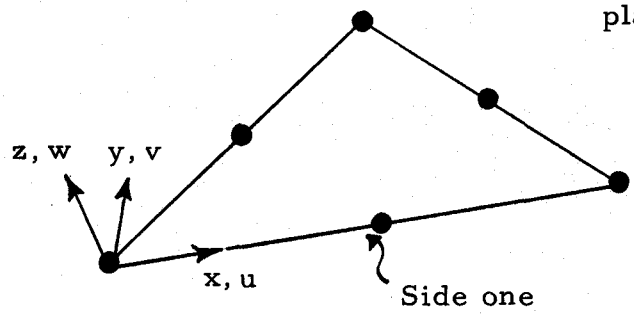

Triangular element

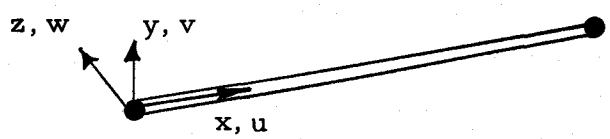

Linear element

Figure B. 2. Local coordinate systems.

B.4 Job Control for IBM 360-50

The following information is systems oriented and describes IBM operating system job control cards placed atop the data deck. Sequential read-write access devices used in the computer program are listed and defined as to their size.

```
//JOBLIB    DD  DSN=LIBRARY,DISP=SHR
//        EXEC  PGM=FINITELE
//FT06F001 DD  SYSOUT=A
//FT02F001 DD  UNIT=SSYSQ,DISP=(NEW,DELETE),
                SPACE=(CYL,(5,5))
//FT03F001 DD  UNIT=SSYSQ,DISP=(NEW,DELETE),
                SPACE=(CYL,(5,5))
//FT15F001 DD  UNIT=SSYSQ,DISP=(NEW,DELETE),
                SPACE=(CYL,(5,5))
//FT16F001 DD  UNIT=SSYSQ,DISP=(NEW,DELETE),
                SPACE=(CYL,(5,5))
//FT17F001 DD  UNIT=SSYSQ,DISP=(NEW,DELETE),
                SPACE=(CYL,(5,5))
//FT18F001 DD  UNIT=SSYSQ,DISP=(NEW,DELETE),
                SPACE=(CYL,(5,5))
//FT21F001 DD  UNIT=SSYSQ,DISP=(NEW,DELETE),
                SPACE=(CYL,(5,5))
//FT22F001 DD  UNIT=SSYSQ,DISP=(NEW,DELETE),
                SPACE=(CYL,(5,5))
//FT05F001 DD  *
                Data
```

B.5 Preparation of Input Data

The following describes the cards and sets of cards shown in Figure B.3 which form the necessary input data to the program. All integer data should be right adjusted in their respective columns.

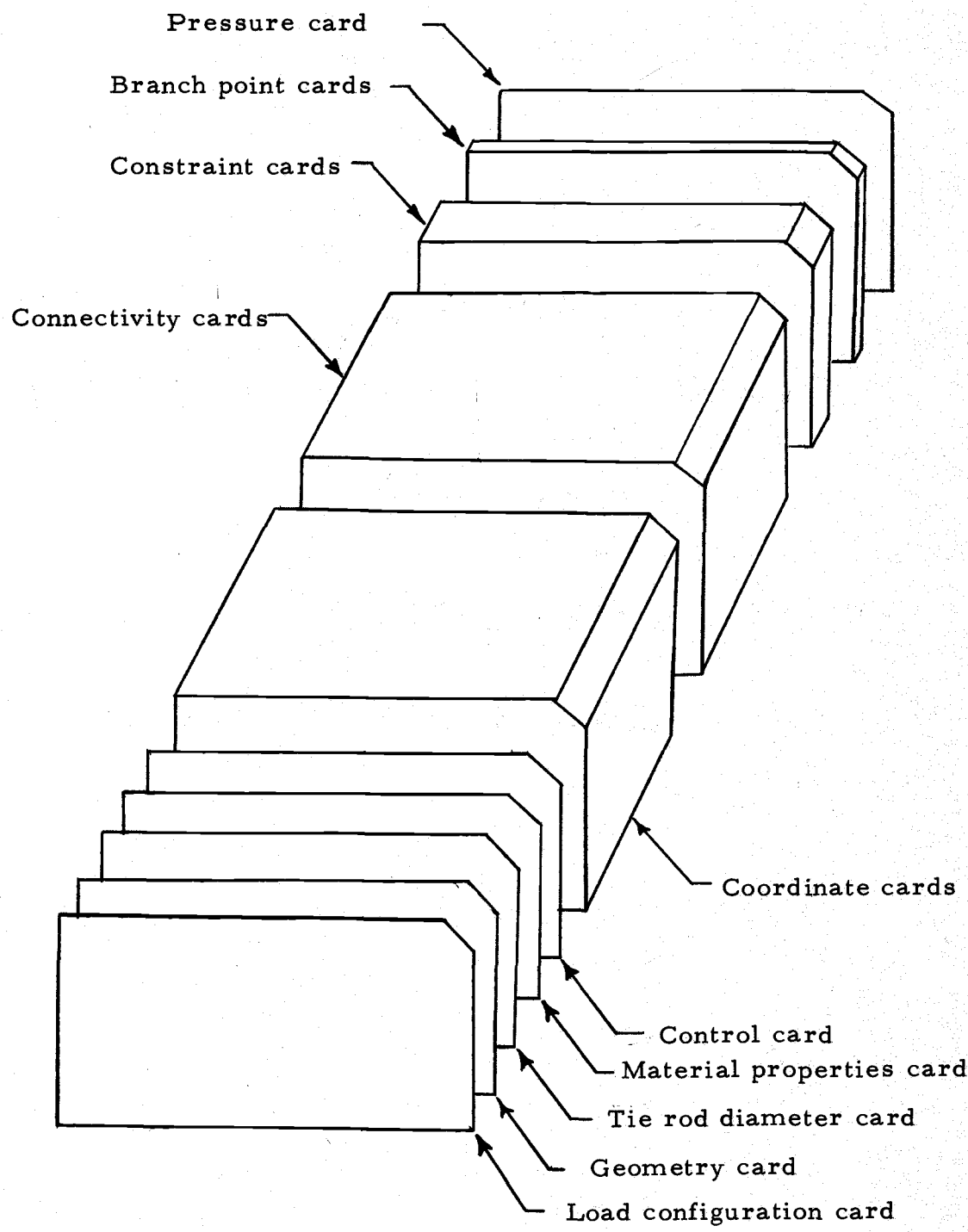

Figure B.3.. Input data for the penstock bifurcation program.

B.5.1 Load Configuration Card (I5)

Columns 1-5 Place a 1 for the hydrostatic test condition or a zero (blank card) for the operating load configuration.

B.5.2 Geometry Card (8F8.5)

Columns 1-8 Radius of the cylinder (feet).

9-16 Outlet radius of the cone (feet).

17-24 Angle change in flow direction (degrees).

25-32 Cone half-angle (degrees).

33-40 Crotch girder thickness (inches). Because the crotch girder is bisected by a plane of symmetry, the program halves this value.

41-48 Ring girder thickness (inches).

49-56 Cylinder thickness (inches).

57-64 Cone thickness (inches).

B.5.3 Tie Rod Diameter Card (F8.1)

Columns 1-8 The tie rod diameter (inches). If a tie rod exists in the finite element model and the user does not wish it to participate structurally, then the diameter may be made extremely

small (.0001). A zero diameter should not be used in this instance. If a tie rod does not exist, the card is left blank.

B.5.4 Material Properties Card (2X, E10.3, F10.3)

Columns 3-12 Modulus of elasticity for the steel (ksi).

13-22 Poisson's ratio for the steel.

B.5.5 Control Card (5I5)

Columns 1-5 Number of node points. (See Section B.2.)

6-10 Number of elements or connectivity cards. (See Section B.5.7.)

11-15 Number of constraint cards. (See Section B.5.8.)

16-20 Number of branch point cards. A branch point occurs only at side points along the intersection between the ring girder and the shell. (See Section B.5.9.)

21-25 Number of coordinate cards. Note that this number is considerably less than the number of node points. (See Section B.5.6.)

B.5.6 Coordinate Cards (I8, 2F10.2, 3F5.0)

This data set describes primarily the overall geometry of the structure in terms of two coordinates for each corner node point of an element. In addition the number of unknowns to be assigned various nodes are described in this data set. Because of this, branch points are also included in these cards even though, as side points, their coordinates are of no interest and are not entered by the user.

The coordinates for each node point will be referenced to one of the four sub-structure reference systems shown in Figure B.4 provided for convenient data input. Numbers 1 through 4 are used to to indicate the reference system for corner node points on the crotch girder, ring girder, cylinder, and cone, respectively. The end nodes for linear members which also occur on a boundary are assigned a 5 in the case of members along the outlet face of the cone and a 6 in the case of a tie rod member. Numbers 5 and 6 do not represent additional reference systems but special cases of reference systems 4 and 1, respectivelv.

Coordinates for corner node points occurring along intersections involving the ring girder should be referenced to the ring girder system (reference system 2). If the intersection involves the crotch girder and does not involve the ring girder, the coordinates should be referenced to the crotch girder system (reference system 1).

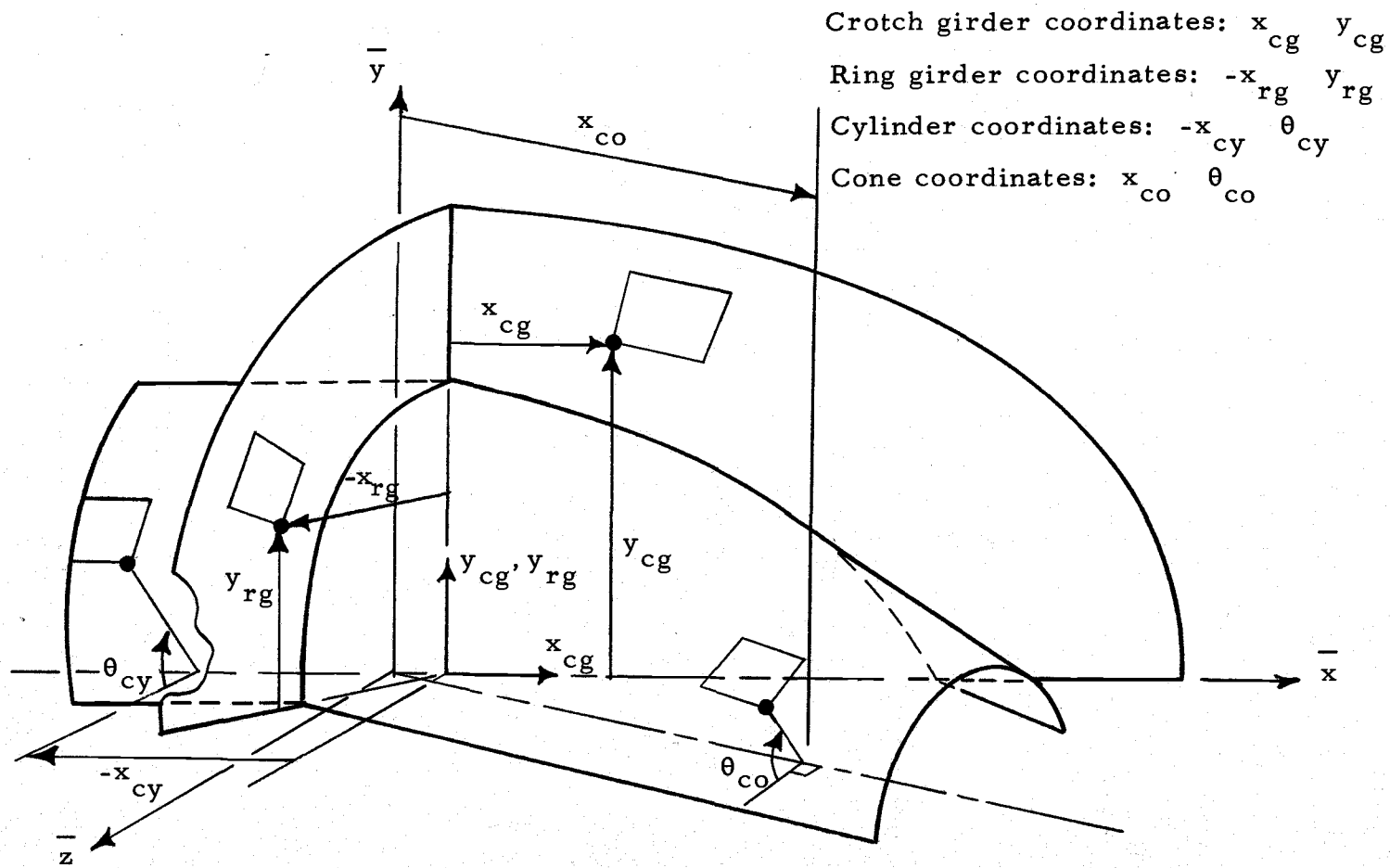

Figure B. 4. Sub-structure reference systems.

In the case of a branch point card a 2 is placed in column 33 and all other columns are left blank.

Columns 1-8 Node number. (Number assigned to the node.)

9-18 The x coordinate of the node (feet).

19-28 The y coordinate (feet) if the node is on the ring girder or crotch girder. The angular coordinate (degrees) if the node is on the cylinder or cone.

33 This entry indicates the number of unknowns the program will assign the node point. In the finite element formulation used, this will predominantly mean 3 unknowns. However, a 2 should be assigned the following node points: node points whose coordinates are cast in the crotch girder reference system and branch points.

38 Sub-structure coordinate reference system number 1, 2, 3, or 4. A 5 is entered for the node point on the constrained end of a linear element, and a 6 is entered for the constrained node point on a tie rod element.

43 Most cards will not contain an entry here. Only those corner point nodes on the inlet face of the

cylinder and outlet face of the cone are of concern. A 1 is entered for both the 0° and 90° nodes on the cylinder and intermediate nodes are assigned a 2. A node located at $\theta = 0°$ (see Figure B. 4) on the outlet face of the cone is referred to as a 0° node, etc. A 3 is entered for the 0° and 180° nodes on the cone and a 4 is assigned to the intermediate nodes. These entries signify the location of tensioning loads produced by bulkheads when the hydrostatic test condition is specified. The loads are computed automatically from internal pressure and geometry.

B. 5. 7 Connectivity Cards (I5, 5X, 8I5, 2I10)

This data connects the element number with the node point numbers on the element's perimeter. The node points for a quadrilateral and triangle are listed counterclockwise on the perimeter beginning with a corner point node and ending with a side point node. The first two or three nodes, as the case may be, define side one of the element and the resulting output data will be referenced to a local x axis collinear with this side (see Figure B. 2). For example, the stress in the x direction for the element will act parallel to side

one. The "top surface" of the element is also defined as the surface that is viewed when numbering counterclockwise (a positive moment creates compression on the "top surface"). For linear members the smallest numbered node should be listed first. There must be a card in this data set for every element. Each card, besides the above information, contains an entry indicating to which part of the structure the element belongs. The indicators are 1, 2, 3, and 4 and they represent the crotch girder, ring girder, cylinder, and cone, respectively. A 5 indicates a linear element along the outlet face of the cone and a 6 indicates a tie rod element. These indicators are similar to those in Section B.5.5 but here they refer to elements and not nodes.

Columns 1-5 Element number (number assigned to the element).

13-15 Corner point node.

18-20 Side point node only. Columns are left blank if the element is on the crotch girder or is a linear element because no side point should have been assigned to these elements.

23-25 Corner point node or end point node if element is a linear element.

28-30 Side point node or blank.

33-35 Corner point node or blank.

38-40 Side point node or blank.

43-45 Corner point node or blank.

48-50 Side point node or blank.

60 A number 1 through 6 as indicated above.

70 Enter a 1 if the element is a triangle otherwise leave blank.

B. 5. 8 The Constraint Cards (415)

These cards apply primarily to corner node points (as opposed to side point nodes) on the boundaries of the finite element model. A constraint is a "fixing against movement" of a displacement component in one of the three global directions $(\bar{x}, \bar{y}, \bar{z})$. The constraints are dictated by symmetry of the structure along those boundaries that are formed by intersections with the symmetrical $\bar{x} - \bar{y}$ plane and symmetrical $\bar{x} - \bar{z}$ plane (see Figure B. 4). For example, a corner node point in the $\bar{x} - \bar{z}$ plane cannot move in the $\bar{y}$ direction and therefore is constrained in the $\bar{y}$ direction. In the same way a corner node point in the $\bar{x} - \bar{y}$ plane is constrained in the $\bar{z}$ direction.

An exception to this procedure occurs for corner node points on the crotch girder to which 2 unknowns have been assigned in column 33 of Section B. 5. 6. Though these node points lie in the $\bar{x} - \bar{y}$ plane they do not receive a constraint in the $\bar{z}$ direction. Those node points which are also common to the $\bar{x} - \bar{z}$ plane are assigned

a constraint in the $\bar{y}$ direction. This is a consequence of the crotch girder being a plane stress component in the $\bar{x}$ - $\bar{y}$ plane.

In addition to boundary conditions resulting from symmetry, constraints will exist because of load conditions along the inlet face of the cylinder and outlet face of the cone. If the hydrostatic test configuration is chosen in step B. 5. 1 above, the user must constrain the $\bar{y}$ and $\bar{z}$ displacements of corner node points along the inlet face of the cylinder. In this manner he is consistent with assuming infinitely rigid bulkheads welded to the structure. If the operating configuration is chosen, only the $\bar{x}$ displacements must be constrained along the same boundary. Boundary conditions on the outlet face of the cone are subject to the same considerations but they cannot be case in terms of global directions $(\bar{x}, \bar{y}, \bar{z})$. The linear elements along the cone outlet face were developed to approximate these boundary conditions (see Figure B. 1). The end nodes of these elements must be completely fixed against displacement by the user by constraining them in all three directions; $\bar{x}$, $\bar{y}$, and $\bar{z}$. This is all that need be done regardless which of the two load configurations are chosen. The user should note, however, that step B. 5. 1 and this step are related insofaras the boundary conditions along the cylinder inlet face are concerned. That is, when the load configuration is changed the constraints along the inlet face of the cylinder must be changed accordingly.

The majority of cards will represent constraint conditions for corner node points but the user must also generate a card for each of the side points along the free edge of the ring girder. The purpose is to constrain the moment at these side points to zero. These are the only side points that are assigned constraints by the user. This is done by entering a 1 in all three columns normally reserved for displacement constraints. The user should note that this does not mean the displacements are constrained along the free edge.

In the following columns a 1 is used when the constraint is desired, otherwise the column is left blank.

Columns 3-5 Node point number.

10 $\bar{x}$ direction constraint. (1 or blank.)

15 $\bar{y}$ direction constraint. (1 or blank.)

20 $\bar{z}$ direction constraint. (1 or blank.)

B.5.9 Branch Point Cards (4I5)

These cards pertain to side points along the intersection of the ring girder with the shell.

Columns 3-5 Side point number.

9-10 Adjacent cylinder element number.

14-15 Adjacent cone element number.

19-20 Adjacent ring girder element number.

B.5.10 Pressure Card (F5.3)

Columns 1-5 Pressure (ksi).

B.6 Checking Input Coordinates and Connectivity

It is important in a finite element investigation of this magnitude that the user have confidence in the accuracy of the input coordinates (B.5.5) and input connectivity (B.5.6). The preferable way to check this data is by plotting the finite element mesh using a mechanical or electronic plotting device. The information needed from the program will be contained in subroutine GLOCOR and may be obtained on card output by removing the comment designation on the appropriate statements. Specifically, the computed global coordinate variables XBAR, YBAR, and ZBAR are written out on cards along with the connectivity matrix ICONN. This information must then be converted by an appropriate program so that a plotting device can interpret and plot the finite element mesh. Development of the program will depend in part on the type of plotting device used and therefore such a program is not included.

B.7 Printed Information and Data

The input data is printed first. This includes the selected load configuration, the dimensions and angles, the material properties,

the control numbers, the element connectivity, the node point coordinates, the constraint data, the branch points, and the internal pressure.

Some useful computed information is printed out next. First, the generated displacement or moment numbers for each node point in the model are printed. For each corner node point there are three possible displacements depending on the constraints. For a side point node there is only one moment, and thus one number assigned to it (if the side point is a branch point, two numbers are assigned). Each number, whether a displacement or moment number, represents one equation in the system. The largest number represents the number of simultaneous equations in the system. Secondly, the code numbers for each element are printed. This information is generated from the input connectivity and the displacement or moment numbers and is used to assemble the system of simultaneous equations. Third, the global coordinates for each node are printed. These coordinates are referenced to the global system and are computed from the input coordinates which are referenced to the four sub-structure reference systems. Finally, the maximum half-bandwidth for the system of simultaneous equations is printed. In the FORTRAN program the named common area SLOW must have dimensions equal to or exceeding the product of the half-bandwidth and the largest displacement number. Also, the named common area F1 must be dimensioned in

excess or equal to the largest displacement number.

The output data is printed next. First, for every node point the global displacement components (UBAR, VBAR, WBAR) or side point moments, as the case may be, are printed. The units are inches for displacement and kip-inches per inch for side point moments. In the finite element formulation, the side point moment values in the direction of curvature of the shell are to be treated as suspect as are the element moments for triangular elements. Side point moment values on the ring girder and elsewhere should be reasonable data. When a side point node is also a branch point, two side point moments will be printed. The first moment will be for the cylinder (M_{n1}) and the second moment will be for the cone (M_{n2}). The side point moment in the ring girder (M_{n3}) at that branch point can be computed by $M_{n3} = -(M_{n1}-M_{n2})$.

The next data printed is the corner point displacement components referenced in the local coordinate systems (see Figure B. 2). These components (u, v, w) are listed by element number. A quadrilateral element will have four sets of components, one for each corner point. A triangular element will have one set of components as will a linear element. The units are inches.

The membrane strains, membrane stresses, and bending moments for the center of each element are printed next. Listed for each element are the rectangular cartesian components (as referenced

in the local system with side one of the element collinear with the x axis) the maximum value, the minimum value, the maximum shear strain, maximum shear stress, or maximum twisting moment, as the case may be, and the angle between side one and the outward normal of the face containing the maximum value. Bending stresses can be computed by multiplying the bending moment by $6/t^2$ where t is the thickness of the element.

APPENDIX C

DESCRIPTION OF COMPUTER PROGRAM

Eighteen subroutines comprise the body of the computer program. They are controlled by call statements which comprise the main program. Extensive use of common storage is made to transfer information from one subroutine to another. Approximately 294,000 bytes of storage are required for the program in its present state, of which 180,000 are allotted to fast core and 114,000 are allotted to slow core. The former amount comprises the system matrix and the latter amount comprises the remainder of the program. Sharing the storage of the program between fast and slow core in this manner made it possible for the program to be run on a 200,000 byte fast core partition set up for normal operation of a batch processing system.

A brief description of the function of each subroutine is given below.

1) Subroutine INPUT. This subroutine reads into storage the input data according to control card information described in Section B. 5. 5. p160

2) Subroutine SUBCOD. This subroutine generates the 4 x 12 matrix of code numbers used subsequently to combine four triangular elements into one quadrilateral element. p160

3) Subroutine GENCOD. This subroutine generates a code

number for each element in the finite element model. These are subsequently used to assemble the system matrix of algebraic equations.

4) Subroutine GLOCOR. This subroutine computes the global coordinates for the node points whose coordinates were given in terms of sub-structure reference systems.

5) Subroutine INTABC. This subroutine initializes the system matrix and system load vector to zero.

6) Subroutine QUASYA. This subroutine computes the center point of each quadrilateral element and thus begins the procedure for subdividing these elements.

7) Subroutine TRISYS. This is a very large subroutine as it performs many functions. Its overall function is to compute triangular element matrices for each of the four triangles composing a quadrilateral element and then use code numbers to assemble the 23 x 23 quadrilateral element matrix and associated load vector.

8) Subroutine QUASYB. This subroutine performs the static condensation process which reduces the 23 x 23 element matrix to a 16 x 16 element matrix.

9) Subroutine SYMAG. This subroutine uses the code numbers to assemble the element matrices into a system matrix and system load vector.

10) Subroutine MAINV2. This is a standard matrix inversion subroutine. It is used to invert only small matrices such as required by the static condensation process.

11) Subroutine REARR. This subroutine rearranges or permutates triangular element matrices and their associated load vectors prior to their synthesis into quadrilateral element matrices.

12) Subroutine SYLMOD. This subroutine is used only in the hydrostatic load configuration and it modifies the system load vector to include the tensioning loads induced by the bulkheads.

13) Subroutine BANWID. This subroutine computes the band width of the system of simultaneous equations prior to the solution process.

14) Subroutine SYMSOL. This is a standard subroutine used to solve the system of simultaneous equations by Gaussian elimination.

15) Subroutine STREMO. This subroutine uses the global displacements and side point moments which are direct solutions of the system of simultaneous equations and computes the local displacements, stresses, and moments for the elements in the finite element model.

16) Subroutine ROTVA. This subroutine is used to rotate the

reference system for each triangular element into a quadrilateral element reference system so that the correct average of stresses and moments can be computed within each quadrilateral element.

17) Subroutine PRINC. p169 This subroutine computes the principal stresses, principal moments and the principal directions for each element.

18) Subroutine OUTPUT. p165 This subroutine controls the printing out of input information and output data.

```
C*********************************************************************
      EXTERNAL EDUMP
      CALL ERRSET(208,2,2,0,EDUMP,209)
      COMMON /A1/ CCOR(315,5)
      COMMON /A3/ ICODE (4,12)
      COMMON /A4/ ICONN(116,10)
      COMMON /A5/ QEMAA(16,16), QEMAB(16,7), QEMT3(16,7),
     1QEMT1(7,16), QEMT2(16,16), CRA(16)
      COMMON /A6/ TQEM(23,23)
      COMMON /A7/ QRT(23)
      COMMON /A8/ B(3,3), BP(3), CP(3), AI(3,3), AJ(3,3), AK(3,3), SI(3)
     1, CO(3),          GI(3,3), D(3,3), Q(3,3),PT(3,3), H(3,3),
     2TEM(12,12),PL(12), TEMP(12,12), RPL(12)
      COMMON /A9/ E,PR,CON,P
      COMMON /B1/ NCODE(116,16)
      COMMON /B2/ PHIA(16),PHIT(7),CRBT(7),PHIB(7),PHI(12),A(3,6),C(3,3)
     1,DISP(7),SMOM(3),TESI(4,3),TEEP(4,3),TEMO(4,3),PHIP(12)
      COMMON /B3/  F(3,3), T(12,12)
      COMMON /B4/  X2,X3,Y3,AREA
      COMMON /B6/ TEMT(12,12),RPLT(12)
      COMMON /B7/ RCY,RCO,BET,GAM,AC,TCG,TRG,TCY,TCO,DITR
      COMMON /B9/ NP,NE,NCONP,NCBPT,NNP
      COMMON /BCD/ KNOVA(47,4), NCOCM(315,3), KNOMO(4,4)
      COMMON /C1/ MB
      COMMON /C2/ XBAR(315), YBAR(315), ZBAR(315)
      COMMON /C4/ QEM (16,16), CR(16)
      COMMON /CDE/ LAOCM
      COMMON /D1/  TH,XBARR,YBARR,ZBARR
      COMMON /E1/ QEEP(116,3), CESI(116,3), QEMO(116,3)
      COMMON /F1/ SYLVEC(486)
      COMMON /H1/ CIS(4)
      COMMON /I1/ QT(16)
      COMMON /L1/ NCASE
      COMMON /Y2/  BB(3)
      COMMON /SLOW/ BGK(486,87)
      DIMENSION   QEMBA(7,16),QEMBB(7,7),CRB(7)
      DOUBLE PRECISION P
      DOUBLE PRECISION QEMBB
      DOUBLE PRECISION    QEMBA
      CALL INPUT
      CALL GLCCOR
      CALL SUBCOD
      CALL GENCOD ( NP,NE,NCONP,NCBPT)
      CALL  INTABC
      DO 250 M=1,NE
      CALL QUASYA (M)
      CALL TRISYS(M)
      N=7
      IF(ICONN(M,9).EQ.1) N=2
      CALL QUASYB (M,LN,N,QEMBB,QEMBA,CRB)
      CALL SYMAG(LN,M)
  250 CONTINUE
      IF(NCASE.EQ.1)  GO TO 150
      GO TO 200
  150 CALL SYLMOD
  200 CONTINUE
      CALL BANKID (NE,MB)
      CALL SYMSOL (MB)
      REWIND 2
      REWIND 3
      REWIND 18
      DO 300 IL=1,NE
      N=7
      IF(ICONN(IL,9).EQ.1) N=2
  300 CALL STREMD (NOBPT,N,QEMBB,QEMBA,CRB,IL)
      CALL OUTPUT
      STOP
      END
C *********************************************************************
      SUBROUTINE INPUT
      COMMON /A1/ CCOR(315,5)
      COMMON /A4/ ICONN(116,10)
      COMMON /A9/ E,PR,CON,P
      COMMON /B7/ RCY,RCO,BET,GAM,AC,TCG,TRG,TCY,TCO,DITR
      COMMON /B9/ NP,NE,NCONP,NCBPT,NNP
      COMMON /BCD/ KNOVA(47,4), NCOCM(315,3), KNOMO(4,4)
      COMMON /L1/ NCASE
      READ(5,200)NCASE
  200 FORMAT (I5)
      READ(5,253) RCY,RCO,BET,GAM,    TCG,TRG,TCY,TCO
      BET=.01745328*BET
      GAM=.01745328*GAM
  253 FORMAT  (8F8.5)
      READ(5,254) DITR
      DITR=DITR*0.5
  254 FORMAT(F8.1)
      AC=(RCY-RCO*COS(GAM))/SIN(GAM)
      READ(5,255) E,PR
      CON= (1.-PR)*.5
  255 FORMAT (2X,E10.3,F10.3)
      READ(5,271)  NP,NE,NCONP,NCBPT,NNP
  271 FORMAT (5I5)
      DO 800 I=1,NP
      DO 800 J=1,5
  800 CCOR(I,J)=0.0
      DO 275 I=1,NNP
      READ(5,280)   K, (CCOR(K,J),J=1,5)
      IF(CCOR(K,4).EQ.3.OR.CCOR(K,4).EQ.4)CCOR(K,2)=.01745328*CCOR(K,2)
  275 CONTINUE
  280 FORMAT    (I8,2F10.2,3F5.0)
      DO 300 I=1,NE
  300 READ(5,305) I,(ICONN(I,J),J=1,10      )
  305 FORMAT (I5,5X,8I5,211C)
      DO 334  I=1,NCONP
  334 READ(5,335)   (KNOVA(I,J),J=1,4)
  335 FORMAT (4I5)
      DO 340 I=1,NCBPT
  340 READ (5,341)    (KNOMO(I,J), J=1,4)
  341 FORMAT (4I5)
      READ(5,344) P
  344 FORMAT (F5.3)
      RETURN
      END
C *********************************************************************
      SUBROUTINE SUBCOD
      COMMON /A3/ ICODE (4,12)
      DO 199 I=1,4
      DO 199 J=1,12
  199 ICODE(I,J)=0
      DO 200 J=1,7
      I=1
```

```
      2C0 ICODE(I,J)=J
          DO 2C1 J=1,7
          I=2
      2C1 ICODE(I,J)=J+4
          DO 2C2 J=1,7
          I=3
      2C2 ICODE(I,J)=J+8
          DO 2C3 J=1,3
      2C3 ICODE(4,J)=ICODE(3,J+4)
          DO 2C5 I=1,4
          ICODE(I,9)=17
          ICODE(I,1C)=18
      2C5 ICODE(I,11)=19
          ICODE (4,4) = 16
          DO 2C7 J=1,3
      2C7 ICODE (4,J+4) = ICODE (1,J)
          DO 2C9  I=1,4
      2C9 ICODE (I,8)= 2C+I
          ICODE (4,8) = 2C
          DO 211 I=1,4
      211 ICODE (I,12) = I+19
          RETURN
          END
C *************************************************************************
          SUBROUTINE GENCOD ( NP,NE,NCCAP,NCBPT)
          COMMON /A1/ CCOR(315,5)
          COMMON /A4/ ICONN(116,1C)
          COMMON /B1/ NCODE(116,16)
          COMMON /BCD/ KNOVA(47,4), NCOCM(315,3), KNCMO(4,4)
          COMMON /CDE/ LADCM
          DO 22 I=1,NE
          DO 23 J=1,16
       23 NCODE(I,J)=0
          DO 3C I=1, NP
          DO 3C J=1,3
       30 NCOCM(I,J)=0
          K=C
          DO 12 I=1, NP
          DO 2  N=1,NCONP
          IF (KNOVA(N,1).EQ.I) GO TC 3
          GC TO 2
        3 DO 4 M=2,4,1
          IF (KNOVA(N,M).EQ.1) GO TC 4
          K=K+1
          J=M-1
          NODOM(I,J)=K
        4 CONTINUE
          GO TO 12
        2 CONTINUE
          IF (CCOR(I,3)-2.) 7,8,9
        7 J=1
          GO TO 11
        8 J=2
          GO TC 11
        9 J=3
       11 DO 31 L=1,J
          K=K+1
          NODOM(I,L)=K
       31 CONTINUE
       12 CONTINUE
          LADOM=K
          DO 15 L=1,NP
          N=C
          IF(ICONN(L,1C).EQ.1) NL=3
          IF (ICONN(L,1C).NE.1) NL=4
          DO 14 LCUM=1,NL
          K=N*4
          J=N*2
          DO 13 I=1,3
       13 NCODE (L,I+K)=NODOM(ICONN(L,1+J),I)
          IF(CCOR(ICONN(L,3),4).GT.4) GC TC 15
          IF(ICONN(L,2+J).EQ.C) GC TC 19
          NCODE (L,4+K)=NCOOM(ICONN(L,2+J),1)
       14 N=N+1
          GO TC 15
       19 K=0
          J=C
          NU=NL-1
          DO 2C LCUM=1,NU
          K=K+4
          J=J+2
          DO 2C I=1,3
       20 NCODE(L,I+K)=NODOM(ICONN(L,1+J),I)
       15 CONTINUE
          DO 18 I=1,NOBPT
          DO 18 K=2,4
          IF (ICONN(I,1C).EQ.1) LN=6
          IF (ICONN(I,1C).NE.1) LN=8
          DO 16 J=2,LN,2
          IF (ICONN(KNCMO(I,K),J).EQ.KNCMO(I,1)) GO TO 17
       16 CONTINUE
       17 L=J*2
          M=K-1
       18 NCODE(KNCMO(I,K),L)=NCOOM(KNCMO(I,1),M)
          RETURN
          END
C *************************************************************************
          SUBROUTINE INTABC
          COMMON /CDE/ LADOM
          COMMON /F1/ SYLVEC(486)
          COMMON /SLOW/ SYMA(486,87)
          DO 1C I=1,486
       10 SYLVEC(I) = 0.0
          DO 99 I=1,486
          DO 99 J=1,87
       99 SYMA(I,J) =  0.0
          RETURN
          END
C *************************************************************************
          SUBROUTINE GLECCR
          COMMON /A1/ CCOR(315,5)
          COMMON /A4/ ICONN(116,10)
          COMMON /B7/ RCY,RCC,BET,GAM,AC,TCC,TRC,TCY,TCC,DITR
          COMMON /B9/ NP,NE,NCCAP,NCBPT,NAP
          COMMON /BCD/ KNOVA(47,4), NCCCM(315,3), KNCMO(4,4)
          COMMON /C2/ XBAR(315), YBAR(315), ZBAR(315)
          COMMON /L1/ NCASE
          TANCM= SIN(BET)/(2.C*COS( .5*(BET+GAM))*COS(.5*(BET-GAM)))
          FS= (RCY*TANCM*SIN(GAM))/SIN(BET)
          ALPHA=(3.1416/2.0)-ATAN(TANCM)
          COAL=COS(ALPHA)
          SIAL=SIN(ALPHA)
          COBET=COS(BET)
          SIBET=SIN(BET)
          TAGAM=TAN(GAM)
```

```
      DO 550  I=1,NP
      XBAR(I)=0.0
      YBAR(I)=0.0
  550 ZBAR(I)=0.0
      DO 371 I=1, NP
      IF (CCOR(I,1).NE.0) GO TO 500
      IF (CCOR(I,2).NE.0) GO TO 500
      IF(CCOR(I,4).EQ.1 .OR. CCCR(I,4).EQ.6) GO TO 500
      GO TO 371
  500 IF (CCOR(I,4).EQ.1 .OR. CCCR(I,4).EQ.6) GO TO 351
      IF (CCOR(I,4).EQ.2) GO TO 361
      IF (CCOR(I,4).EQ.3) GO TO 364
      IF (CCOR(I,4).EQ.4 .OR. CCCR(I,4).EQ.5) GO TO 369
  351 XBAR(I)=CCOR(I,1)      + FS
      YBAR(I)=CCOR(I,2)
      ZBAR(I)=0.0
      GO TO 371
  361 XBAR(I)= COAL*COOR(I,1)+FS
      YBAR(I)= COOR(I,2)
      ZBAR(I)= -SIAL*COOR(I,1)
      GO TO 371
  364 XBAR(I)= COOR(I,1)+FS
      YBAR(I)= RCY*SIN(COOR(I,2))
      ZBAR(I)= RCY*COS(CCOR(I,2))
      GO TO 371
  369 TA=TAGAM
      RA=RCO
      IF (CCOR(I,4).EQ.4) GO TO 370
      IF (NCASE.EQ.0) TA=0.0
      IF (NCASE.EQ.1) RA=RCC/5.10
      IF (NCASE.EQ.1) COOR(I,1)=A0
  370 COCO    =COS(COOR(I,2))
      SICC    =SIN(CCOR(I,2))
      TEM1    = RA+(A0-CCOR(I,1))*TA
      TEM2    = COOR(I,1)
      XBAR(I)= TEM2    *COBET-TEM1*SIBET*CCCC
      YBAR(I)= TEM1    *SICC
      ZBAR(I)= TEM2    *SIBET+TEM1*CCBET*COCC
  371 CONTINUE
```

```
      DO 4CC I=1,NOBPT
      YBAR(ICONN(KNOMO(I,2),3)) = YBAR(ICONN(KNOMO(I,2),1))
  400 ZBAR(ICONN(KNOMO(I,2),3)) = ZBAR(ICONN(KNOMO(I,2),1))
      YBAR(ICONN(KNOMO(NOBPT,2),5)) = YBAR(ICONN(KNOMO(NOBPT,2),7))
      ZBAR(ICONN(KNOMO(NOBPT,2),5)) = ZBAR(ICONN(KNOMO(NOBPT,2),7))
      DO 908 I=1,NP
  908 WRITE (7,11)  I,XBAR(I),YBAR(I),ZBAR(I)
   11 FORMAT(I4,3X,F12.4,8X,F12.4,8X,F12.4,8X,A4)
      DO 911 I=1,NE
      J=I+1CCC
  911 WRITE(7,321)      J,(ICONN(I,K),  K=1,8,2)
  321 FORMAT (16(I4,1X))
      RETURN
      END
C*********************************************************************
      SUBROUTINE GLASYA (M)
      COMMON /A4/ ICONN(116,10)
      COMMON /B7/ RCY,RCO,BET,GAM,AL,TCG,TRG,TCY,TCO,DITR
      COMMON /C2/ XBAR(315), YBAR(315), ZBAR(315)
      COMMON /D1/  TH,XBARR,YBARR,ZBARR
      DX=0.
      DY=0.
      DZ=0.
      IF (ICONN(M,10).EQ.1) GO TO 161
      IF(ICONN(M,9).GT.4) GO TO 161
      DO 8 J=1,8,2
      DX=DX + XBAR(ICONN(M,J))
      DY=DY + YBAR(ICONN(M,J))
    8 DZ=DZ + ZBAR(ICONN(M,J))
  161 XBARR= DX*.25
      YBARR= DY*.25
      ZBARR= DZ*.25
      IF(ICONN(M,9).EQ.1) GO TO 11
      IF(ICONN(M,9).EQ.2) GO TO 12
      IF(ICONN(M,9).EQ.3) GO TO 13
      IF(ICONN(M,9).EQ.4) GO TO 14
      IF(ICONN(M,9).EQ.5) GO TO 9
      IF(ICONN(M,9).EQ.6) GO TO 15
   11 TH=TCG
      GO TO 9
   12 TH=TRG
      GO TO 9
   13 TH=TCY
      GO TO 9
   14 TH=TCO
      GO TO 9
   15 TH=DITR
    9 RETURN
      END
C*********************************************************************
      SUBROUTINE TRISYS(M)
      COMMON /A3/ ICODE (4,12)
      COMMON /A4/ ICONN(116,10)
      COMMON /A6/ TQEM(23,23)
      COMMON /A7/ QRT(23)
      COMMON /A8/ B(3,3), BP(3), CP(3), AI(3,3), AJ(3,3), AK(3,3), SI(3)
     1, CO(3),          G(3,3), D(3,3), Q(3,3),PT(3,3), H(3,3),
```

```
     2TEM(12,12),PL(12), TEMP(12,12), RPL(12)
      COMMON /A9/ E,PR,CON,P
      COMMON /B3/  F(3,3), T(12,12)
      COMMON /B4/  X2,X3,Y3,AREA
      COMMON /B6/ TEMT(12,12),RPLT(12)
      COMMON /B7/ RCY,RCO,BET,GAM,AC,TCG,TRG,TCY,TCO,DITR
      COMMON /C2/ XBAR(315), YBAR(315), ZBAR(315)
      COMMON /D1/  TH,XBARR,YBARR,ZBARR
      COMMON /L1/ NCASE
      COMMON /Y2/  BB(3)
      DOUBLE PRECISION F,BB,DET
      DO 145 I=1,23
      QRT(I)=0.0
      DO 145 J=1,23
  145 TQEM(I,J)=0.0
      DO 155 L=1,4
      IF (L.EQ.1) GO TO 10
      IF (L.EQ.2) GO TO 20
      IF (L.EQ.3) GO TO 30
      IF (L.EQ.4) GO TO 40
   10 XBAR1=XBAR(ICONN(M,1))
      YBAR1=YBAR(ICONN(M,1))
      ZBAR1=ZBAR(ICONN(M,1))
      XBAR2=XBAR(ICONN(M,2))
      YBAR2=YBAR(ICONN(M,2))
      ZBAR2=ZBAR(ICONN(M,2))
      IF(ICONN(M,10).NE.1) GO TO 45
      XBAR3=XBAR(ICONN(M,5))
      YBAR3=YBAR(ICONN(M,5))
      ZBAR3=ZBAR(ICONN(M,5))
      GO TO 55
```

```
   20 XBAR1=XBAR(ICONN(M,3))
      YBAR1=YBAR(ICONN(M,3))
      ZBAR1=ZBAR(ICONN(M,3))
      XBAR2=XBAR(ICONN(M,5))
      YBAR2=YBAR(ICONN(M,5))
      ZBAR2=ZBAR(ICONN(M,5))
      GO TO 45
   30 XBAR1=XBAR(ICONN(M,5))
      YBAR1=YBAR(ICONN(M,5))
      ZBAR1=ZBAR(ICONN(M,5))
      XBAR2=XBAR(ICONN(M,7))
      YBAR2=YBAR(ICONN(M,7))
      ZBAR2=ZBAR(ICONN(M,7))
      GO TO 45
   40 XBAR1=XBAR(ICONN(M,7))
      YBAR1=YBAR(ICONN(M,7))
      ZBAR1=ZBAR(ICONN(M,7))
      XBAR2=XBAR(ICONN(M,1))
      YBAR2=YBAR(ICONN(M,1))
      ZBAR2=ZBAR(ICONN(M,1))
   45 A1 = ((XBAR2-XBAR1)*(XBAR2-XBAR1)+(YBAR2-YBAR1)*(YBAR2-YBAR1)+
     1    (ZBAR2-ZBAR1)*(ZBAR2-ZBAR1))**.5
      IF(ICONN(M,9).GT.4) GO TO 56
      A2 = ((XBARR-XBAR2)*(XBARR-XBAR2)+(YBARR-YBAR2)*(YBARR-YBAR2)+
     1    (ZBARR-ZBAR2)*(ZBARR-ZBAR2))**.5
      A3 = ((XBARR-XBAR1)*(XBARR-XBAR1)+(YBARR-YBAR1)*(YBARR-YBAR1)+
```

```
     1    (ZBARR-ZBAR1)*(ZBARR-ZBAR1))**.5
      GO TO 56
   55 A1 = ((XBAR2-XBAR1)*(XBAR2-XBAR1)+(YBAR2-YBAR1)*(YBAR2-YBAR1)+
     1    (ZBAR2-ZBAR1)*(ZBAR2-ZBAR1))**.5
      A2 = ((XBAR3-XBAR2)*(XBAR3-XBAR2)+(YBAR3-YBAR2)*(YBAR3-YBAR2)+
     1    (ZBAR3-ZBAR2)*(ZBAR3-ZBAR2))**.5
      A3 = ((XBAR1-XBAR3)*(XBAR1-XBAR3)+(YBAR1-YBAR3)*(YBAR1-YBAR3)+
     1    (ZBAR1-ZBAR3)*(ZBAR1-ZBAR3))**.5
   56 B(1,1)=(XBAR2-XBAR1)/A1
      B(1,2)=(YBAR2-YBAR1)/A1
      B(1,3)=(ZBAR2-ZBAR1)/A1
      IF(ICONN(M,10).EQ.1) GO TO 57
      IF(ICONN(M,9).GT.4) GO TO 54
      C1=(XBARR-XBAR1)/A3
      C2=(YBARR-YBAR1)/A3
      C3=(ZBARR-ZBAR1)/A3
      GO TO 58
   57 C1=(XBAR3-XBAR1)/A3
      C2=(YBAR3-YBAR1)/A3
      C3=(ZBAR3-ZBAR1)/A3
   58 SINSI= ((B(1,2)*C3-B(1,3)*C2)*(B(1,2)*C3-B(1,3)*C2) + (B(1,3)*C1
     1         -B(1,1)*C3)* (B(1,3)*C1-B(1,1)*C3) + (B(1,1)*C2-B(1,2)*C1)
     2         *(B(1,1)*C2-B(1,2)*C1))**.5
      COSSI=  B(1,1)*C1+B(1,2)*C2+B(1,3)*C3
      B(3,1)= (B(1,2)*C3-B(1,3)*C2)/SINSI
      B(3,2)= (B(1,3)*C1-B(1,1)*C3)/SINSI
      B(3,3)= (B(1,1)*C2-B(1,2)*C1)/SINSI
      B(2,1)= B(3,2)*B(1,3)-B(3,3)*B(1,2)
      B(2,2)= B(3,3)*B(1,1)-B(3,1)*B(1,3)
      B(2,3)= B(3,1)*B(1,2)-B(3,2)*B(1,1)
      GO TO 49
   54 IF (ICONN(M,9).EQ.5 .AND. NCASE.EQ.0) GO TO 51
      IF (ICONN(M,9).EQ.5 .AND. NCASE.EQ.1) GO TO 52
      IF (ICONN(M,9).EQ.6) GO TO 53
      WRITE(6,6) M
    6 FORMAT (' ERROR IN ICONN FOR ELEMENT',I5)
   51 B(2,1)=C.0
      B(2,2)=1.0
      B(2,3)=C.0
      B(3,1)=-B(1,3)
      B(3,2)=C.C
      B(3,3)=B(1,1)
      GO TO 49
   52 ALPHA=1.57079-BET
      B(3,1)=SIN(ALPHA)
      B(3,2)=C.C
      B(3,3)=COS(ALPHA)
      B(2,1)=-B(1,2)*B(3,3)
      B(2,2)=B(1,1)/B(3,3)
      B(2,3)=B(1,2)*B(3,3)
      GO TO 49
   53 B(2,1)=1.0
      B(2,2)=C.0
      B(2,3)=C.0
      B(3,1)=C.0
      B(3,2)=C.0
      B(3,3)=1.0
```

```
   49 CONTINUE
      DO 59 I=1,3
      DO 59 J=1,3
   59 IF(ABS(B(I,J)).LE. .03500) B(I,J) = 0.0
      A1=A1*12.
      IF(ICONN(M,9).GT.4) GO TO 72
      A2=A2*12.
      A3=A3*12.
      X2=A1
      X3=A3  *COSSI
      Y3=A3  *SINSI
      AREA=(X2*Y3/2.0)
      BP(1)=-Y3
      BP(2)=Y3
      BP(3)=0.
      CP(1)=(X3-X2)
      CP(2)=-X3
      CP(3)=X2
      ETA=E*TH/(4.*AREA*(1.-PR*PR))
      DO 50 I=1,3
      DO 50 J=1,3
      AI(I,J)=ETA * (BP(I)*BP(J)+CP(I)*CP(J)*CON)
      AJ(I,J)=ETA * (BP(I)*CP(J)*PR+BP(J)*CP(I)*CON)
   50 AK(I,J)=ETA * (CP(I)*CP(J)+BP(I)*BP(J)*CON)
      SI(1)=-1.
      SI(2)=(X2-X3)/A2
      IF (ICONN(M,7).NE.0) WRITE(18) SINSI, SI(2)
      DO 61 I=1,3
      DO 61 J=1,3
   61 F(I,J)=C.0
      IF (ICONN(M,9).EQ.1) GO TO 72
      SI(3)=COSSI
      CO(1)=0.
      CO(2)=Y3/A2
      CO(3)=-SINSI
      F(1,1)=C.
      F(1,2)=1.
      F(1,3)=C.
      F(2,1)=CO(2)*CO(2)
      F(2,2)=SI(2)*SI(2)
      F(2,3)=2.*CO(2)*SI(2)
      F(3,1)=CO(3)*CO(3)
      F(3,2)=SI(3)*SI(3)
```

```
      F(3,3)=2.*CO(3)*SI(3)
      CALL MAINV2 (F,3,BB,C,DET)
      ETAP= 12.*AREA/(E*TH*TH*TH)
      DO 6C I=1,3
      DO 6C J=1,3
   6C G(I,J)=-ETAP*(2.*(1.+PR)*F(3,I)*F(3,J)+F(1,I)*F(1,J)+F(2,I)*F(2,J)
     1       -PR*(F(2,I)*F(1,J)+F(1,I)*F(2,J)))
      D(1,1)=C.
      D(1,2)=C.
      D(I,3)=-1.
      D(2,1)=-SI(2)*CO(2)
      D(2,2)=-D(2,1)
      D(2,3)=2.*CO(2)*CC(2)-1.0
      D(3,1)=-SI(3)*CC(3)
      D(3,2)=-D(3,1)
      D(3,3)=2.*CO(3)*CC(3)-1.0
      DO 7C I=1,3
      CO 7C J=1,3
      PT(I,J)=-BP(J)*SI(I)/(2.*AREA)+CP(J)*CC(I)/(2.*AREA)
      Q(I,J)=C.
      CO 7C K=1,3
   7C Q(I,J)= Q(I,J)+D(I,K)*F(K,J)
      DO 79 I=1,3
      CO 79 J=1,3
   79 H(I,J)=      (+A1*Q(1,I)*PT(1,J)+A2*Q(2,I)*PT(2,J)+A3*Q(3,I)*PT(3,J
     1))
   72 DO 80 I=1,12
      DO 80 J=1,12
   80 TEM(I,J)=C.C
      IF(ICONN(M,9).LT.5) GC TO 83
      AREA=1CCCCCC.
      IF(ICONN(M,9).EQ.6) AREA= 3.14159*TH*TH/8.0
      AXST= AREA*E/A1
      TEM(1,1)= AXST
      TEM(1,2)=-AXST
      TEM(2,1)= TEM(1,2)
      TEM(2,2)= AXST
      X2=A1
      GO TC 99
   83 CONTINUE
      DO 85 I=1,3
      CC 85 J=1,3
      TEM(I,J)=AI(I,J)
      TEM(I,J+3)=AJ(I,J)
      TEM(I+3,J)=AJ(J,I)
      TEM(I+3,J+3)=AK(I,J)
      IF(ICONN(M,9).EQ.1) GL TC 85
      TEM(I+9,J+6)=H(I,J)
      TEM(I+6,J+9)=H(J,I)
      TEM(I+9,J+9)=G(I,J)
   85 CONTINUE
      DO 87 I=1,12
   87 PL(I)=C.C
      IF (ICONN(M,9).LT.7) GO TL 99
      DO 89 I=7,9
   89 PL(I)=   P*AREA/3.0
      DO 98 I=1,12
   98 RPL(I)=C.C
   99 CALL REARR (TEM,PL,RPL)
      DO 1CC I=1,12
      DO 1CC J=1,12
  1CC T(I,J)=C.C
      DO 11C I=1,3
      DO 11C J=1,3
      T(I,J)=B (I,J)
      T(I+4,J+4)=B (I,J)
  11C T(I+8,J+8)=B (I,J)
      CO 12C I=4,12,4
      J=I
  12C T(I,J)=1.0
      WRITE (2) X2,X3,Y3,AREA,F,T
      DO 13C I=1,12
      DO 13C J=1,12
      TEMP(I,J)=C.C
      DO 13C K=1,12
  13C TEMP(I,J)=TEMP(I,J)+TEM(I,K)*T(K,J)
      CO 14C I=1,12
      DO 14C J=1,12
      TEMT(I,J)=C.C
      DO 14C K=1,12
  14C TEMT(I,J)=TEMT(I,J)+T(K,I)*TEMP(K,J)
      IF(ICONN(M,9).GT.4) GC TO 156
      DO 142 I=1,12
      RPLT(I)=C.C
      DO 142 K=1,12
  142 RPLT(I)=RPLT(I)+T(K,I)*RPL(K)
      IF (ICONN(M,10).EQ.1) GC TO 156
      DO 35C J=1,12
      DO 35C N=J,12
      KA=ICODE(L,J)
      KB=ICODE(L,N)
      IF (KA.LE.KB)  GO TC 15C
      NTEMP=KA
      KA=KB
      KB=NTEMP
  15C TQEM(KA,KB)=TQEM(KA,KB)+TEMT(J,N)
  35C CONTINUE
      DO 152 I=1,23
      DO 152  J=I,23
      TQEM(J,I)=TQEM(I,J)
  152 CONTINUE
      DO 154 J=1,23
      DO 153 K=1,12
      IF (ICODE(L,K).NE.J) GO TC 153
      QRT(J)=QRT(J)+RPLT(K)
  153 CONTINUE
  154 CONTINUE
  155 CONTINUE
  156 RETURN
      END
C ***********************************************************************
      SUBROUTINE QUASYB (M,LN,N,CEMBB,CEMBA,CRB)
      COMMON /A4/ ICONN(116,10)
      COMMON /A5/ QEMAA(16,16), CEMAB(16,7), CEMT3(16,7),
     1CEMT1(7,16), CEMT2(16,16), CRA(16)
      COMMON /A6/ TQEM(23,23)
      COMMON /A7/ QRT(23)
      COMMON /C4/ QEM (16,16), CR(16)
      COMMON /I1/ QT(16)
      COMMON /Z2/ BD(7)
      DIMENSION  CEMBB(N,N), CEMBA(N,16),CRB(N)
      DOUBLE PRECISION CEMBB,DET,BD
      DOUBLE PRECISION QEM ,QEMAA, CEMAB,QEMBA,CEMT1,CEMT2,CEMT3
      IF(ICONN(M,10).EQ.1) GC TC 302
      IF(ICONN(M,9).GT.4) GC TO 3C3
```

```
      DO 160 I=1,16
      DO 160 J=1,16
  160 QEMAA(I,J)=TQEM(I,J)



      DO 170 I=1,16
      DO 170 J=1,N
  170 QEMAB(I,J)=TQEM(I,J+16)
      DO 180 I=1,N
      DO 180 J=1,16
  180 QEMBA(I,J)=TQEM(I+16,J)
      DO 190 I=1,N
      DO 190 J=1,N
  190 QEMBB(I,J)=TQEM(I+16,J+16)
      CALL MAINV2(QEMBB,N,BD,C,DET)
      DO 210 I=1,N
      DO 210 J=1,16
      QEMT1(I,J)=C.C
      DO 210 K=1,N
  210 QEMT1(I,J)=QEMT1(I,J)+QEMBB(I,K)*QEMBA(K,J)
      DO 220 I=1,16
      DO 220 J=1,16
      QEMT2(I,J)=C.C
      DO 220 K=1,N
  220 QEMT2(I,J)=QEMT2(I,J)+QEMAB(I,K)*QEMT1(K,J)
      DO 230 I=1,16
      DO 230 J=1,16
  230 QEM(I,J)= QEMAA(I,J)-QEMT2(I,J)
      DO 233 I=1,16
  233 QRA(I)=QRT(I)
      DO 235 I=1,N
  235 QRB(I)=QRT(I+16)
      WRITE (3) QEMBA,QEMBB,QRB
      DO 237 I=1,16
      DO 237 J=1,N
      QEMT3(I,J)=0.0
      DO 237 K=1,N
  237 QEMT3(I,J)=QEMT3(I,J)+QEMAB(I,K)*QEMBB(K,J)
      DO 240 I=1,16
      QT(I)=0.0
      DO 239 K=1,N
  239 QT(I)= QT(I)+QEMT3(I,K)*QRB(K)
  240 QR(I)=QRA(I)-QT(I)
      LN=16
      GO TO 301
  302 LN=12
      GO TO 301
  303 LN=7
  301 RETURN
      END
C *********************************************************************
      SUBROUTINE SYMAG(LN,M)
      COMMON /A4/ ICONN(116,10)
      COMMON /B1/ NCODE(116,16)
      COMMON /B6/ TEMT(12,12),RPLT(12)
      COMMON /B9/ NP,NE,NCONP,NEPPT,NAP     /
      COMMON /BCD/ KNOWA(47,4), NCOCM(315,3), KNOMO(4,4)
      COMMON /C4/ QEM (16,16), QR(16)
      COMMON /C8E/ LADOM /
      COMMON /F1/ SYLVEC(486)
      COMMON /SLOW/ SYMA(486,87) /
      DOUBLE PRECISION QEM
```

```
      DO 250 I=1,LN
      DO 250 J=I,LN
      K=NCODE(M,I)
      L=NCODE(M,J)
      IF (K.EQ.0 .OR. L.EQ.0) GO TO 250
      IF(K.LE.L) GO TO 248
      TEMPO=K
      K=L
      L=TEMPO
  248 MPACK=L-K+1
      IF(ICONN(M,10).EQ.1 .OR. ICONN(M,9).GT.4) GO TO 303
      SYMA(K,MPACK)=SYMA(K,MPACK)+QEM(I,J)
      GO TO 250
  303 SYMA(K,MPACK)=SYMA(K,MPACK)+TEMT(I,J)
  250 CONTINUE
      IF(ICONN(M,9).GT.4) GO TO 243
      IF (ICONN(M,10).EQ.1) NL=12
      IF (ICONN(M,10).NE.1) NL=16
      DO 240 I=1,LADOM
      DO 241 J=1,NL
      IF(NCODE(M,J).NE.I) GO TO 241
      IF(ICONN(M,10).EQ.1) QR(J)=RPLT(J)
      SYLVEC(I)=SYLVEC(I)+QR(J)
  241 CONTINUE
  240 CONTINUE
  243 RETURN
      END
C *********************************************************************
      SUBROUTINE MAINV2 (A,N,B,M,DETERM)                                  C0409
C     MATRIX INVERSION WITH ACCOMPANYING SOLUTION OF LINEAR               C0410
C      EQUATIONS OF THE FORM AX = B.  JORDAN'S METHOD                     C0411
C     A IS THE ARRAY TO BE INVERTED.                                      C0412
C     B IS THE COLUMN OF CONSTANTS FOR LINEAR EQUATION SOLUTION.          C0413
C     N IS THE ORDER OF A                                                 C0414
C     M IS THE INDICATOR FOR SPECIFYING INVERSION OR SOLUTION             C0415
C      OF LINEAR EQUATIONS.                                               C0416
C          M=0, INVERSION IS PERFORMED.                                   C0417
C          M=1, SOLUTION OF LINEAR EQUATIONS IS PERFORMED.                C0418
C     AT THE RETURN TO THE CALLING PROGRAM, A INVERSE                     C0419
C      IS STORED AT A AND X AT B.                                         C0420
C     NOTE.. IF USED SOLELY FOR INVERSION, THE CALL STATEMENT             C0421
C      MUST STILL CONTAIN AN ENTRY CORRESPONDING TO B.                    C0422
C     DETERM IS THE LOCATION IN WHICH THE DETERMINANT IS STORED.          C0423
      DIMENSION IPIVOT(7), A(N,N), B(1,1), INDEX(7,2), PIVOT(7)           C0424
      DOUBLE PRECISION A,DETERM,AMAX,SWAP,T,B
      DO 20 J=1,N                                                         C0426
   20 IPIVOT(J)=0                                                         C0427
      DO 550 I=1,N                                                        C0428
C     SEARCH FOR PIVOT ELEMENT                                            C0429
      AMAX=0.0                                                            C0430
      DO 105 J=1,N                                                        C0431
      IF (IPIVOT(J)-1) 60, 105, 60                                        C0432
   60 DO 100 K=1,N
      IF (IPIVOT(K)-1) 80, 100, 740                                       C0434
   80 IF (DABS(AMAX)-DABS(A(J,K))) 85,100,100
   85 IROW=J                                                              C0436
      ICOLUM=K                                                            C0437
```

```
      AMAX=A(J,K)
  100 CONTINUE
  105 CONTINUE
      IPIVOT(ICOLUM)=IPIVOT(ICOLUM)+1
C     INTERCHANGE ROWS TO PUT PIVOT ELEMENT ON DIAGONAL
      IF (IROW-ICOLUM) 140, 260, 140
  140 CONTINUE
      DO 200 L=1,N
      SWAP=A(IROW,L)
      A(IROW,L)=A(ICOLUM,L)
  200 A(ICOLUM,L)=SWAP
      IF(M) 260, 260, 210
  210 DO 250 L=1, M
      SWAP=B(IROW,L)
      B(IROW,L)=B(ICOLUM,L)
  250 B(ICOLUM,L)=SWAP
  260 INDEX(I,1)=IROW
      INDEX(I,2)=ICOLUM
      PIVOT(I)=A(ICOLUM,ICOLUM)
C     DIVIDE PIVOT ROW BY PIVOT ELEMENT
      A(ICOLUM,ICOLUM)=1.0
      DO 350 L=1,N
  350 A(ICOLUM,L)=A(ICOLUM,L)/PIVOT(I)
      IF(M) 380, 380, 360
  360 DO 370 L=1,M
  370 B(ICOLUM,L)=B(ICOLUM,L)/PIVOT(I)
C     REDUCE NON-PIVOT ROWS
  380 DO 550 L1=1,N
      IF(L1-ICOLUM) 400, 550, 400
  400 T=A(L1,ICOLUM)
      A(L1,ICOLUM)=0.0
      DO 450 L=1,N
  450 A(L1,L)=A(L1,L)-A(ICOLUM,L)*T
      IF(M) 550, 550, 460
  460 DO 500 L=1,M
  500 B(L1,L)=B(L1,L)-B(ICOLUM,L)*T
  550 CONTINUE
C     INTERCHANGE COLUMNS
      DO 710 I=1,N
      L=N+1-I
      IF (INDEX(L,1)-INDEX(L,2)) 630, 710, 630
  630 JROW=INDEX(L,1)
      JCOLUM=INDEX(L,2)
      DO 705 K=1,N
      SWAP=A(K,JROW)
      A(K,JROW)=A(K,JCOLUM)
      A(K,JCOLUM)=SWAP
  705 CONTINUE
  710 CONTINUE
  740 RETURN
      END
C *********************************************************************
      SUBROUTINE REARR (TEM,PL,RPL)
      DIMENSION A1(12,12), A2(12,12),TEM(12,12),TEMP(12,12),
     1 PL(12),RPL(12)
      DO 4 I=1,12
      DO 4 J=1,12
      A1(I,J)=0.0
    4 A2(I,J)=0.0
      I=1
      J=1
      GO TO 9
    5 J=2
      GO TO 9
    6 J=3
      GO TO 9
    7 J=4
    9 A2(I,J)=1.0
      I=I+1
      J=J+4
      IF(J.EQ.13)GO TO 5
      IF(J.EQ.14)GO TO 6
      IF(J.EQ.15)GO TO 7
      IF(J.EQ.16)GO TO 10
      GO TO 9
   10 DO 11 I=1,12
      DO 11 J=1,12
   11 A1(I,J)=A2(J,I)
      DO 12 I=1,12
      DO 12 J=1,12
      TEMP(I,J)=0.0
      DO 12 K=1,12
   12 TEMP(I,J)=TEMP(I,J)+TEM(I,K)*A2(K,J)
      DO 13 I=1,12
      DO 13 J=1,12
      TEM(I,J)=0.0
      DO 13 K=1,12
   13 TEM(I,J)=TEM(I,J)+A1(I,K)*TEMP(K,J)
      DO 14 I=1,12
      RPL(I)=0.0
      DO 14 K=1,12
   14 RPL(I)=RPL(I)+A1(I,K)*PL(K)
      RETURN
      END
C *********************************************************************
      SUBROUTINE SYLMOD
      COMMON /A1/ COOR(315,5)
      COMMON /A9/ E,PR,CON,P
      COMMON /B7/ RCY,RCO,BET,GAM,AD,TCG,TRG,TCY,TCO,DITR
      COMMON /B9/ NP,NE,NCONP,NCBPT,NNP
      COMMON /BCD/ KNOVA(47,4), NODOM(315,3), KNOMO(4,4)
      COMMON /F1/ SYLVEC(486)
      COMMON /CDE/ LADOM
      ALPHA=1.57079-BET
      C1=SIN(ALPHA)
      C2=COS(ALPHA)
      N=0
      M=0
      DO 10 K=1,NP
      IF (COOR(K,5).EQ.1.OR.COOR(K,5).EQ.2)  N=N+1
      IF (COOR(K,5).EQ.3.OR.COOR(K,5).EQ.4)  M=M+1
   10 CONTINUE
      NU=N-1
      FCY=((P*(RCY*RCY)*3.14159)/(4.0*NU))*144.
      NU=M-1
      FCO=((P*(RCO*RCO)*3.14159)/(2.0*NU))*144.
      DO 100 K=1,NP
      IF (COOR(K,5).EQ.0)  GO TO 100
      IF (COOR(K,5).EQ.2 .OR. COOR(K,5).EQ.4)  GO TO 25
      F=FCY
      IF (COOR(K,5).EQ.2)  F=0.5*FCY
      ID=NODOM(K,1)
      SYLVEC(ID)=SYLVEC(ID)+F
      GO TO 100
   25 F=FCO
      IF (COOR(K,5).EQ.4)  F=0.5*FCO
      ID1=NODOM(K,1)
```

```
      ID2=NCODCM(K,3)
      SYLVEC(ID1)=SYLVEC(ID1)+F*C1
      SYLVEC(ID2)=SYLVEC(ID2)+F*C2
  100 CONTINUE
      RETURN
      END
C *********************************************************************
      SUBROUTINE BANWID (NE,MB)
      COMMON /B1/ NCODE(116,16)
      J=0
      DO 259 N=1,NE
      DO 258 I=1,16
      IF(NCODE(N,I).EQ.0) GO TO 258
      DO 257 L=I,16
      IF(NCODE(N,L).EQ.0) GO TO 257
      KK=IABS(NCODE(N,I)-NCODE(N,L))
      IF(KK-J) 257,257,256
  256 J=KK
  257 CONTINUE
  258 CONTINUE
  259 CONTINUE
      MB=J+1
      RETURN
      END
C *********************************************************************
      SUBROUTINE SYMSOL (MB)
      COMMON /B9/ NP,NE,NCONP,NCBPT,NAP
      COMMON /BCD/ KNOVA(47,4), NCODCM(315,3), KNCMO(4,4)
      COMMON /CDE/ LADOM
      COMMON /F1/ Q(486)
      COMMON /SLOW/ BGK(486,87)
      DIMENSION F(486)
      NO=LADOM
      N=0
  500 N=N+1
C
C     REDUCE N TH EQUATION
C
C        1. DIVIDE RIGHT SIDE BY DIAGONAL ELEMENT
C
      Q(N)=Q(N)/BGK(N,1)
C
C        2. CHECK FOR LAST EQUATION
C
```

```
      IF(N-NO) 550,700,550
C
C        3. DIVIDE N TH EQUATION BY DIAGONAL ELEMENT
C
  550 DO 600 K=2,MB
      F(K)=BGK(N,K)
      BGK(N,K)=BGK(N,K)/BGK(N,1)
  600 CONTINUE
C
C        4. REDUCE REMAINING EQUATIONS
C
      DO 660 L=2,MB
      I=N+L-1
      IF(NO-I) 660,640,640
  640 J=0
      DO 650 K=L,MB
      J=J+1
  650 BGK(I,J) = BGK(I,J) - F(L) * BGK(N,K)
      Q(I)=Q(I)-F(L)*Q(N)
  660 CONTINUE
      GO TO 500
C
C     BACK SUBSTITUTION
C
  700 N=N-1
C
C        1. CHECK FOR FIRST  EQUATION
C
      IF(N) 750,900,750
C
C        2. CALCULATE UNKNOWN DISPLACEMENTS
C
  750 DO 800 K=2,MB
      L=N+K-1
      IF(NO-L) 800,770,770
  770 Q(N)=Q(N)-BGK(N,K)*Q(L)
  800 CONTINUE
      GO TO 700
  900 CONTINUE
      DO 10 I=1,NP
      K1=NCODOM(I,1)
      K2=NCODOM(I,2)
      K3=NCODOM(I,3)
      IF(K1.EQ.0) Q(K1)=0.0
      IF(K2.EQ.0) Q(K2)=0.0
      IF(K3.EQ.0) Q(K3)=0.0
   10 WRITE(16) I,Q(K1),Q(K2),Q(K3)
      RETURN
      END
C *********************************************************************
      SUBROUTINE STREMO (NCBPT,N,QEMBB,QEMBA,QRB,IL)
      COMMON /A4/ ICONN(116,10)
      COMMON /A9/ E,PR,CON,P
      COMMON /B1/ NCODE(116,16)
      COMMON /B2/ PHIA(16),PHIT(7),QRBT(7),PHIB(7),PHI(12),A(3,6),C(3,3)
     1,CISP(7),SMOM(3),TESI(4,3),TEEP(4,3),TEMO(4,3),PHIP(12)
      COMMON /B3/  F(3,3), T(12,12)
```

```
      COMMON /B4/  X2,X3,Y3,AREA
      COMMON /BCD/ KNOVA(47,4), NCODCM(315,3), KNCMO(4,4)
      COMMON /E1/ QEEP(116,2), QESI(116,3), QEMO(116,3)
      COMMON /F1/ SYLVEC(486)
      COMMON /H1/ DIS(4)
      COMMON /L1/ COM(1,4)
      COMMON /V1/ B(8)
      DIMENSION  QEMBA(N,16),QEMBB(N,N),QRB(N)
      DOUBLE PRECISION F
      DOUBLE PRECISION QEMBB
      DOUBLE PRECISION QEMBA
      NL=16
      IF(ICONN(IL,10).EQ.1) NL=12
      IF(ICONN(IL,9).GT.4) NL=7
      DO 100 I=1,NL
      IF (NCODE(IL,I).EQ.0) GO TO 105
      PHIA(I) =SYLVEC(NCODE(IL,I))
      GO TO 100
  105 PHIA(I) = 0.0
  100 CONTINUE
      IF((ICONN(IL,10).EQ.1 .OR. ICONN(IL,9).GT.4) GO TO 51
      READ(3) QEMBA,QEMBB,QRB
      DO 30 I=1,N
      PHIT(I)=0.0
```

```
      DO 30 K=1,16
   30 PHIT(I)=PHIT(I)+GEMBA(I,K)*PHIA(K)
      DO 40 I=1,N
   40 GRBT(I)= GRB(I)-PHIT(I)
      DO 50 I=1,N
      PHIB(I)=0.0
      DO 50 K=1,N
   50 PHIB(I)= PHIB(I)+GEMBB(I,K)*GRBT(K)
      IF (N.EQ.2) GO TO 7
      GO TO 9
    7 DO 8 I=3,7
    8 PHIB(I)=0.0
    9 CONTINUE
      NN = 0
   51 DO 80 L=1,4
      IF (ICONN(IL,7).EQ.0)  GO TO 52
      READ(18) SINSI,SI
      NN = NN + 1
      B(NN)  = SINSI
      NN = NN + 1
        B(NN) = SI
   52 CONTINUE
      READ(2) X2,X3,Y3,AREA,E,T
      IF(ICONN(IL,10).EQ.1 .OR. ICONN(IL,9).GT.4) GO TO 67
      DO 63 M=1,7
      K=M+4*(L-1)
      IF(K.LE.16) GO TO 63
      K=M-4
   63 PHIP(M)=PHIA(K)
      IF(L.EQ.4) GO TO 65
      K=4+L
      PHIP(8)=PHIB(K)
      GO TO 66

   65 PHIP(8)=PHIB(4)
   66 PHIP(9)=PHIB(1)
      PHIP(10)=PHIB(2)
      PHIP(11)=PHIB(3)
      K=3+L
      PHIP(12)=PHIB(K)
   67 CONTINUE
      NJ=12
      IF(ICONN(IL,9).GT.4) NJ=7
      DO 72 I=1,NJ
      PHI(I)=0.0
      DO 72 K=1,NJ
      IF(ICONN(IL,10).EQ.1 .OR. ICONN(IL,9).GT.4) PHIP(K)=PHIA(K)
   72 PHI(I)=PHI(I)+T (I,K)*PHIP(K)
      IF(ICONN(IL,9).GT.4) GO TO 69
      DO 71 I=1,NORPT
      IF (IL.EQ.KNOMO(I,4)) GO TO 73
   71 CONTINUE
      GO TO 220
   73 IF (L.EQ.1) GO TO 83
      GO TO 220
   83 II=NODOM (KNOMO(I,1),1)
      JJ=NODOM (KNOMO(I,1),2)
      PHI(4)=-(SYLVEC(II)-SYLVEC(JJ))
  220 DUM1=      (2.*AREA)
      DO 74 I=1,3
      DO 74 J=1,6
   74 A(I,J)=0.0
      A(1,1)=-Y3/DUM1
      A(1,2)= Y3/DUM1
      A(3,4)= A(1,1)
      A(3,5)= A(1,2)
      A(2,4)=(X3-X2)/DUM1
      A(2,5)=-X3/DUM1
      A(2,6)= X2/DUM1
      A(3,1)=A(2,4)
      A(3,2)=A(2,5)
      A(3,3)=A(2,6)
      DUM2=E/(1.-(PR*PR))
      DO 75 I=1,3
      DO 75 J=1,3
   75 C(I,J)=0.0
      C(1,1)= DUM2
      C(2,2)= C(1,1)
      C(1,2)= PR*DUM2
      C(2,1)= C(1,2)
      C(3,3)= CON*DUM2
      DO 76 I=1,7
   76 DISP(I)=0.0
      DO 77 I=1,3
   77 SMOM(I)=0.0
   69 CONTINUE
      DISP(1)=PHI(1)
      DISP(2)=PHI(5)
      DISP(3)=PHI(9)
      DISP(4)=PHI(2)
      DISP(5)=PHI(6)

      DISP(6)=PHI(10)
      DISP(7)=PHI(3)
      DIS(1)=IL
      DIS(2)=DISP(1)
      DIS(3)=DISP(4)
      DIS(4)=DISP(7)
      WRITE(15) DIS
      IF(ICONN(IL,9).GT.4) GO TO 91
      SMOM(1)=PHI(4)
      SMOM(2)=PHI(8)
      SMOM(3)=PHI(12)
   91 CONTINUE
      DO 79 I=1,3
      TESI(L,I)=0.0
      TEEP(L,I)=0.0
   78 TEMO(L,I)=0.0
      IF(ICONN(IL,9).GT.4) GO TO 92
      DO 79 I=1,3
      DO 79 K=1,6
   79 TEEP(L,I)=TEEP(L,I)+A(I,K)*DISP(K)
      DO 81 I=1,3
      DO 81 K=1,3
   81 TESI(L,I)=TESI(L,I)+C(I,K)*TEEP(L,K)
      CALL PRINC (TESI(L,1),TESI(L,2),TESI(L,3),2)
      DO 82 I=1,3
      DO 82 K=1,3
   82 TEMO(L,I)=TEMO(L,I)+E(I,K)*SMOM(K)
      GO TO 93
   92 TEEP(L,1)=-DISP(1)/X2
      TESI(L,1)= E*TEEP(L,1)
   93 CONTINUE
      WRITE(17) IL,L,(TESI(L,I),I=1,3),(CCM(1,I),I=1,4)
      IF(ICONN(IL,10).EQ.1 .OR. ICONN(IL,9).GT.4) GO TO 85
   80 CONTINUE
      CALL RCIVA
      DO 87 M=1,3
      CHEP(IL,M)=0.0
```

```
      QESI(IL,M)=C.C
      QEMO(IL,M)=C.C
      CO 87 I=1,4
      QEEP(IL,M)= QEEP(IL,M)+ TEEP(I,M)/4.0
      QESI(IL,M)= QESI(IL,M)+ TESI(I,M)/4.0
      QEMO(IL,M)= QEMO(IL,M)+ TEMO(I,M)/4.0
   87 CONTINUE
      GO TO 9C
   85 DO 86 J=1,3
      QEEP(IL,J)=TEEP(1,J)
      QESI(IL,J)=TESI(1,J)
   86 QEMO(IL,J)=TEMO(1,J)
   9C CONTINUE
      CALL PRINC (QESI(IL,1),QESI(IL,2),QESI(IL,3),2)
      WRITE(21) IL,(QESI(IL,I),I=1,3),(COM(1,I),I=1,4)
      CALL PRINC (QEMO(IL,1),QEMO(IL,2),QEMO(IL,3),2)
      WRITE(22) IL,(QEMO(IL,I),I=1,3),(COM(1,I),I=1,4)
      RETURN
      END
C ***************************************************************************
```

```
      SUBROUTINE ROTVA
      COMMON /B2/ PHIA(16),PHIT(7),CRBT(7),PHIB(7),PHI(12),A(3,6),C(3,3)
     1,DISP(7),SMOM(3),TESI(4,3),TEEP(4,3),TEMO(4,3),PHIP(12)
      COMMON /V1/  B(8)
      DIMENSION  TEER(4,3), TESR(4,3), TEMR(4,3)
      DO 1C I=1,8
   1C B(I)= ARSIN(B(I))
      A2=C.C
      DO 2C L=2,4
      I= (L-1)*2
      J= I+1
      A2= -(1.57079-B(J)+B(I)-A2)
      B2= A2-1.57079
      SA= SIN(2.C*A2)
      CA= COS(2.C*A2)
      SB= SIN(2.C*B2)
      CB= COS(2.C*B2)
      TEER(L,1)= (TEEP(L,1)+TEEP(L,2))/2.0 + (TEEP(L,1)-TEEP(L,2))/2.0
     1           *CA + TEEP(L,3)/2.C*SA
      TEER(L,2)= (TEEP(L,1)+TEEP(L,2))/2.0 + (TEEP(L,1)-TEEP(L,2))/2.0
     2           *CB + TEEP(L,3)/2.C*SB
      TEER(L,3)= -(TEEP(L,1)-TEEP(L,2))/2.C*SA + TEEP(L,3)/2.0*CA
      TESR(L,1)= (TESI(L,1)+TESI(L,2))/2.0 + (TESI(L,1)-TESI(L,2))/2.0
     1           *CA + TESI(L,3)*SA
      TESR(L,2)= (TESI(L,1)+TESI(L,2))/2.0 + (TESI(L,1)-TESI(L,2))/2.0
     2           *CB + TESI(L,3)*SB
      TESR(L,3)= -(TESI(L,1)-TESI(L,2))/2.C*SA + TESI(L,3)*CA
      TEMR(L,1)= (TEMO(L,1)+TEMO(L,2))/2.0 + (TEMO(L,1)-TEMO(L,2))/2.0
     1           *CA + TEMO(L,3)*SA
      TEMR(L,2)= (TEMO(L,1)+TEMO(L,2))/2.0 + (TEMO(L,1)-TEMO(L,2))/2.0
     2           *CB + TESI(L,3)*SB
      TEMR(L,3)= -(TEMO(L,1)-TEMO(L,2))/2.C*SA + TEMO(L,3)*CA
   2C CONTINUE
      DO 3C I=2,4
      DO 3C J=1,3
      TEEP(I,J)= TEER(I,J)
      IF (J.EQ.3) TEEP(I,J)= 2.C*TEER(I,J)
      TESI(I,J)= TESR(I,J)
      TEMO(I,J)= TEMR(I,J)
   3C CONTINUE
      RETURN
      END
C ***************************************************************************
```

```
      SUBROUTINE PRINC  (A,B,C,N)
      COMMON /C1/ COM(1,4)
      IF (B.EQ.0 .AND. C.EQ.0) GO TO 1C
      AVE=(A+B)/2.C
      BASE=(A-B)/2.C
      OPP=C
      IF(N.EQ.1) OPP=C/2.C
      RAD=(BASE*BASE+OPP*OPP)**.5
      DIV= -OPP/BASE
      COM(1,1)=AVE+RAD
      COM(1,2)=AVE-RAD
      COM(1,3)=RAD
      IF(N.EQ.1) COM(1,3)=RAD*2.C
      COM(1,4)=(C.5*ATAN(DIV))/C.C1745329
```

```
      GO TO 2C
   1C DO 15 I=1,4
   15 COM(1,I)=C.C
      IF (A.NE.0) COM(1,1)=A
   2C RETURN
      END
C ***************************************************************************
      SUBROUTINE OUTPUT
      COMMON /A1/ CCOR(315,5)
      COMMON /A4/ ICONN(116,10)
      COMMON /A9/ E,PR,CON,P
      COMMON /B1/ NCODE(116,16)
      COMMON /B2/ PHIA(16),PHIT(7),CRBT(7),PHIB(7),PHI(12),A(3,6),C(3,3)
     1,DISP(7),SMOM(3),TESI(4,3),TEEP(4,3),TEMO(4,3),PHIP(12)
      COMMON /B7/ RCY,RCO,BET,GAM,AC,TCG,TRG,TCY,TCO,DITR
      COMMON /B9/ NP,NE,NCONP,NCBPT,NNP
      COMMON /BCD/ KNOVA(47,4), NCOCM(315,3), KNOMO(4,4)
      COMMON /C1/ MH
      COMMON /C2/ XBAR(315), YBAR(315), ZBAR(315)
      COMMON /E1/ QEEP(116,3), QESI(116,3), QEMO(116,3)
      COMMON /H1/ DIS(4)
      COMMON /L1/ NCASE
      COMMON /U1/ COM(1,4)
      REWIND 15
      REWIND 16
      REWIND 17
      REWIND 21
      REWIND 22
      WRITE(6,260)
  260 FORMAT (1H1,5CX,'I N P U T  D A T A')
      IF(NCASE.EQ.1) GO TO 8CC
      GO TO 8C1
  8CC WRITE (6,802)
  8C2 FORMAT (///' LOAD CONFIGURATION:   HYDROSTATIC TEST CONDITION,BULKH
     1EADS ASSUMED')
      GO TO 264
  8C1 WRITE (6,8C3)
  8C3 FORMAT (///' LOAD CONFIGURATION:   OPERATING CONDITION USING EQUIVA
     1LENT STATIC PRESSURE,NO BULKHEADS ASSUMED')
  264 CONTINUE
      BET=BET/.C1745328
      GAM=GAM/.C1745328
      DITR=DITR*2.C
      WRITE(6,265) RCY,RCO,BET,GAM,AC,TCG,TRG,TCY,TCO,DITR
  265 FORMAT (///' CYLINDER INLET RADIUS = ',F6.3,2X,' FEET',/' CONE OUTL
     1ET RADIUS = ',F6.3,2X,' FEET',/' ANGLE CHANGE IN FLOW DIRECTION =
     2',F6.3,2X,' DEGREES',/' CONE APEX HALF ANGLE = ',F6.3,2X,' DEGREES
     3',/
     4' CROTCH GIRDER THICKNESS = ',F6.3,2X,' INCHES',/' RING GIRDER THI
```

```
     5CKNESS = ',F8.3,2X,' INCHES',/' CYLINDER THICKNESS = ',F8.3,2X,' I
     6NCHES',/' CONE THICKNESS = ',F8.3,2X,' INCHES',/' DIAMETER OF TIE
     7ROD = ',F8.5,' INCHES')
      WRITE(6,270) E,PR
  270 FORMAT (/' MODULUS OF ELASTICITY = ',E10.2,2X,' KSI',/' POISSON RA
     1TIO = ',F5.2)
      WRITE (6,272)  NP,NE,NCONP,NOBPT,NNP
  272 FORMAT (//,' NUMBER OF NODE POINTS = ',I5,10X,' NUMBER OF ELEMENTS
     1 = ',I5,10X,' NUMBER OF CONSTRAINED NODES = 'I5,/' NUMBER OF BRANC
     2H POINTS =  ',I5,10X,' NUMBER OF INPUT NODES = ',I5)
      WRITE(6,310)
  310 FORMAT (//,' ELEMENT CONNECTIVITY')
      DO 315 I=1,NE
  315 WRITE(6,320) I,(ICONN(I,J),J=1,10)
  320 FORMAT (/,I5,2X,8I5,5X,I5,2X,I5)
      WRITE(6,285)
  285 FORMAT (//,10X,' NODAL POINT COORDINATES')
      DO 290 I=1, NP
      IF(CCOR(I,4).EQ.3.OR.CCOR(I,4).EQ.4)CCOR(I,2)=CCOR(I,2)/.01745328
      WRITE(6,295) I,(CCOR(I,J),J=1,5)
  290 CONTINUE
  295 FORMAT (/,5X,I5,2F10.2,3F9.0)
      WRITE(6,336)
  336 FORMAT (//,' CONSTRAINED NODE POINTS',/,6X,' NODE     U      V      W
     1')
      DO 337 I=1,NCONP
  337 WRITE(6,500) I,(KNCVA(I,J),J=1,4)
  500 FORMAT (215,316)
      WRITE(6,342)
  342 FORMAT (//,' BRANCH POINTS',/,5X,' NODE   ADJACENT ELEMENTS')
      DO 343 I=1,NOBPT
  343 WRITE(6,500) I,(KNOBC(I,J),J=1,4)
      WRITE (6,345)  P
  345 FORMAT (//,' INTERNAL PRESSURE=', F9.3,2X,' KSI')
      WRITE(6,351)
  351 FORMAT (1H1,40X,'C O M P U T E D  I N F O R M A T I O N')
      WRITE(6,352)
  352 FORMAT (//,' NODE',5X,'DISPLACEMENT OR MOMENT NUMBER')
      DO 20 I=1, NP
   20 WRITE(6,21) I, (NCDOM(I,J),J=1,3)
   21 FORMAT (/,4I5)
      WRITE(6,353)
  353 FORMAT(//,' ELEMENT',30X,'CODE NUMBER')
      DO 16 I=1,NE
   16 WRITE(6,17) I,(NCODE(I,J),J=1,16)
   17 FORMAT (/ ,I5,5X,16I5)
      WRITE (6,372)
  372 FORMAT (//,7X,' GLOBAL COORDINATES',/,' NODE',8X,' XBAR',8X,' YBAR
     1',8X,' ZBAR')
      DO 374 I=1,NP
  374 WRITE(6,373) I,XBAR(I),YBAR(I),ZBAR(I)
  373 FORMAT(/,I5,3(5X,F8.3))
      WRITE(6,261) MB
  261 FORMAT (//,' BAND WIDTH=',I5)
      WRITE(6,350)
  350 FORMAT (1H1,50X,'O U T P U T  D A T A')
      KK=4*NE
      WRITE(6,354)
  354 FORMAT(//,44X,'GLOBAL DISPLACEMENTS AND SIDE POINT MOMENTS',/,40X,
     1'NODE',6X,'UBAR',10X,'VBAR',10X,'WBAR')
      DO 355 I=1,KK
      READ (16,END=356) I,C1,C2,C3
  355 WRITE(6,357) I,C1,C2,C3
      WRITE (6,6CC)
 6CC FORMAT (///,'DISPLACEMENTS IN LOCAL COORDINATE SYSTEM',/ 'ELEMENT',
     I14X,'X',18X,'Y',18X,'Z')
      DO 601 I=1,KK
      READ(15,END=602) DIS
 601 WRITE(6,407) DIS
 6C2 CONTINUE
      WRITE (6,608)
 608 FORMAT ('1',5CX,'MEMBRANE STRESSES',//'  ELE',3X,'TRI', 8X,'SIGMA
     1X', 8X,'SIGMA Y', 8X,'TAU XY', 8X,'MAX SIGMA', 8X,'MIN SIGMA', 8X,
     2'MAX TAU', 8X,'THETA')
      DO 6C5 N=1,KK
      READ(17,END=607) IL,L,(TESI(L,I),I=1,3),(COM(I,I),I=1,4)
 6C5 WRITE(6,6C6) IL,L,(TESI(L,I),I=1,3),(COM(1,I),I=1,4)
 6C6 FORMAT (2I5,7(3X,E13.5))
 607 CONTINUE
 4C7 FORMAT (F7.0,2X,3(5X,E13.5))
1CC6 FORMAT (I5,5X,7(3X,E13.5))
      WRITE (6,1018)
1018 FORMAT ('1',45X,'MEMBRANE STRESS   AT CENTER OF ELEMENT',//' ELEME
     1NT',9X,'SIGMA X',9X,'SIGMA Y',10X,'TAU XY',9X,'MAX SIGMA',7X'MIN S
     2IGMA',8X,'MAX TAU', 9X,'THETA')
      DO 1015 N=1,KK
      READ(21,END=1017) IL,(QESI(IL,I),I=1,3),(COM(1,I),I=1,4)
1015 WRITE(6,1CC6) IL,(QESI(IL,I),I=1,3),(COM(1,I),I=1,4)
1017 CONTINUE
      WRITE (6,1028)
1028 FORMAT ('1',45X,'BENDING MOMENT  AT CENTER OF ELEMENT',//' ELEMENT
     1',8X,'MOMENT X',8X,'MOMENT Y',7X,'MOMENT XY',8X,'MAX MOMENT',6X,'M
     2IN MOMENT',6X,'MAX TWIST',6X,'THETA')
      DO 1025 N=1,KK
      READ(22,END=1027) IL,(QEMO(IL,I),I=1,3),(COM(1,I),I=1,4)
1025 WRITE(6,1CC6) IL,(QEMO(IL,I),I=1,3),(COM(1,I),I=1,4)
1027 CONTINUE
      RETURN
      END
C ***************************************************************************
/*
```